# 21st FERROFLUIDWORKSHOP

#### Benediktbeuern

September 30<sup>th</sup> - October 2<sup>nd</sup> 2025

## **Program Overview**

Opening Session 1 Coffee Break Session 2 Postersession	30.09.2025	13:20 - 13:40 13:40 - 15:40 15:40 - 16:10 16:10 - 18:10 18:10 - 20:00
Walking / Bus Tour Mountain Talks Session 3	01.10.2025	08:30 - 16:00 17:30 - 18:10
Winners of the Docto Workshop-Dinner	ral Thesis Award	18:10 - 18:45 19:00
Session 4 Coffee Break Session 5 Closing	02.10.2025	08:30 - 09:50 09:50 - 10:20 10:20 - 12:20 12:20 - 12:30
	next trains to Munich will leave	e 12:59 and 13:58

1

## **Content**

Program

Abstracts	9
List of Participants	65



## Preliminary Program for the







## Tuesday, September 30<sup>th</sup>

13:40	Session 1	
13:40 - 14:00	I. Rehberg, P. Blümler	Tailoring Magnet Setups for Field Homogeneity: An Interactive GUI for Design and Exploration
14:00 – 14:20	M. Kermarrec, Y. Suffren, P. Roquefort, S. Triki, T. Aubry	Viscoelasticity and Fluorescence of polymer- based magnetically switchable composite gels
14:20 – 14:40	A. Leon-Cecilla,F. J. Vazquez-Perez, L. Álvarez de Cienfuegos, J. E. Martin, M. T. Lopez-Lopez	Chirality and Instabilities in Ferrogel Torsional Actuators under Uniaxial Magnetic Fields
14:40 – 15:00	M.D. Contreras-Mateus, C. Friedrich, S. Odenbach	Mechanistic insights into the magnetorheology of ferrofluid emulsions with tunable nanoparticle localization: Droplet-dispersed nanoparticles
15:00 – 15:20	K. Gerstenberger, G. K. Auernhammer	Cluster growth dynamics of nickel particles in viscoelastic matrices
15:20 – 15:40	N. Magin, D. Borin, S. Odenbach	Influence of microstructure on magnetic properties of anisotropic magnetic elastomers

## 15:40 Coffee break & Posters

16:10	Session 2	
16:10 - 16:30	R. Stephan, S. Ranoo, P. Kreissl, C. Pabshettiwar, J. Kubis, C. Holm, R. von Klitzing, A. Schmidt, R. Weeber	Exploring the Mechanisms of Particle-Matrix Coupling in Magnetic Gels by Means of Simulations and Experiments

16:30 – 16:50	M. Heiber, L. Fischer, H. Reinken, A. M. Menzel	Structuring magnetic elastomers
16:50 – 17:10	H. T. Roth, P. Gebhart, K. A. Kalina, T. Wallmersperger, M. Kästner	A data-driven decoupled multiscale scheme for the modeling of structured magnetorheological elastomers
17:10 – 17:30	O. Bilous, K.A. Okrugin, A. Lakkis, R. Richter, S.S. Kantorovich	Cracking the Code of Anomalous Diffusion: Simulation Meets Experiment in Ferrogranular
17:30 – 17:50	M. Raphael, A. M. Schmidt	Micromagnetic Simulations of Magneto- Plasmonic Nano-Objects with Tunable Domain Architectures
17:50 – 18:10	K. Xiao, S. Lyer, J. Kirchner, G. Fischer	Molecular dynamics simulation of zipped chain- like agglomeration of the SPIONs

#### 18:10 Poster Session

## Wednesday, October 1st

## approx. 08:30 Mountain and Alternative Tour

#### approx. 13:30 Mountain Talks

J. Kirchner The body perspective: How magnetic nanoparticles move in the body and how we find out

17:30	Session 3	
17:30 – 17:50	T. Becker, M. Reiche, L. Zentner	Multipolar magnetized magnetoactive elastomers for actuation and locomotion applications
17:50 - 18:10	Y. Remane, S. Hestermann, A. Wagner, M. Ehresmann, G. Herdrich	Ferrofluidic gears and seals for space applications
18:10	Presentations of the awardee	s of the "Promotionspreis des

### 18:10 Presentations of the awardees of the "Promotionspreis des Ferrofluidverein Deutschland e.V."

## 19:00 Workshop dinner

# Thursday, October 2<sup>nd</sup>

8:30	Session 4	
8:30 - 8:50	A. Weidner, M. Kurniawan, B. Hankiewicz, S. Dutz, A. Bund	Light induced coating of iron oxide nanoparticles with Cu and assessment of their catalytic activity for electrochemical reduction of NO3- to NH4+
8:50 – 9:10	M. Weißpflog, G. Signorato, P. Schütz, B. Hankiewicz, V. Abetz	Hyperthermal-active and reprocessable composites based on magnetic nanoparticles in responsive polymer networks
9:10 – 9:30	D. Eberbeck, A. Knöchel, F. Mickoleit, D. Schüler, F. Wiekhorst	Alteration of MPS signal due to strong magnetic dipolar interactions within structurally different aggregates of magnetosomes
9:30 – 9:50	J. Landers, S. Salamon, H. Nádasi, A. Eremin, H. Wende	Ultralow-frequency AC-susceptometry for the analysis of complex fluids
9:50	Coffee break & Posters	
10:20	Session 5	
10:20 – 10:40	C. M. Huber, H. Ermert, I. Ullmann, M. Vossiek, C. Alexiou, S. Lyer	Ultrasound-based Methods for Imaging Superparamagnetic Iron Oxide Nanoparticles in Biomedical Applications
10.40 11.00		
10:40 – 11:00	M. Löffler, B. Kluwe, C. Fiedler, F. Wiekhorst, S. Dutz	harmoMPI: Phantoms for Harmonizing Magnetic Particle Imaging Across Global Scanner Systems
11:00 – 11:20		Magnetic Particle Imaging Across Global
	F. Wiekhorst, S. Dutz  B. Kluwe, L. Truttenbach, M. Löffler, U. Heinen, S. Dutz,	Magnetic Particle Imaging Across Global Scanner Systems Time-resolved magnetic particle spectroscopy
11:00 – 11:20	F. Wiekhorst, S. Dutz  B. Kluwe, L. Truttenbach, M. Löffler, U. Heinen, S. Dutz, F. Wiekhorst  F. Wolgast, R. Sack, Y. Wang, R. Amin, A. Lak, M. Schilling,	Magnetic Particle Imaging Across Global Scanner Systems Time-resolved magnetic particle spectroscopy to investigate aneurysm phantoms  Magnetic particle spectroscopy based
11:00 - 11:20 11:20 - 11:40	F. Wiekhorst, S. Dutz  B. Kluwe, L. Truttenbach, M. Löffler, U. Heinen, S. Dutz, F. Wiekhorst  F. Wolgast, R. Sack, Y. Wang, R. Amin, A. Lak, M. Schilling, T. Viereck  L. Wille, S. Lyer, G. Fischer,	Magnetic Particle Imaging Across Global Scanner Systems  Time-resolved magnetic particle spectroscopy to investigate aneurysm phantoms  Magnetic particle spectroscopy based biosensing for antigens and nucleic acids  Advection of superparamagnetic nanoparticles

# 21st FERROFLUIDWORKSHOP

# **Abstracts**



#### **Abstracts**

T. Becker, M. Reiche, L. Zentner	Multipolar magnetized magnetoactive elastomers for actuation and locomotion applications	9
S. Behrens	Hydrothermal synthesis of ferrite nanoparticles	11
O. Bilous, K.A. Okrugin, A. Lakkis, R. Richter, S.S. Kantorovich	Cracking the code of anomalous diffusion: simulation meets experiment in ferrogranular	12
D. Borin, S. Odenbach	Quasi-static shear of the structured magnetic suspensions	14
M.D. Contreras-Mateus, C. Friedrich, S. Odenbach	Mechanistic insights into the magnetorheology of ferrofluid emulsions with tunable nanoparticle localization: Droplet-dispersed nanoparticles	15
D. Eberbeck, A. Knöchel, F. Mickoleit, D. Schüler, F. Wiekhorst	Alteration of MPS signal due to strong magnetic dipolar interactions within structurally different aggregates of magnetosomes	17
C. Friedrich, M.D. Contreras- Mateus, S. Odenbach	Mechanistic insights into the magnetorheology of ferrofluid emulsions with tunable nanoparticle localization: Interfacial-active nanoparticles	19
Y. Gandhi, C. Holm, R. Weeber	Towards studying viscoelastic properties of soft magnetic materials using computer simulations	21
P. Gebhart, T. Wallmersperger	A unified variational-based modeling approach for soft and hard magnetic magneto-active polymers	22
K. Gerstenberger, G. K. Auernhammer	Cluster growth dynamics of nickel particles in viscoelastic matrices	23
Y. Hadadian, H. Kim, T. L. Cao, F. Wiekhorst, J. Yoon	Tumor-Size effects on magnetic hyperthermia efficiency: a simulation-guided in vivo validated study	24
M. Heiber, L. Fischer, H. Reinken, A. M. Menzel	Structuring magnetic elastomers	26
C. M. Huber, H. Ermert, I. Ullmann, M. Vossiek, C. Alexiou, S. Lyer	Ultrasound-based methods for imaging superparamagnetic iron oxide nanoparticles in biomedical applications	28
M. Kermarrec, Y. Suffren, P. Roquefort, S. Triki, T. Aubry	Viscoelasticity and Fluorescence of polymer-based magnetically switchable composite gels	30
B. Kluwe, L. Truttenbach, M. Löffler, U. Heinen, S. Dutz, F. Wiekhorst	Time-resolved magnetic particle spectroscopy to investigate aneurysm phantoms	32

A. Lakkis, M. Biersack, O. Bilous, S.S. Kantorovich, R. Richter	Two time scales drive the formation of transient networks in a ferrogranular experiment, and how to control them	34
J. Landers, S. Salamon, H. Nádasi, A. Eremin, H. Wende	Ultralow-frequency AC-susceptometry for the analysis of complex fluids	36
A. Leon-Cecilla,F. J. Vazquez- Perez, L. Álvarez de Cienfuegos, J. E. Martin, M. T. Lopez-Lopez	Chirality and instabilities in ferrogel torsional actuators under uniaxial magnetic Fields	37
M. Löffler, B. Kluwe, C. Fiedler, F. Wiekhorst, S. Dutz	harmoMPI: Phantoms for harmonizing magnetic particle imaging across global scanner systems	39
N. Magin, D. Borin, S. Odenbach	Influence of microstructure on magnetic properties of anisotropic magnetic elastomers	41
N. Magin, S. Odenbach	Application of the Scharr edge detection algorithm for microstructure assessment of magnetic composites	43
P. Patel, M. Saphiannikova, D. Romeis	Structured magneto-active elastomers under inclined fields and an approximation for the near-field effect in particle clusters	45
M. Raphael, A. M. Schmidt	Micromagnetic simulations of magneto-plasmonic nano- objects with tunable domain architectures	47
I. Rehberg, P. Blümler	Tailoring magnet setups for field homogeneity: an interactive GUI for design and exploration	49
Y. Remane, S. Hestermann, A. Wagner, M. Ehresmann, G. Herdrich	Ferrofluidic gears and seals for space applications	51
H. T. Roth, P. Gebhart, K. A. Kalina, T. Wallmersperger, M. Kästner	A data-driven decoupled multiscale scheme for the modeling of structured magnetorheological elastomers	53
R. Stephan, S. Ranoo, P. Kreissl, C. Pabshettiwar, J. Kubis, C. Holm, R. von Klitzing, A. Schmidt, R. Weeber	Exploring the mechanisms of particle-matrix coupling in magnetic gels by means of simulations and experiments	54
A. Weidner, M. Kurniawan, B. Hankiewicz, S. Dutz, A. Bund	Light induced coating of iron oxide nanoparticles with Cu and assessment of their catalytic activity for electrochemical reduction of NO3- to NH4+	55
M. Weißpflog, G. Signorato, P. Schütz, B. Hankiewicz, V. Abetz	Hyperthermal-active and reprocessable composites based on magnetic nanoparticles in responsive polymer networks	57
L. Wille, S. Lyer, G. Fischer, J. Kirchner	Advection of superparamagnetic nanoparticles in branched arterial networks	59

F. Wolgast, R. Sack, Y. Wang, R. Amin, A. Lak, M. Schilling, T. Viereck	Magnetic particle spectroscopy based biosensing for antigens and nucleic acids	61
K. Xiao, S. Lyer, J. Kirchner, G. Fischer	Molecular dynamics simulation of zipped chain-like agglomeration of the SPIONs	63

# Multipolar magnetized magnetoactive elastomers for actuation and locomotion applications

## T.I. Becker, M. Reiche, L. Zentner

Mechanics of Compliant Systems Group, Department of Mechanical Engineering, Technische Universität Ilmenau, 98684 Ilmenau, Germany

During the last three decades of intensive research on magnetoactive elastomers (MAEs) containing magnetically soft (MS) micron-sized particles, a growing interest has emerged in studying elastomers filled with magnetically hard (MH) particles. Due to their high coercivity and ability to retain significant remanence over time after magnetization, MH particles enable the synthesis of permanently magnetized MAEs that open new application opportunities as functional elements in advanced devices.

#### Shape-programmable bending

The form of a cantilever is one of the most common mechanical spring-mass systems, widely used for sensor elements and various technical applications. Cantilevers made of permanently magnetized MAEs offer advanced capabilities, as their deflection shape can be programmed by applying magnetic fields of low to moderate strength. The extent of this programmability depends on the type of material composition and the manner in which the cantilever is initially magnetized.

Figure 1: Bending shapes of the bipolar magnetized MAE cantilever containing only MH particles under gravity and under different vertically applied uniform magnetic fields  $H_0$ : solid lines – numerical calculations; markers – experimental measurements

We study, both theoretically and experimentally, the static bending deformation of horizontally fixed, initially straight MAE cantilevers with bipolar permanent magnetization along the length axis. The cantilevers are examined under the combined action of vertically applied gravity and uniform magnetic fields of varying strength (Figure 1). All four studied cantilevers have a fixed concentration of 10 vol.% MH particles, while the content of MS particles varies between 0 and 30 vol.%. In [1], we developed a magnetomechanical model based on finite-strain theory under the plane-stress approximation for a two-dimensional cantilever. The model demonstrates good agreement between numerically calculated and experimentally measured equilibrium shapes of the cantilevers up to moderate concentrations of MS particles.

The developed modeling framework requires only a few material parameters and can be extended without additional level of complexity on any multipole magnetized MAE beam of application interest. Figure 2 shows that the three-pole MAE

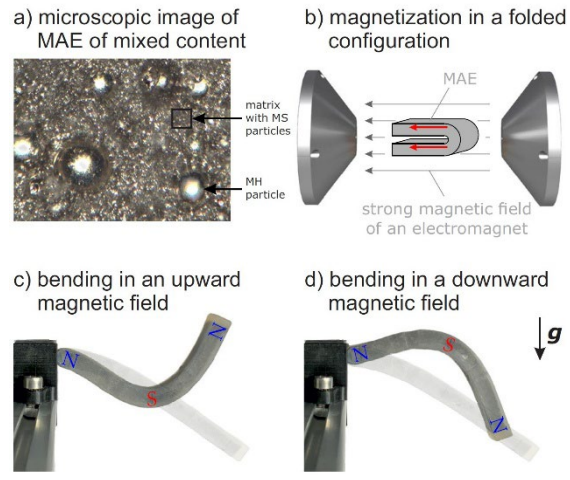


Figure 2: MAE cantilever of mixed content: a) microscopic image of the surface; b) imparting a three-pole magnetization profile; c) and d) bending in a vertical uniform magnetic field of 40 kA/m, compared to the original shape caused by gravity (transparent gray)

cantilever exhibits a more intricate bending shape in a uniform magnetic field compared to the two-pole cantilevers discussed above. This highlights the increased flexibility and programmability offered by higher-order magnetization patterns.

# Locomotion based on magnetic field-induced bending

On the basis of three-pole magnetized MAE beams of mixed (MH & MS) content, we develop different prototypes of vibration-driven locomotion systems for:

- one- and bi-directional locomotion along a straight or inclined line;
- vertical upward locomotion;
- planar locomotion on a horizontal surface,

featuring additional capabilities such as load carrying and step-like obstacle overcoming [2,3,4]. All our locomotion systems employ the motion principle of cyclic interplay between asymmetric friction forces due to bristles and inertial forces from magnetic field-induced bending vibrations of the magnetized MAE beam. Obliquely oriented bristles set a preferred motion direction. The use of a minimal number of actuators, implemented as alternately voltage-driven electromagnetic coils to generate MAE bending vibrations, is beneficial for soft robotics applications. Experiments reveal that the locomotion systems exhibit a strong resonance dependence of linear velocity on the excitation frequency of the integrated coil (Figure 3). The resonant motion is theoretically analyzed using a rigid-body model with two degrees of freedom, based on the principles of vibrational mechanics. An

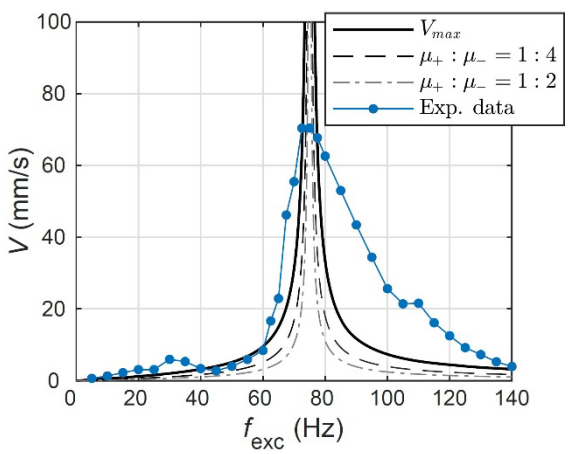


Figure 3: Linear velocity of the vibration-driven multipole MAE bristlebot as a function of the coil's excitation frequency (see [3] for details)

analytical expression is derived for the maximum velocity achievable under magnetic excitation, independent of the surface on which the rigid-body model moves. Furthermore, a design recommendation for the optimal bristle inclination angle is proposed, depending only on the length ratio of the model's rods.

The motion capture analysis performed for the planar locomotion system reveals that the excitation frequencies of two coils control the system velocity and the movement direction (Figure 4).

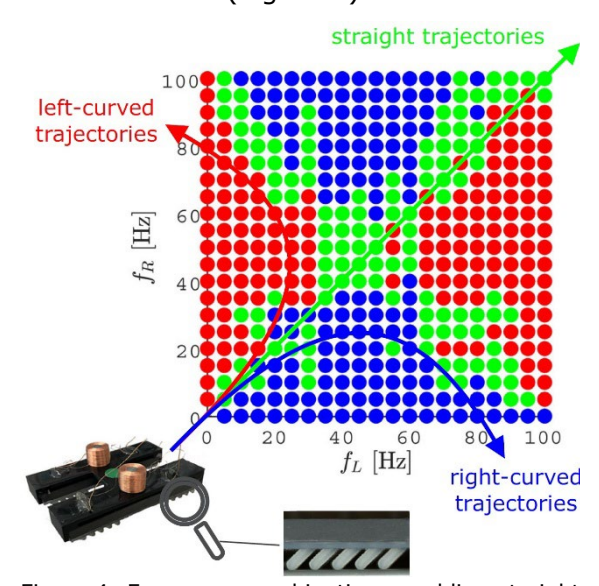


Figure 4: Frequency combinations enabling straight and curved trajectories of the vibration-driven multipole MAE bristlebot for planar locomotion

#### **Acknowledgments**

The study is funded by the Deutsche Forschungsgemeinschaft under the project BE 6553/2-1. The authors thank Dr. D. Borin for synthesizing the elastomers.

- [1] T.I. Becker, O.V. Stolbov, A.M. Biller, D.Yu. Borin, O.S. Stolbova, K. Zimmermann, Yu. L. Raikher. Shape-programmable cantilever made of a magnetoactive elastomer of mixed content. Smart Materials and Structures 31 (2022) 105021 (14pp).
- [2] M. Reiche, L. Zentner, D. Borin, F. Becker, T. Becker. Bi-directional vibration-driven mobile robots based on multipole magnetoactive elastomers. IEEE Robotics and Automation Letters 9(10) (2024) 8961-8966.
- [3] M. Reiche, L. Zentner, T.I. Becker. On the dynamics of the vibration-driven multipole magnetoactive bristlebot. Archive of Applied Mechanics 95 (2025) article number 160.
- 4] M. Reiche, L. Zentner, D. Borin, T.I. Becker. Mobile robot based on multipole magnetoactive elastomer for controllable planar locomotion. IEEE Transactions on Magnetics 61(6) (2025) 4900304.

## **Hydrothermal Synthesis of Ferrite Nanoparticles**

#### S. Behrens

Institut für Katalyseforschung und -technologie, Karlsruher Institut für Technologie

Due to their low cost, interesting magnetic properties and high stability in air, ferrite nanoparticles are of great interest for various biomedical and technical applications. In a new project, the continuous hydrothermal synthesis of highly crystalline ferrite nanoparticles (i.e., spinel-type  $MFe_2O_4$  and magnetoplumbite-type  $MFe_1O_1$ ) will be addressed.

Scandium-doped BaFe $_{12}O_{19}$  platelets were obtained by hydrothermal synthesis in an autoclave from the corresponding nitrate precursors and NaOH. The lateral dimensions depended on the reaction temperature and increased from 7 nm (160 °C) to 70 nm (240 °C) to 168 nm (340 °C) (Fig. 1a-d), while their height was about 5 nm [1, 2]. The easy axis is parallel to the crystallographic c axis and perpendicular to the platelet plane.

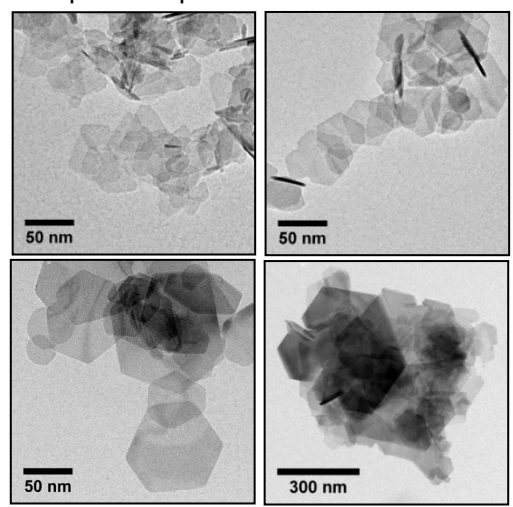


Fig. 1. Sc-doped BaFe<sub>12</sub>O<sub>19</sub> platelets synthesized in a batch autoclave (reaction temperature: a) 210 °C, b) 260 °C, c) 310 °C, und d) 340 °C) [1, 2].

Continuous flow processes, in which the reactants are continuously dosed and the process parameters are automatically controlled, are suitable for scaling the synthesis of clusters or nanoparticles to larger quantities [3, 4]. Continuous hydrothermal synthesis (CHTS) in near- or supercritical water enables the rapid and continuous production of highly crystalline particles in an environmentally friendly reaction medium. Supercritical water

(scH<sub>2</sub>O 374 °C, 22.1 MPa) has liquid-like densities and mass transfer properties that are intermediate between those of gases and liquids. Therefore, scH<sub>2</sub>O has many interesting properties with respect to particle synthesis. A CHTS plant designed by M. Türk [6] was recently set up and put into operation in our laboratories (Fig. 2). We successfully demonstrated the synthesis of CeO<sub>2</sub> particles (300°C, 400 bar) using SEM and online monitoring of nanoparticle formation by dynamic light scattering.



Fig. 2. Batch autoclave and plant for continuous hydrothermal synthesis in scH<sub>2</sub>O.

Future work will address the continuous flow hydrothermal synthesis of spineland magentoplumbite-type magnetic nanoparticles in supercritical water for use in 3D-printed polymer composites.

#### **Acknowledgments**

We acknowledge funding from the German Science Foundation (project BE 2243/10-1).

- [1] M. Hähsler, I. Appel, S. Behrens, Magnetic hybrid materials in liquid crystals, Phys. Sci. Rev., (2020), De Gruyter, DOI: 10.1515/psr-2019-0090.
- [2] M. Hähsler, M. Zimmermann, S. Heißler, S. Behrens, Sc-doped barium hexaferrite nano-discs: Tuning morphology and magnetic properties, J. Magn. Magn. Mater., 500, 166349 (2020), DOI:1016/j.jmmm.2019.166349.
- [3] C. Schmitt, N. Da Roit, M. Neumaier, C. Maliakkal, D. Wang, T. Henrich, C. Kübel, M. Kappes, S. Behrens, Nanoscale Adv., 6, 2459-2468 (2024), DOI: 10.1039/d4na00074a
- [5] C. Schmitt, S. Behrens, Patent Pending, EP4406642A1 (2024).
- [6] C. Schüßler, M. Zürn, T. Hanemann, M. Türk, Chem. Ing. Tech., 94, 3, 281–288 (2022), DOI: 10.1002/cite.202100146

# Cracking the Code of Anomalous Diffusion: Simulation Meets Experiment in Ferrogranular

O. Bilous<sup>1</sup>, Kirill A. Okrugin<sup>1</sup>, A. Lakkis<sup>2</sup>, R. Richter<sup>2</sup>, S.S. Kantorovich<sup>1</sup>

<sup>1</sup>University of Vienna, Kolingasse 14-16, Vienna, 1090 (Austria) <sup>2</sup>Experimentalphysik V, Universtät Bayreuth, 95440 Bayreuth (Germany)

#### Introduction

Anomalous diffusion in driven granular suspensions defies classical Brownian paradigms, as evidenced by recent studies of vibrated granular monolayers and active particulate systems [1-3]. In ferrogranular layers, which couple magnetic, hydrodynamic, and contact forces, transport becomes highly nontrivial with subdiffusive transport and hopping dynamics [4, 5]. While qualitative models exist, no study to date has achieved a quantitatively accurate match to experimental diffusion metrics in such strongly interacting, driven systems. We investigate this dynamic using both theoretical [4, 5] and experimental [4-6] methods. This investigation was conducted with and without a magnetic field applied perpendicular to the layer. We focus on the ferrogranulate system, which contains different total area fractions and changes the concentration of magnetic and steel beads.

#### **Methods**

We consider a quasi-two-dimensional layer of millimetre-sized magnetic  $\sigma_m$ = 3 and glass  $\sigma_a$ = 4 spheres. The spheres are modeled with combined Stockmayer and Weeks-Chandler-Andersen potentials, while magnetic interactions are captured via central dipoles. Thermal fluctuations are simulated through effective shaking amplitudes. Leveraging simulation with ESPResSo 4.1.4 alongside experiments, we evaluate the interplay of particle arrangements, clustering, and diffusion properties, expanding on previous work that highlighted subdiffusive particle dynamics in vibrated films and magnetic systems [4-6].

Both experiments and simulations cover varying particle area fractions  $\phi g$ ,  $\phi m$  and three magnetic inductions  $B^* = 0.0$ , 0.5, 1.0.

#### **Numerical results**

Key metrics such as the diffusion exponent an and the normalized diffusion coefficient D/D0 reveal critical insights into ferrogranular dynamics:

- Diffusion exponent a (Fig. 1) from mean square displacement (MSD).
- Effective diffusion coefficient  $D/D_0$ , normalized by the single-particle diffusion coefficient  $D_0 = k_BT/\gamma$ .

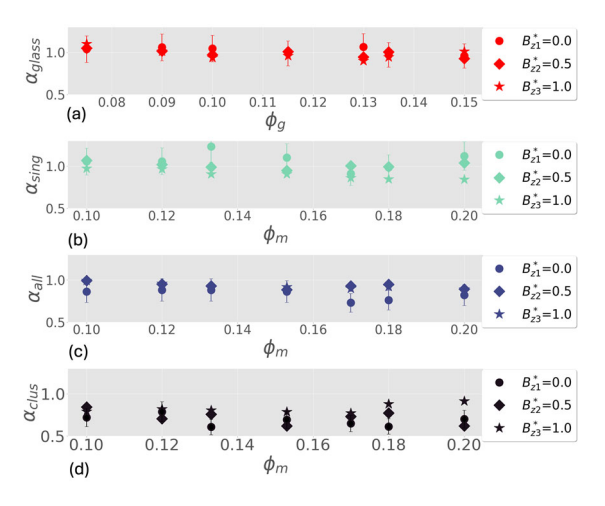


**Figure 1:** Diffusion exponent a versus particle area fraction for glass (a), single magnetic (b), all magnetic (c), and clustered particles (d). Circular, diamond, and star markers correspond to B\* = 0.0, 0.5, 1.0.

As we can see from Figure 1 the diffusion exponent,  $a_n$ , indicate for: 1) **Glass particles (Fig. 1a):**  $a \approx 1$  across all area fractions and magnetic inductions, indicating normal diffusion; 2) **Single magnetic particles (Fig. 1b):** a remains near unity, showing weak dependence on  $\phi_m$  or  $B^*$ ; 3) All magnetic particles (Fig. 1c): a < 1 at high  $\phi_m$  and low  $B^*$ , indicating cluster-mediated subdiffusion. 4) **Clustered magnetic particles (Fig.** 

**1d):** Strongly subdiffusive at high  $\phi_m$ ; effect diminishes at higher B\*.

Figure 2 shows the effective diffusion coefficient,  $D/D_0$ , normalized by single-particle diffusion, highlighting the role of area fraction and magnetic induction: 1) Glass particles maintain nearly constant  $D/D_0$ . 2) Clustered particles exhibit reduced mobility due to crowding and magnetic interactions. 3) Single magnetic particles show enhanced  $D/D_0$  at high  $B^*$ , reflecting dipolar repulsion. 4) Increasing  $\phi_m$  suppresses diffusion for clustered particles, with the effect amplified at intermediate and high  $B^*$ .

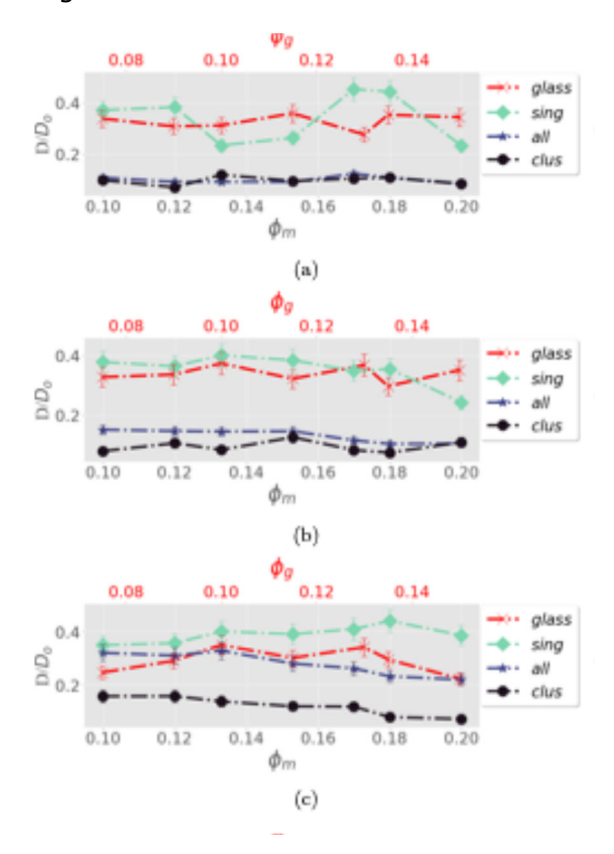


**Figure 2:** Effective diffusion coefficient  $D/D_0$  as a function of  $\phi_g$  (top axis) and  $\phi_m$  (bottom axis) for three magnetic inductions: (a)  $B^* = 0.0$ , (b)  $B^* = 0.5$ , (c)  $B^* = 1.0$ .

These results reveal a competition between magnetic clustering and field-induced dispersion, modulated by particle area fractions and supplementing theoretical predictions [4, 5]. Increasing magnetic induction promotes mobility for single particles while constraining clustered particles, capturing the complex interplay governing diffusion in ferrogranulate systems.

This study demonstrates that anomalous diffusion in ferrogranulates results from the interplay between magnetic clustering and field-induced particle dispersion, both governed by area fraction and magnetic induction. By combining experimental and theoretical analyses, it provides a physics-based framework to unravel transport phenomena in driven granular systems with long-range interactions.

#### **Acknowledgements**

The authors acknowledge financial support for the German-Austrian project "Coarsening dynamics of ferromagnetic granular networks: experiment and simulation" through Ri 1054/7-1 and I5160 FWF.

- [1] Bechinger, C., Di Leonardo, R., Löwen, H., Reichhardt, C., Volpe, G., Volpe, G., Rev. Mod. Phys. 88 (2016) 045006.
- [2] Aranson, I.S., Tsimring, L.S., Rev. Mod. Phys. 78 (2006) 641.
- [3] Ramaswamy, S., Annu. Rev. Condens. Matter Phys. 1 (2010) 323.
- [4] Kögel A., Sanchez P., Maretzki R., Dumont T., Pyanzina E. S., Kantorovich, S.S., and Richter R.. Soft Matter, 14 (2018) 1001.
- [5] Biersack, M., Lakkis, A., Richter, R., Bilous, O., Sanchez, P.A., Kantorovich, S.S., Phys. Rev. E 108 (2023) 054905.
- [6] Lakkis A., Biersack M., Bilous O., Kantorovich S.S., Richter R., Soft Matter (2025) submitted. For movies of the experiment cf. https://doi.org/10.17605/OSF.IO/6S4FM.

# Quasi-static shear of structured magnetic suspensions

#### D. Borin, S. Odenbach

Technische Universität Dresden, 01069 Dresden, Germany

The standard method for studying the rheological behaviour of magnetorheological (MR) suspensions is rotational or oscillatory rheometry using a plate-plate geometry. To avoid the influence of magnetostatic forces on the rheometer rotor, non-magnetic plate-plate configurations, in particular those made of titanium, are typically used in laboratory experiments. However, in the case of a non-magnetic surface, smooth measured yield of the magnetic suspension is associated with the slippage of particle structures on the upper plate of the rheometer, rather than with the breakup of aggregates. Moreover, in MR devices, the suspension is usually in contact with ferromagnetic material. Accordingly, for the correct characterisation of the behaviour of the MR suspension in terms of its potential application, the working geometry of the rheometer must correspond to the conditions in which the suspension is exposed into the MR de-Replacing the standard nonmagnetic plate-plate geometry with ferromagnetic steel plates has been done in a few studies before and a significant increase in the transmitted shear stress was demonstrated using conventional flow curve measurements, see e.g. [1,2]. In this study, we examine the influence of the magnetic properties of the rheometer plate surfaces on the quasi-static deformation of a structured magnetic suspension. Quasi-static shear allows us to obtain values of the static yield stress of the MR suspension and make observations about the possible physical mechanisms of interaction between magnetic particle aggregates and the surface of the measuring geometry, as well as the mechanisms of particle structure fracture under the action of the applied shear load. In our investigation, we take into account the morphology of magnetic particle aggregates formed as a result of structuring. Known researches consider highly filled suspensions characterised by the formation of network-like clusters, but not separate chain aggregates. Based on the data of microstructural studies, we vary the concentration of magnetic particles in order to analyse the rheological behaviour of structures of diverse morphology. Figure 1 demonstrates an example of the different response of a structured MR suspension with chain-like aggregates to an applied quasi-static shear load.

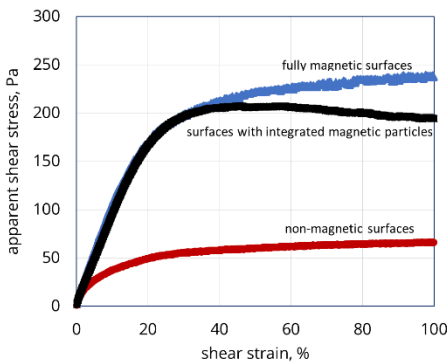


**Figure 1** Response of a structured MR suspension (1 vol.%, 250 mT) to an applied quasi-static shear load

In addition to the fundamental importance, the expected results are essential from an applied point of view for the choice of MR suspension and operating conditions for devices using magnetic control of the static yield stress. This is particularly the case for MR disc brakes or MR dampers with MR valve operating in a shear mode. Preliminary results of our research will be presented at the workshop.

#### **Acknowledgments**

The financial support by German Federal Ministry of Education and Research within the KMU-innovativ - collaborative project "COGNAC" under contract number 13GW0632D is gratefully acknowledged.

- [1] Laun et al 2011, Rheo Acta 50, 141-157
- [2] Jonkkari et al 2012, Smart Mater. Struct. 21, 075030

# Mechanistic insights into the magnetorheology of ferrofluid emulsions with tunable nanoparticle localization: Droplet-dispersed nanoparticles

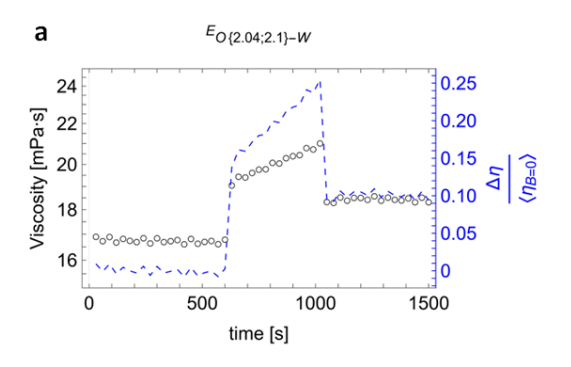
M.D. Contreras-Mateus, C. Friedrich, S. Odenbach

Chair of Magnetofluiddynamics, Measuring and Automation Technology, TU Dresden, 01069 Dresden, Germany

Magnetorheological (MR) fluids are fieldresponsive materials that undergo millisecond-scale, reversible transitions from a liquid to a semi-solid state upon the application of an external magnetic stimulus, a phenomenon known as MR effect [1]. At a fundamental level, dominant phenomena involve changes in the viscosity spanning several orders of magnitude (occurring within 10-20 ms) [2, 3], the development of yield stresses (up to 100 kPa) [2], and the enhancement of viscoelastic properties [4]. The underlying mechanism lies in the induction of strong magnetostatic (dipole-dipole) interactions between particles, leading to the subsequent formation of field-aligned columnar/network structures that, simultaneously, obstruct the flow [5]. Owing to these properties, MR fluids have demonstrated extensive applicability across various fields, including aerospace, ultra-fine processing, civil engineering, fluid mechanics, targeted drug delivery, among others [4, 6]. However, several physicochemical challenges continue to constrain the performance of MR fluids, with particle sedimentation, arising from inherent density differences between the dispersed particles and the carrier fluid, constituting the most critical and irreversible limitation [3, 6]. This heterogeneous particle distribution significantly accelerates the degradation of magnetorheological responsiveness. Accordingly, plenty of strategies have been proposed to enhance stability, mainly focused on modifications of the material composition, or the design of devices incorporating remixing or self-homogenization functions during operation [6]. Although these strategies are effective, they can only temporarily inhibit sedimentation; the inherent thermodynamic instability of MR fluids, combined with the remnant magnetization of the particles, ultimately leads to particle settling over time.

The above prompts a fundamental question regarding alternative design strategies focused on the development of magnetic fluid systems that exhibit significant magnetorheological responses, but using colloidal nanoparticles, which inherently ensure long-term stability by minimizing gravitational separation and aggregation through sustained Brownian motion. In this context, Bibette [7] and Chernobai et al.[8] introduced a novel approach by formulating biphasic systems, in which ferrofluid droplets are dispersed within a non-magnetic and immiscible carrier liguid, commonly known as ferrofluid emulsions. The main advantage of this configuration lies in the close density parity between the ferrofluid and the surrounding liquid, which reduces sedimentation rates by suppressing buoyancy-driven motion while maintaining a dense particle concentration and a narrow nanoparticle size distribution. While this concept has been primarily investigated within magneto-optics, essentially focusing on the interplay between magneto-optical effects and selfassembly dynamics [9], its potential for inducing strong MR effects remains largely unexplored, particularly regarding the development of stable formulations capable of producing reversible and longlasting functional responses. In a previous research [10], we demonstrated a relative increase in viscosity of up to 17-fold in oilbased ferrofluid emulsions (with nanoparticle volumetric fractions  $\phi \sim 0.1\%$ ) stabilized using hexadecylpyridinium(droplet size  $\sim$ 3-4 µm), when exposed to a linearly increasing magnetic field of up  $796.73 \, \text{mT}$  at a shear rate of  $1 \, \text{s}^{-1}$ . The observed magnetoviscous effect remained reproducible for up to one year after preparation. In this research, an innovative formulation procedure for highly stable ferrofluid emulsions was proposed using nonionic surfactant mixtures of Span 80/Tween 80, considering their multiple benefits, which include enhanced stability and formulation flexibility. Moreover, as an initial nanoparticle localization strategy, highly hydrophobic iron oxide nanoparticles were used to improve their dispersibility within the oil droplets and reduce migration to the interface. As a result, a system predominantly composed of surfactant-covered droplets was obtained. Thus, under zero-field conditions, tensoactive dynamics regulate local interfacial tension and induce Marangoni stress that counteract deformation. The oilbased ferrofluid emulsions were prepared using nanoparticle volumetric concentrations  $\phi$ <0.2%, and the droplet size distribution was reduced and optimized to reach values in the order of  $\sim 1 \mu m$ . The rheological and magnetorheological properties of the formulated emulsions were characterized using an Anton Paar MCR 502 rheometer coupled to a Magneto-Rheological Device (MRD170/1T), generating magnetic flux densities (B) of up to 1 T, which were oriented perpendicular to the flow direction.

The formation of highly stable ferrofluid was demonstrated, emulsions creaming completely suppressed. Likewise, under an external magnetic field, it was proven that the formation of nanoparticle aggregates within the droplets may have perturbed interfacial tension gradients through localized changes in surfactant distribution, thereby modifying the balance of Marangoni stress. This effect became more pronounced as surfactant concentration decreased. A critical threshold was identified that enabled externally controlled droplet deformation, potentially leading to the development of droplet microscopic anisotropic structures that significantly modified the magnetorheological response. Particularly, it was proven that reducing surfactant concentration significantly increased the observed changes in viscosity and exhibited a time-dependent magnetoviscous effect, as shown in Figure 1.



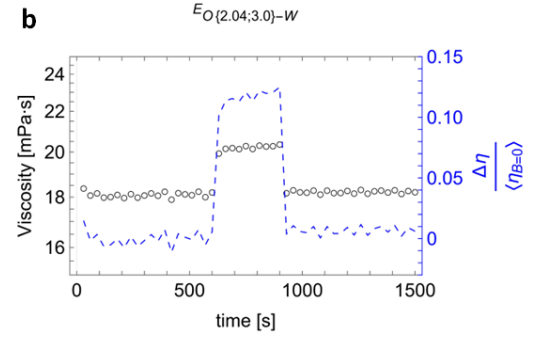


**Figure 1** Transient viscosity curves at  $\dot{\gamma}=10\,s^{-1}$  of (a)  $E_{O\{2.04;2.1\}-W}$ , where 2.04 and 2.1 refer to the  $\frac{wL}{vol}$  % of nanoparticles and Span 80/Tween 80 in the oil phase, respectively, and (b)  $E_{O\{2.04;3.0\}-W}$  samples. The test was divided into three intervals: (i) in the absence of a magnetic field, (ii) under the effect of a perpendicular magnetic flux density of 347.8 mT for 5 min, and (iii) after removing the magnetic field.

- [1] Rabinow J. Electrical Engineering 1948;67(12):1167-.
- [2] Bossis G, Lacis S, Meunier A, et al. Journal of Magnetism and Magnetic Materials 2002:252:224-8.
- [3] Ashtiani M, Hashemabadi SH, Ghaffari A. Journal of Magnetism and Magnetic Materials 2015;374:716-30.
- [4] Socoliuc V, Avdeev MV, Kuncser V, et al. Nanoscale 2022;14(13):4786-886.
- [5] López-López MT, Gómez-Ramírez A, Rodríguez-Arco L, et al. Langmuir 2012;28(15):6232-45.
- [6] Zhu T, Wu T, Gao Z, et al. International Journal of Mechanical Sciences 2024;266:108980.
- [7] Bibette J. Journal of Magnetism and Magnetic Materials 1993;122(1):37-41.
- [8] Chernobai VA, Yarmol'chik YP. Magnetohydrodynamics 1993;28(2):130-4.
- [9] Ivey M, Liu J, Zhu Y, et al. Physical Review E 2000;63(1):011403.
- [10] Gómez-Sanabria V, Contreras-Mateus MD, Chaves-Guerrero A, et al. Physics of Fluids 2024;36(12):123107.

# Alteration of MPS signal due to strong magnetic dipolar interactions within structurally different aggregates of magnetosomes

D. Eberbeck<sup>1</sup>, A. Knöchel<sup>2</sup>, F. Mickoleit<sup>2</sup>, D. Schüler<sup>2</sup>, F. Wiekhorst<sup>1</sup>

Magnetosomes are a novel class of MNP naturally formed by magnetotactic bacteria as geomagnetic sensors. Purified magnetosomes are very suited as tracers for MPI (Magnetic Particle Imaging) because of their large core size naturally being in the range of the prognosed optimum of 30 nm. The corresponding large magnetic moment may lead to high dipol-dipole interaction (DDI) energy with an interaction parameter  $\lambda_d \approx 20 ... 30$  at contact distance of 30 nm cores promoting the aggregation of these MNP. The, in such clusters a fluxclosure might occur strongly reducing the dynamic magnetic response measurable by, e.g. MPS (Magnetic Particle Spectroscopy) [1].

In this study we present how the MPS signals of magnetosomes (purified from the magnetic bacterium *Magnetospirillum gryphiswaldense*,  $\bar{d}=40~\rm nm$ ,  $\sigma_{\rm d}=0.13$ , coated with a proteinaceous lipid bilayer membrane with a thickness of ca. 6-8 nm [2]) behave in dependence on MNP-concentration and the matrix where they were embedded into. Then we quantify the corresponding short-range structure by means of SAXS (Small Angle X-Ray Scattering) data to explain the magnetic behaviour.

For iron concentrations lower than  $c_{\rm Fe} =$ 0.3 mM we measured MPS-spectra of typical shape for non-interacting MNP. While for classical MPI-suitable MNP-systems, like for example Resovist®, the MPS-amplitudes will be attenuated at high concentrations, we here observe with increasing MNP-concentration first a structuring of the spectra and later a further restructuring and also an increase of the specific MPS-amplitudes (Figure 1). Obviously, there appear MNP-arrangements where DDI induces a rather like-ferromagnetic short-range order of the moments. Such an order is evident for chains of MNP here generated by immobilization of the MNP in

a polyacrylamide (PAam) matrix under an external field of  $B_{\rm im}=1\,\rm T$ . These structures enhance the MPS spectra strongly although the immobilization in zero field usually diminish the amplitudes, here by 50% at k=3 for PAam and even by a factor of 1/3 in gelatine matrix (Figure 1).

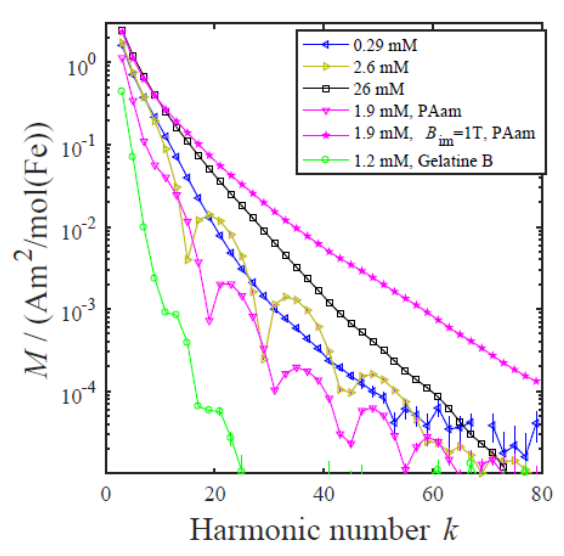


**Figure 1**: MPS-data, amplitudes of higher odd harmonics of magnetisation at the indicated different iron concentrations and embedded within different matrices.  $B_{\rm im}$ : external field while immobilisation.

In order to elucidate this behaviour, we next investigated the structure of possible aggregates with SAXS. While the PDDF (Pair Distance Distribution Function) of the most diluted sample does not show any spatial correlation of the MNP, second maximum comes up which shifts towards smaller distances r with increasing concentration. From the nearest neighbour distances  $r_{\rm nn}$  (maximum position of PDDF) we inferred to the interaction parameter which increases with concentration up to  $\lambda_d=20$  but attains 43 for MNP embedded in gelatine (Table 1).

<sup>&</sup>lt;sup>1</sup> Physikalisch-Technische Bundesanstalt, Berlin, Germany

<sup>&</sup>lt;sup>2</sup> Dept. of Microbiology, University of Bayreuth, Germany

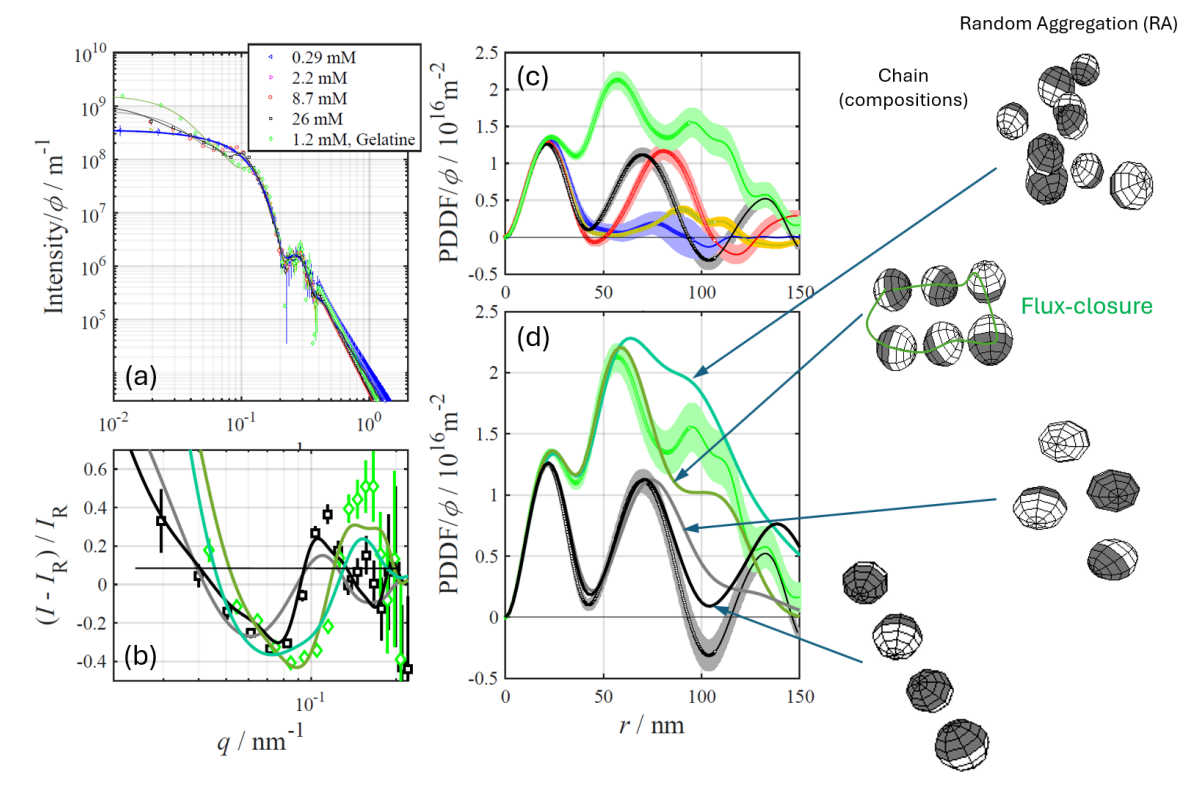


**Figure 2:** (a) SAXS-intensities after background correction and desmearing, normalized to the magnetite volume fraction,  $\phi$ , with (b) its normalised differences where the fit curve of the first data set (blue line) serves as reference  $I_R$ . (c,d) Pair distance distribution function (PDDF). The lighter-colored band around PDDF represents its uncertainty however disregarding the effect of imperfection of the model for the extrapolation according to Guinier law. PDDF resulting from extrapolated values are drawn with a thinner line instead of symbols. Accordingly, the resolution limit amounts to about 100 nm. Thicker lines in (b,d) and color-matching thin lines in (a): calculations of the depicted models of oligomers.

**Table 1**: Interaction parameter  $\lambda_d$  corresponding to the nearest neighbour distances  $r_{nn}$  of the different samples.

C Fe	r <sub>nn</sub>	$\lambda_{d}$	
mM	nm		
2.2	94 ± 3	8 ± 1	
8.7	$83 \pm 2$	11 ± 1	
25.9	68 ± 1	20 ± 2	
in Gelatine			
1.2	53 ± 1	$43 \pm 3$	

Using  $r_{\rm nn}$  we calculated the SAXS curves with oligomers created by random aggregation (RA) and with chains and aggregated small chains (Figure 2). The chain-like models match significantly better the data (Figure 2b,d). Hence, we hypothesise that in the dispersions with increasing concentration a net-like structure of chains occurs which prefers a local parallel orientation of the MNP's moments enhancing the MPS-amplitudes. The embedment within gelatine leads to clusters with

a reduced  $r_{\rm nn}$  where local flux-closure may take place which reduces the MPS-amplitudes strongly (Figure 1).

It was shown that the change of the arrangement of magnetosomes evoke large changes of the dynamic magnetic response making these MNP suitable for functional MPI or other magnetic sensor applications, for example within material monitoring.

- [1] A. Remmo et al., ACS Appl. Nano Mater., 2024.
- [2] D. Schüler et al., Nat. Rev. Microbiology, 2025, in press

# Mechanistic insights into the magnetorheology of ferrofluid emulsions with tunable nanoparticle localization: Interfacial-active nanoparticles

C. Friedrich, M.D. Contreras-Mateus, S. Odenbach

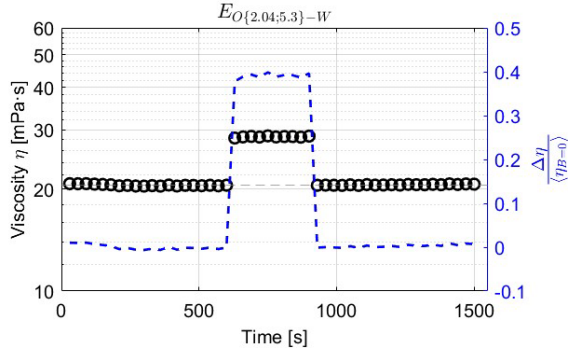
Chair of Magnetofluiddynamics, Measuring and Automation Technology, TU Dresden, 01069 Dresden, Germany

Magnetorheological (MR) fluids are suspensions of ferro- or ferrimagnetic mesoscale particles (1-10 µm) dispersed in a liquid carrier. Upon exposure to a magnetic field, these fluids exhibit rapid (millisecond-scale) and reversible increases in apparent viscosity and yield stress, resulting from field-induced particle structuring (1). These properties enable applications such as adaptive damping, controllable brakes, or seismic vibration control. However, a fundamental drawback of MR fluids lies in their thermodynamic instability. The relatively large and dense particles are prone to sedimentation, undermining the homogeneity and long-term functionality of these fluids. Despite mitigation strategies such as particle surface functionalization, the addition of thickeners, or the integration of viscoelastic (or viscoplastic) carrier liquids, sedimentation constitutes a significant and persistent challenge (1-3).

To overcome these stability limitations, strategies from ferrofluids composed of nano-scale magnetic colloidal particles can be adopted. While such systems typically exhibit lower magnetorheological responses than MR fluids, their superior colloidal stability offers a promising pathway. Magnetically responsive emulsions, in which magnetic nanoparticles are confined within the dispersed phase stabilized by surfactants or by the combined action of surfactants and nanoparticles, represent a hybrid strategy that couples high colloidal stability with tunable, field-induced viscosity. Previous studies by Bibette (4) and Chernobai et al. (5) demonstrated that ferrofluid emulsions can reach long-term stability and markedly reduced sedimentation rates, primarily due to a high degree of density matching between the ferrofluid phase and the surrounding liquid. Despite these promising stability characteristics, their capability to generate strong MR effects has not yet been systematically explored.

Building on this research gap, Gómez-Sanabria et al. (6) demonstrated that long-term stable, magneto-responsive oil-in-water emulsions can be formulated by dispersing magnetic nanoparticles within the oil phase and stabilizing the system through appropriate surfactant combinations, using hexadecylpyridinium. Based on this research, the present study investigates a new formulation strategy employing a mixture of the non-ionic surfactants Tween 80 and Span 80, which offers increased flexibility in tailoring interfacial properties and improved emulsion stability. Furthermore, the approach explores the use of amphiphilic-functionalized iron oxide nanoparticles to promote their preferential localization at the oilwater interface, thereby potentially enhancing both the structural stability and the magnetorheological responsiveness of the emulsions. Furthermore, the droplets in the emulsions are expected to exhibit superparamagnetic behavior, noscale iron oxide particles undergo rapid thermal fluctuations of their magnetic moments, preventing permanent magnetization and enabling reversible response to an applied magnetic field. As shown in Figure 1, transient viscosity measurements at a constant shear rate of 10 s<sup>-1</sup> using an Anton Paar MCR 502 rheometer equipped with a magneto-rheological device (MRD170/1T) revealed that, under a perpendicular pulse of magnetic field of 347.8 mT, the ferrofluid emulsion wt./vol.% nanoparticles, wt./vol.% Span 80/Tween 80 in oil) exhibited an approximately 40% time-independent increase in viscosity, demonstrating a significant magnetorheological response.

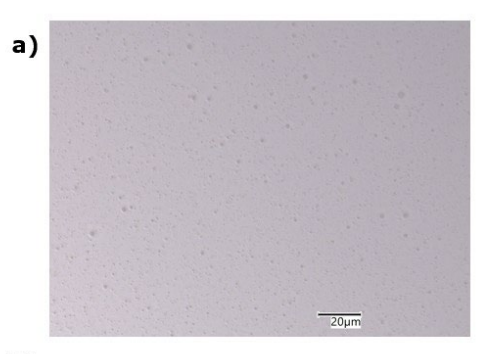
This behavior can be attributed to the preferential localization of the nanoparticles at the oil-water interface, which causes the droplets to behave like rigid spheres by enhancing interfacial elasticity and mechanical resistance to deformation. In the presence of an external magnetic field, the magnetic dipoles at the surfaces of the droplets align, leading to chain formation or agglomeration and, thereby, strengthening the macroscopic magnetorheological effect.



**Figure 1:** Time-dependent viscosity of the ferrofluid emulsion (2.04 wt./vol.% nanoparticles, 5.3 wt./vol.% Span 80/Tween 80 in oil) at  $\dot{\gamma}=10~s^{-1}$ . The test was divided into three intervals: (i) in the absence of a magnetic field, (ii) under the effect of a perpendicular magnetic flux density of 347.8 mT for 5 min, and (iii) after removing the magnetic field.

Equally important, the droplet size distribution in emulsions strongly influences their mechanical stability and MR performance. To quantify this effect, droplet sizes were measured using optical microscopy, employing a sandwich configuration with partial coaxial illumination. Images acquired with a KEYENCE Digital Microscope VHX-7000 were processed using an edge-detection algorithm based on a Sobel filter applied in eight directions, enabling precise determination of droplet size distribution. As summarized in Figure 2, the results provided quantitative insight into the emulsion microstructure, showing that most droplets are approximately 1-2 µm in diameter. Smaller droplets may be present but remain undetected due to the optical resolution limits of the microscope. This limitation is not critical, as larger droplets dominate the volume fraction and, therefore, exert a greater influence on the macroscopic properties of the emulsion.

Collectively, these findings indicate that the combined interfacial activity of surfactants and nanoparticles exhibits a strong, reversible, and time-independent magnetorheological response, while maintaining long-term structural stability. The above highlights the potential of ferrofluid emulsions to provide a foundation for further studies aimed at optimizing droplet size distribution, surfactant combinations, and nanoparticle surface nature, to enhance both stability and magnetorheological performance.



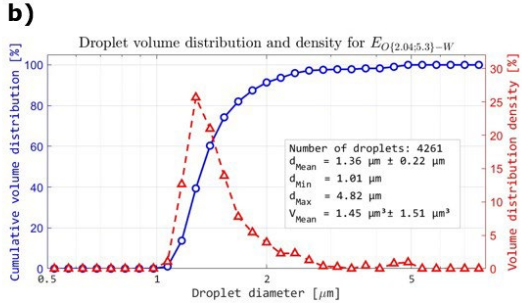


**Figure 2:** (a) Optical micrograph of the magnetizable oil-in-water emulsion  $E_{O\{2.04;5.3\}-W}$  showing a homogeneous droplet dispersion. Scale bar: 20 µm. (b) Droplet size distribution and cumulative volume distribution determined from image analysis

- [1] Rabinow J. The magnetic fluid clutch. Electrical Engineering. 1948;67(12):1167–1167.
- [2] Bossis G, Lacis S, Meunier A, Volkova O. Magnetorheological fluids. Journal of Magnetism and Magnetic Materials. 2002;252:224–8.
- [3] Choi SB. Sedimentation stability of magnetorheological fluids: the state of the art and challenging issues. Micromachines. 2022;13(11):1904.
- [4] Bibette J. Monodisperse ferrofluid emulsions. Journal of Magnetism and Magnetic Materials. 1993;122(1):37–41.
- [5] Chernobai VA, Yarmol'chik YuP. The effective viscosity of magnetofluid emulsions. Magnetohydrodynamics. 2025 Jan;28(2).
- [6] Gómez-Sanabria V, Contreras-Mateus MD, Chaves-Guerrero A, Mercado R, Nassar NN (نشات). Rheology and magnetorheology of ferrofluid emulsions: Insights into formulation and stability. Physics of Fluids. 2024 Dec;36(12):123107.

# Towards studying viscoelastic properties of soft magnetic materials using computer simulations

Y. Gandhi, C. Holm, R. Weeber

Institute for Computational Physics, University of Stuttgart (ygandhi@icp.uni-stuttgart.de)

Magnetic gels are of particular interest due to their combination of magnetic and viscoelastic properties. The viscoelastic properties are determined by both the underlying hydrogel and the embedded magnetic nanoparticles, as well as their interactions.

There are two principal approaches to accessing viscoelastic properties: first, through nano-rheology, by applying an AC magnetic field and measuring the magnetic response, with the Gemant–Di-Marzio–Bishop<sup>[1,2]</sup> theory subsequently used to infer local viscoelastic properties; and second, by applying shear to the sample and observing the macroscopic stress–strain relation. In principle, these techniques are available in both experiments and simulations; however, the latter involves a very high computational effort.

Here, we explore the viscoelasticity of hydrogels via simulations using the ES-PResSo<sup>[3]</sup> simulation package. We employ a coarse-grained model that resolves the polymer network as bead-spring chains, with hydrodynamic interactions and thermal fluctuations modeled via momentum-conserving dissipative particle dynamics.

Our initial aim is to parametrize the model to reproduce key experimentally observed features of hydrogels. In the future, magnetic nanoparticles will be incorporated to study the influence of the constraints they impose on local deformation, as well as the role of dipole–dipole interactions.

#### **Acknowledgments**

This project is funded by the Cluster of Excellence EXC 2075, SimTech.

- [1] A. Gemant. (1935). The conception of a complex viscosity and its application to dielectrics. Transactions of the Faraday Society, 31, 1582–1582. https://doi.org/10.1039/tf9353101582
- [2] DiMarzio, E. A., & Bishop, M. (1974). Connection between the macroscopic electric and mechanical susceptibilities. *The Journal of Chemical Physics*, 60(10), 3802–3811. https://doi.org/10.1063/1.1680822
- [3] espressomd. (2024, May 22). GitHub espressomd/espresso: The ESPResSo package. GitHub. https://github.com/espressomd/espresso

# A unified variational-based modeling approach for soft and hard magnetic magneto-active polymers

## Philipp Gebhart, Thomas Wallmersperger

Institute of Solid Mechanics, TU Dresden, 01062 Dresden, Germany

Over the past two decades, there has been a growing interest in both the theoretical modeling and experimental investigation of field-responsive functional composite materials. Among these, magneto-active polymers (MAPs) emerged as a particularly fascinating and versatile class of smart materials. These composites consist of a polymer-based matrix with dispersed magnetizable particles. Owing to this specific microstructural composition, MAPs possess the remarkable ability to undergo large deformation and alter their material properties in direct response to applied magnetic fields. The nature of their response is largely governed by the magnetic characteristics of the embedded ferromagnetic particles. Accordingly, MAP composites are typically classified into two principal categories: (i) soft magnetic MAPs and (ii) hard magnetic MAPs.

Soft MAPs comprising magnetically soft particles, e.g., carbonyl iron, exhibit negligible hysteresis loss and demagnetize completely after the removal of the external magnetic field. This in consequence leads to reversible deformation mechanisms. Conversely, NdFeB particle-filled hard MAPs exhibit distinct nonlinear, dissipative material behavior, such as the characteristic magnetic and "butterfly" field-induced strain hysteresis. The distinctive behaviors of both soft magnetic and hard magnetic MAPs — coupled with the high degree of tunability in their properties achievable through tailored fabrication techniques — render them highly promising candidates for a broad range of engineering applications.

In the present work, we present a comprehensive microstructural guided modeling framework that allows to describe soft magnetic and hard magnetic MAPs in an elegant unifying manner. We outline ingredients of the constitutive theory based on the framework of generalized standard materials, that necessitates suitable definitions of (i) the total energy density function and (ii) the dissipation potential. Key idea of the constitutive approach is an additive split of the material part of the total energy density function into three contributions associated with (i) an elastic ground stress, (ii) the magnetization and (iii) a magnetically induced mechanical stress, respectively [1, 2]. We propose suitable constitutive functions in an energy-based setting that allow to accurately capture the highly nonlinear material behavior of soft and hard MAPs with stochastic microstructures. Subsequently, the two constitutive functions are embedded in an incremental minimization principle that is supplemented by a conforming finite element method.

The performance of the developed variational-based modeling framework is demonstrated by solving some application-oriented boundary value problems. The main emphasis of the numerical studies lies on the investigation of the magnetostrictive effect of hard MAPs at the macroscale level as well as on the in-depth analysis of pre-magnetized beam structures undergoing large deformations.

- [1] P. Gebhart and T. Wallmersperger, A constitutive macroscale model for compressible magneto-active polymers based on computational homogenization data: Part II Magnetic nonlinear regime, International Journal of Solids and Structures 258 (2022) 111984. https://doi.org/10.1016/j.ijsolstr.2022.111984
- [2] P. Gebhart and T. Wallmersperger, Modeling of hysteresis effects in magneto-active polymers: constitutive theory and variational principles, Acta Mechanica (2025) 1-27. https://doi.org/10.1007/s00707-025-04274-0

# Cluster growth dynamics of nickel particles in viscoelastic matrices

### K. Gerstenberger, G. K. Auernhammer

Leibniz Institute of Polymer Research Dresden, Dresden, Germany

Magnetic elastomers can dynamically modify numerous properties in response to a magnetic field. This gives this class of materials potential for new applications, which justifies the scientific interest in researching them [1–2]. A common method of producing these materials involves embedding magnetic particles in a gel or elastomer matrix. In the presence of an applied magnetic field, the particles tend to arrange themselves into chain-like clusters that react to external stimuli, even if the matrix is cross-linked [3].

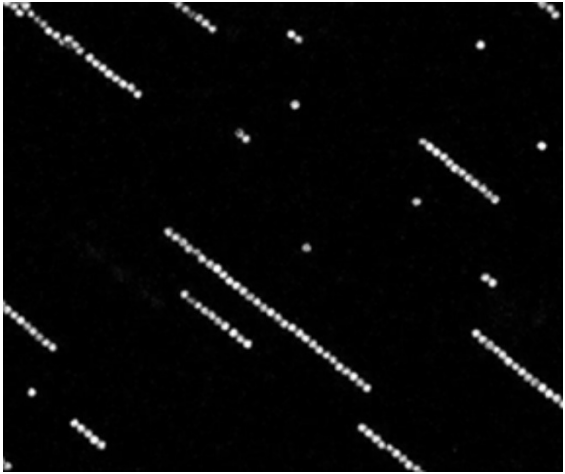


**Figure 1.** Light microscopical picture of nickel particle chains which are formed due to the parallel oriented magnetic field.

Our research focuses on investigating the formation process of these materials, paying particular attention to the interaction between particle cluster formation and simultaneous cross-linking of the surrounding matrix. A magnetic Halbach array generates a homogeneous and controllable magnetic field. Here, we focus on the dynamics of cluster formation under static and slowly varying magnetic fields. We use particle tracking velocimetry techniques to observe how the clusters develop over time and to investigate how this process depends on various parameters. These parameters include matrix

viscosity, particle concentration and applied magnetic field strength. We also consider cluster formation under a rotating magnetic field.

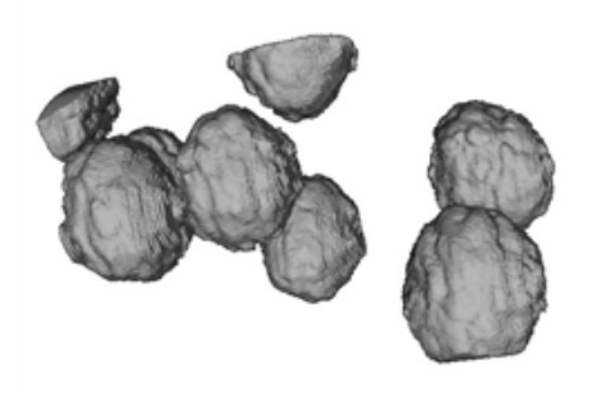


**Figure 2.** CT of the used nickel particles showing the form of them.

Further investigation of larger sample sizes will be possible with a new Halbach array which is currently under construction. This presentation will cover the general idea of the machine, including the variation of the magnetic field, the use of 3D particle tracking and the anti-gravitational aspect.

#### **Acknowledgments**

We thank the Deutsche Forschungsgemeinschaft for support through the Research Unit FOR 5599 on structured magnetic elastomers, project no. 511114185, via DFG grant reference no. AU 321/16-1.

- [1] Z. Rigbi, et al., The response of an elastomer filled with soft ferrite to mechanical and magnetic influences. Journal of Magnetism and Magnetic Materials. 1983, 37, 267.
- [2] Stefan Odenbach (Ed.), Magnetic Hybrid-Materials. Walter de Gruyter GmbH, Berlin/Boston (2022).
- 3] Shilin Huang, et al., Buckling of paramagnetic chains in soft gels. Soft Matter. 2016,12, 228.

# Tumor-Size Effects on Magnetic Hyperthermia Efficiency: A Simulation-Guided In Vivo Validated study

Y. Hadadian<sup>1,2</sup>, H. Kim<sup>2</sup>, T. L. Cao<sup>2</sup>, F. Wiekhorst<sup>1</sup>, J. Yoon<sup>2</sup>

<sup>1</sup> Physikalisch-Technische Bundesanstalt, Abbestr. 2-12, 10587 Berlin, Germany

#### Introduction

Magnetic hyperthermia (MH), for selective tumor cell ablation through heat generated by magnetic nanoparticles (MNPs) under an alternating magnetic field (AMF), is among the most promising biomedical applications of MNPs. However, several technical challenges still hinder its clinical translation, including limited heating efficiency (specific loss power, SLP), accurate delivery and retention of MNPs at the treatment site, and the absence of reliable non-invasive temperature monitoring to avoid overdosing and collateral tissue damage. For a given SLP, the achievable temperature in MH is determined by the AMF parameters and the amount of MNPs delivered (injection dose). Moreover, biological factors such as tumor morphology (size, vascularization, and interstitial fluid pressure) also strongly influence MNP distribution and, consequently, heating performance. Reflecting this complexity, preclinical studies report a wide and inconsistent range of injection doses, from  $<0.1 \text{ mg}_{Fe}/\text{cm}^3$  to  $>10 \text{ mg}_{Fe}/\text{cm}^3$ , with no established standard [1]. This inconsistency underscores the urgent need for systematic investigations, as insufficient dosing leads to inadequate heating while overdosing risks unnecessary toxicity. Here, we present a simulationquided framework validated by in vivo experiments to establish how tumor size and thermal transport constraints dictate the MNPs concentration (injection does) required for therapeutic heating [2].

#### Materials and methods

PEG-coated Synomag®-D nanoflowers (micromod, Germany) were characterized for their intrinsic magnetic properties and SLP under immobilized conditions using agarose phantoms, and the derived SLP was implemented in a COMSOL-based 3D pancreatic tumor model (80–700 mm³).

Tumor temperature (to achieve 45 °C) was simulated by solving a modified bioheat transfer equation:

$$\begin{split} \rho_i \mathcal{C}_i \frac{\partial T_i}{\partial t} &= k_i \nabla^2 T_i + \rho_b \mathcal{C}_b \omega_b^i (T_b - T_i) + Q_m^i + \lambda \\ &\times \text{SLP} \times \theta \end{split}$$

where  $\rho$ , C, T, k and  $\omega$  represent the density, specific heat, arterial temperature, thermal conductivity, and perfusion rate, respectively.  $Q_m$  is metabolic heat generation. The subscripts i and b refer to the specific tissue layer and the blood, respectively. The variable  $\lambda$  takes the value of 1 or 0, indicating tumor or normal tissue, respectively.

#### **Results and discussion**

The required MNP concentration (Fig. 1a) decreased sharply with increasing tumor size and approached an asymptotic minimum of  $\sim$ 2.9  $\mu$ gFe/mm³, following an exponential decay.

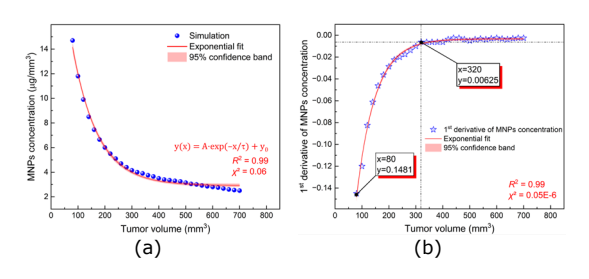


Fig. 1, a) COMSOL simulation for the required MNPs concentration to reach 45  $^{\circ}\mathrm{C}$  with respect to tumor volume and and b) the first derivative of the MNPs concentration

Analysis of the fitted curve (Fig. 1b) identified a critical size of  $\sim 320 \text{ mm}^3$ , marking the transition from a steeply varying to a quasi-steady state dose regime (derivative <0.01, <5% of the initial slope). Therefore, tumors  $\geq 320 \text{ mm}^3$  were defined as "large," requiring  $\sim 3 \mu g_{Fe}/\text{mm}^3$ , while those <320 mm³ were considered

<sup>&</sup>lt;sup>2</sup> Department of AI Convergence, Gwangju Institute of Science and Technology, Gwangju, Republic of Korea

as "small," with substantially higher required MNPs concentration.

Using a 60 mg<sub>Fe</sub>/mL Synomag®-D dispersion, Fig, 2a shows the required injection volumes. For large tumors, a constant 3 µg<sub>Fe</sub>/mm³ dose yielded a linear dependence on tumor volume, whereas for small tumors the required volume plateaued at ~20, obtained by averaging the required injection amount over the 80 to 300 mm³. These findings motivated two dosing strategies: Minimum Injection (MI) for small tumors and Tumor Volume-Normalized Injection (TVNI) for large tumors, which were validated *in vivo* across 31 pancreatic tumor-bearing mice.

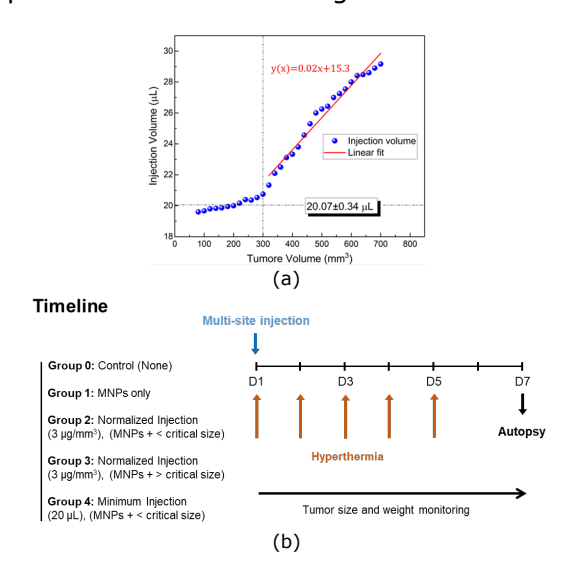


Fig. 2, a) required MNPs injection volumes for different tumor sizes and b) in vivo experiments protocol

The group classifications and the *in vivo* experimental protocols are shown in Fig. 2b. A 30-minutes hyperthermia per session was applied daily for mice in groups 2, 3, and 4 over a period of five consecutive days. During the hyperthermia sessions, tumor surface temperature was monitored using a fiber optic sensor placed on the skin.

Fig. 3a shows the average tumor temperature recorded for each group at Day 1 based on the saturation phase of the heating profile. Groups 2 and 3 agreed well with simulation predictions, while Group 4 (small tumors with MI) showed higher surface temperatures, likely due to non-uniform MNP distribution and local hot spots.

Tumor growth dynamics (Fig. 3b) revealed significant progression in controls

and MNP-only (Group 1) and complete regression in Groups 3 and 4. In group 2 (small tumors with TVNI) five of seven tumors grew, one stabilized, one regressed. To interpret the simulation and in vivo results, we considered a simplified steadystate 1D bioheat equation, whose general solution includes exponential terms, which implies that any heat introduced into the tissue will decay over a characteristic length so-called the thermal penetration depth  $\delta$ . Using tumor-specific parameters,  $\delta$  was calculated as  $\sim$ 9 mm. The simulated critical tumor size (~320 mm<sup>3</sup>) corresponds to a spherical diameter of  $\sim$ 8.4 mm, remarkably close to  $\delta$ . This indicates that tumors smaller than  $\delta$  lose heat too rapidly to sustain therapeutic temperatures, explaining why higher doses were required in small tumors and why uniform and sufficient heating was more reliable in larger ones.

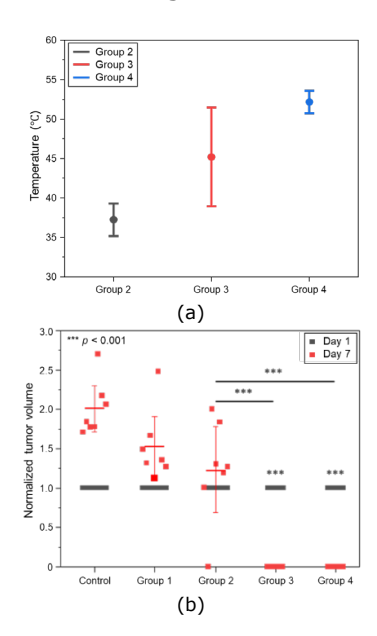


Fig. 3, a) average tumor temperatures and b) tumor size changes in mice

#### **Acknowledgments**

Financial support by the German Federal Ministry for Economic Affairs and Climate within the Special Lipids funding programme (KIWI: future project SPORT - TherSys 16LP301402) is acknowledged.

- [1] Rodrigues, H.F., et. al, Int. J. Hyper., 2020. 37(3): p. 76-99. DOI: 10.1080/02656736.2020.1800831.
- [2] Hadadian, Y., et al. ACS App. Nano. Mat., 2025. DOI: 10.1021/acsanm.5c02473.

## **Structuring magnetic elastomers**

M. Heiber, L. Fischer, H. Reinken, A. M. Menzel

Institut für Physik, Otto-von-Guericke-Universität Magdeburg, Universitätsplatz 2, 39106 Magdeburg, Germany

#### Introduction

Magnetic elastomers combine elastic deformability with excitability of deformations by externally imposed magnetic stimuli [1]. The type of response, that is, the degree and mode of induced deformation strongly depend on the positional arrangement of the magnetizable particles embedded in the elastic carrier medium that cause the magnetic response [2]. Besides the overall shape, also mechanical properties, for example, stressstrain relations and elastic moduli of the materials are affected by external magnetic fields and depend on the particle configuration.

#### Scope

We address these aspects from two different directions by theoretical and computational approaches. On the one hand, we study on the particle scale the dynamic process of structure formation when generating the materials by application of external magnetic fields. Our focus in the current presentation is on anisotropic magnetic particles. On the other hand, we identify spatial arrangements of magnetizable particles that optimize given macroscopic properties. Examples are selected modes of magnetically induced overall deformations and magnetically induced overall changes in mechanical stiffness.

#### Magnetically induced structure formation of anisotropic magnetizable particles

In reality, the particle configurations determining the properties of a structured magnetic elastomer are introduced in a still fluid but reactive suspension by applying strong external magnetic fields during synthesis [3]. These arrangements are then locked in by establishing the permanent elastic carrier medium through chemical crosslinking from the surrounding reactive suspension. We

here aim to develop simulation methods describing this important process of particulate structure formation on the particle scale, including the impact of hydrodynamic, magnetic, and steric interactions between particles. First, we concentrate on the still fluid system.

Hydrodynamic interactions are mediated by the flow of the surrounding fluid, which we take into account explicitly by an appropriate computational method. The dynamics of the combined system of particles and carrier medium is determined by solving the Navier-Stokes equation, coupling the particle dynamics to the velocity field of the carrier fluid. We aim at efficient numerical simulations that still describe hydrodynamic interactions accurately.

Magnetic interactions are treated by explicitly solving Maxwell's equations for spatially resolved particles [4]. To this end, we exploit that the particle dynamics is much slower than magnetic relaxation times. As a result, we are able to accurately resolve the magnetization and the magnetic field in space and calculate the forces acting on the particles.

In the case of isotropic particles, steric interactions are modeled via a Weeks-Chandler-Andersen potential. For anisotropic particles, the complexity of the particle shape necessitates a more involved approach. For example, anisotropic potentials, such as a Gay-Berne potential [5,6], are utilized. Furthermore, torques acting on the particles due to hydrodynamic, magnetic, or steric effects have to be taken into account as well.

Combining these features in our numerical simulations, we are able to study the details of the magnetically induced structure formation. Previous studies on non-magnetizable particles have shown that the presence of hydrodynamic interactions favors the formation of chain-like aggregates, in contrast to more compact structures that emerge in the absence of hydrodynamic interactions. We here investigate how such hydrodynamic inter-

actions affect the emerging configurations in the case of magnetizable particles [7]. Varying particle shape and material parameters of both the carrier medium and the embedded particles, we investigate the structure formation under applied external magnetic fields.

# Optimized spatial arrangements of magnetizable particles

Reversing the perspective, we do not build up the structure from the bottom during dynamic processes as described above. Instead, we request for certain overall properties that we impose and then ask for the associated most beneficial particle configurations.

For this purpose, we first derived an analytical expression that connects the magnetic force on each discrete magnetic inclusion to the overall extension or contraction along the magnetic field direction [8]. We use this formula as an input to an adapted algorithm of simulated annealing [9]. It allows us to determine the optimized particle arrangement for maximized elongation or contraction of spherical example systems upon magnetization by an external magnetic field. As a variant, we address the optimization for maximized magnetically induced stiffening or softening of cubical example systems [9]. Here, in a rather numerical approach, we found underlying particle configurations for maximized magnetically induced changes in mechanical properties during uniaxial stretching or shear-

Recently, we outlined how on that basis the magnitude of this magnetorheological effect can be approximately doubled in magnitude using strategies of computational materials design [10]. Instead of just optimizing the particulate structures for either maximized stiffening or softening of the materials, we simultaneously optimize for both. Stiffening is triggered by one magnetic field direction and softening by a perpendicular field direction. Switching between the two perpendicular fields can have a total effect about twice

in magnitude when compared to the case of simple switching between a nonmagnetized and a magnetized state.

#### Conclusions

We address the topic of structuring magnetic elastomers from two opposite sides. On one hand, we establish theoretical methods to study the formation of particulate aggregates in continuous carrier media by applying external magnetic fields. On the other hand, we identify particulate arrangements that are most beneficial for the overall performance of systems of specified shape. One challenging task for the future is to establish ways that allow us to employ the former process of structuring to generate the arrangements identified during the latter process of optimization.

#### **Acknowledgments**

We thank the Deutsche Forschungsgemeinschaft (DFG) for support of our work through Research Unit FOR 5599 on structured magnetic elastomers, project no. 511114185, via DFG grant reference nos. ME 3571/10-1 and ME 3571/11-1.

- [1] S. Odenbach, Arch. Appl. Mech. **86**, 269 (2016).
- [2] L. Fischer, A. M. Menzel, J. Magn. Magn. Mater. **591**, 171695 (2024).
- [3] D. Günther, D. Yu Borin, S. Günther, S. Odenbach, Smart Mater. Struct. 21, 015005 (2012).
- [4] P. Metsch, K. A. Kalina, C. Spieler, M. Kästner, Comp. Mater. Sci. **124**, 364 (2016).
- [5] J. G. Gay, B. J. Berne, J. Chem. Phys. 74, 3316 (1981).
- [6] R. A. X. Persson, J. Chem. Phys. **136**, 226101 (2012).
- [7] M. Heiber, H. Reinken, A. M. Menzel, in preparation.
- [8] L. Fischer, A. M. Menzel, J. Appl. Math. Mech. 105, e70028 (2025).
- [9] L. Fischer, A. M. Menzel, PNAS Nexus 3, pgae353 (2024).
- [10] L. Fischer, A. M. Menzel, arXiv preprint, ar-Xiv:2507.22777 (2025).

# Ultrasound-based Methods for Imaging Superparamagnetic Iron Oxide Nanoparticles in Biomedical Applications

C. M. Huber<sup>1,3</sup>, H. Ermert<sup>2</sup>, I. Ullmann<sup>3</sup>, M. Vossiek<sup>3</sup>, C. Alexiou<sup>2</sup>, S. Lyer<sup>1</sup>

#### **Motivation**

Superparamagnetic iron oxide nanoparticles (SPIONs) are utilized in various biomedical applications, such as local chemotherapy with Magnetic Durg Targeting (MDT) [1], local magnetic hyperthermia [2] and imaging sentinel lymph nodes [3]. Conventional methods for imaging SPIONs are for example magnetic resonance imaging (MRI) [4] or magnetic particle imaging (MPI) [5]. However, these methods are expensive and cannot be performed e.g. during Magnetic Drug Targeting. Ultrasoundbased methods, such as magnetomotive ultrasound (MMUS) [6, 7], ultrasound elastography [8, 9] or ultrasound-induces cavitation [10] can be used during most biomedical SPION applications and have the potential for real time imaging.

#### **Magnetomotive Ultrasound**

MMUS utilizes the magnetic properties of SPIONs to image their distribution. An applied magnetic field exerts the magnetic gradient force [6]

$$F_m = \frac{\chi_s V}{2\mu_0} \nabla(|\mathbf{B}(\mathbf{r}, t)|^2), \tag{1}$$

on the SPIONs.  $\chi_S$  is the magnetic susceptibility,  $\mu_0$  the permeability, V the volume of magnetic core in each SPION and  $\mathbf{B}(\mathbf{r},t)$  the magnetic flux density and point  $\mathbf{r} = (x, y, z)^T$  and time t. When an alternating magnetic field is applied to tissue interspersed with SPIONs, these particles and the tissue are displaced according to the magnetic field pattern. The displacement of the tissue can be tracked with ultrasound imaging and reconstructed as area of SPIONdistribution. We demonstrated that this method can even be used during Magnetic Drug Targeting [7] (Figure 1).

#### **Ultrasound induced Cavitation**

A completely novel ultrasound based imaging method exploits the utilization of ultrasound induced cavitation on SPIONs. It was shown that certain SPIONs can generate acoustic cavitation, when placed in a focused ultrasound field [8,9]. Cavitation is the generation of gas filled microbubbules, which oscillate and eventually implode. This implosion can be acoustically received as noise signals and used to reconstruct the cavitation source area. As the SPIONs are the cavitation nuclei, imaging the cavitation source area

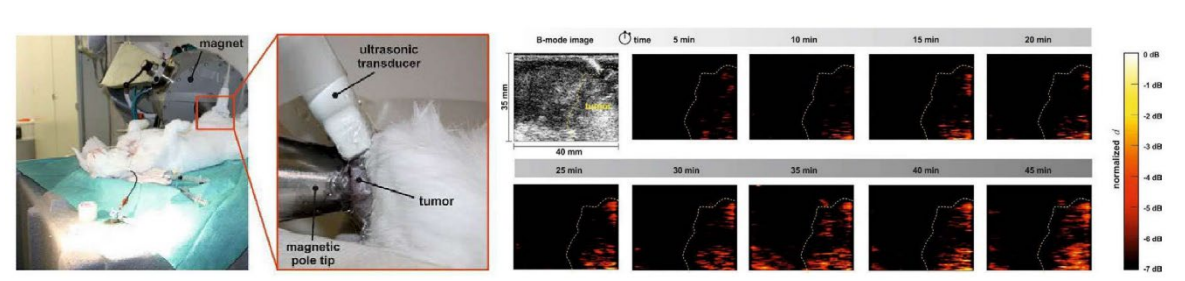


Figure 1: In vivo magnetomotive ultrasound imaging during Magnetic Drug Targeting of a rabbit. The nanoparticle accumulation is demonstrated over a time frame of 5 minutes to 45 minutes [7].

<sup>&</sup>lt;sup>1</sup> Department of Otorhinolaryngology, Head and Neck Surgery, Section of Experimental Oncology and Nanomedicine (SEON), Professorship for AI-Controlled Nanomaterials (KINAM), Universitätsklinikum Erlangen, Glücksstrasse 10a, Erlangen, 91054, Bavaria, Germany

<sup>&</sup>lt;sup>2</sup> Department of Otorhinolaryngology, Head and Neck Surgery, Section of Experimental Oncology and Nanomedicine (SEON), Universitätsklinikum Erlangen, Glücksstrasse 10a, Erlangen, 91054, Bavaria, Germany <sup>3</sup> Institute of Microwaves and Photonics (LHFT), Friedrich-Alexander-Universität Erlangen-Nürnberg, Cauerstrasse 9, Erlangen, 91058, Bavaria, Germany

PCM MMUS Combined

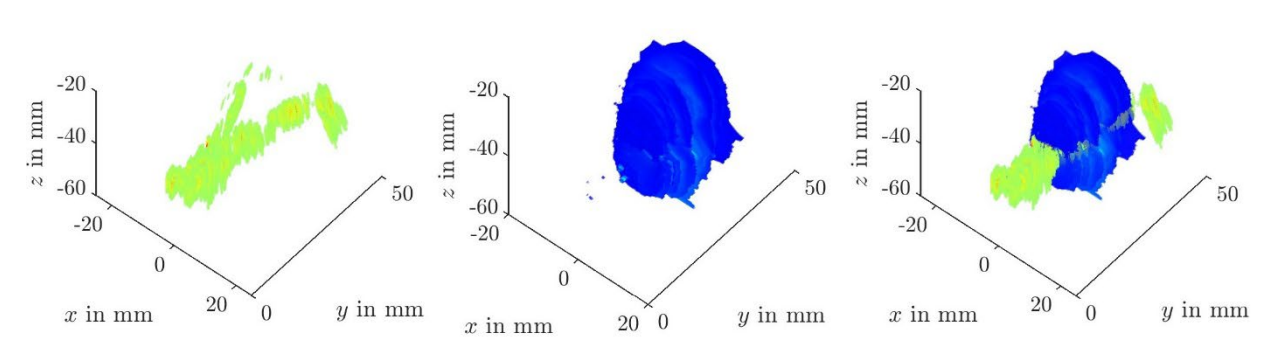


Figure 2: Multimodal Imaging of SPIONs within a flow bifurcation with tumour inclusion. Passive Cavitation Mapping (PCM) showing the flow channel, while Magnetomotive Ultrasound (MMUS) maps the tissue bound SPIONs. The combined image shows the complete structure.

indirectly maps the SPION distribution. Passive Cavitation Mapping [10] can thus be used for SPION imaging.

#### **Multimodal PCM and MMUS Imaging**

Based on the work with MMUS and PCM, A multimodal imaging approach combining MMUS and PCM has been developed. This new method utilizes the imaging strengths of MMUS for detecting SPIONs embedded in tissue, alongside PCM's capability for imaging SPIONs present in fluids. Figure 2 demonstrates the application of this technique using a complex flow phantom with tumor inclusion. By integrating MMUS and PCM imaging maps, the entire structure can be comprehensively visualized.

#### Conclusion

employed various Our research ultrasound-based techniques for SPION imaging. MMUS uses the magnetic properties of SPIONs to visualize their distribution in tissues, while PCM uses the acoustic signals generated by cavitation events to map SPIONs in fluids. The combined multimodal approach provides a thorough imaging solution. Future research will apply this integrated multimodal technique to animal studies and experiments involving SPION-loaded cells.

#### **Acknowledgments**

The authors gratefully acknowledge the financial support of the Deutsche Forschungsgemeinschaft (DFG) – project number 452821018, and the Julitta und Richard Müller Stiftung, Munich, Germany.

- [1] Tietze, R et al. (2013). Efficient drug-delivery using magnetic nanoparticles—biodistribution and therapeutic effects in tumour bearing rabbits. Nanomedicine: Nanotechnology, Biology and Medicine, 9(7), 961-971.
- [2] Dutz, S., & Hergt, R. (2013). Magnetic nanoparticle heating and heat transfer on a microscale: Basic principles, realities and physical limitations of hyperthermia for tumour therapy. International Journal of Hyperthermia, 29(8), 790-800.
- [3] Evertsson, S. et al. (2017). Combined Magnetomotive ultrasound, PET/CT, and MR imaging of 68Ga-labelled superparamagnetic iron oxide nanoparticles in rat sentinel lymph nodes in vivo. Scientific reports, 7(1), 4824.
- [4] Avasthi, A. et al. (2020). Magnetic nanoparticles as MRI contrast agents. Surfacemodified nanobiomaterials for electrochemical and biomedicine applications, 49-91.
- [5] Borgert, J. et al. (2012). Fundamentals and applications of magnetic particle imaging. Journal of cardiovascular computed tomography, 6(3), 149-153.
- [6] Oh, J. et al (2006). Detection of magnetic nanoparticles in tissue using magneto-motive ultrasound. Nanotechnology, 17(16), 4183.
- [7] Fink, M. et al. (2020). In Vivo study on magnetomotive ultrasound imaging in the framework of nanoparticle based magnetic drug targeting. Current Directions in Biomedical Engineering, 6(3), 543-546.
- [8] Huber, C. M. et al. (2022, September). Ultrasound-Mediated Cavitation of Magnetic Nanoparticles for Drug Delivery Applications. In Current Directions in Biomedical Engineering (Vol. 8, No. 2, pp. 568-571). De Gruyter.
- [9] Huber, C. M. et al. (2024, September). Ultrasound-Induced Stable and Inertial Cavitation of Magnetic Nanoparticles for Drug Delivery Applications. In Current Directions in Biomedical Engineering (Vol. 10, No. 4, pp. 328-331). De Gruyter.
- [10] Gyöngy, M., & Coussios, C. C. (2010). Passive cavitation mapping for localization and tracking of bubble dynamics. The Journal of the Acoustical Society of America, 128(4), EL175-EL180.

## Viscoelasticity and Fluorescence of polymerbased magnetically switchable composite gels

M. Kermarrec<sup>1,2</sup>, Y. Suffren<sup>3</sup>, P. Roquefort<sup>2</sup>, S. Triki<sup>1</sup>, T. Aubry<sup>2</sup>

Switchable materials comprise an actual and eclectic area of research covering as well applied as fundamental research questions. While the implementation of magnetic nano- and microparticles into soft matrices principally opens the pathway to magnetically manipulable composites, it still remains a challenge to integrate magnetically switchable particles that fundamentally change their nature under the influence of external fields. One option to achieve this goal is the employment of nanoparticles composed of a spin-crossover Fe(II) complex in a polymer matrix,[1] as they can undergo an abrupt transition from a diamagnetic state (low spin electronic configuration) to a paramagnetic state (high spin configuration) with temperature.[2] Despite their potential, the study of the viscoelastic properties of spin crossover soft nanocomposites remains relatively plored.[3]

In this work, the viscoelastic, fluorescent and spin crossover properties of composite gels are studied. The composites are prepared by dispersing Fe(II)-triazole rod-shaped based particles  $([Fe(Htrz)_2(trz)](BF_4)$ and particle [Fe(NH<sub>2</sub>trz)<sub>3</sub>]Cl<sub>2</sub>) of various lengths in NaPSS aqueous solutions. The [Fe(Htrz)<sub>2</sub>(trz)](BF<sub>4</sub>)/NaPSS composite systems are shown to exhibit a critical gel behavior.[4] This behavior is brought by the percolation of the particles within the NaPSS matrix, similar to what has been reported for various anisometric particle dispersions.[5-7] While their study is limited to the LS state due to their high LS-to-HS transition temperature  $(T_{1/2} \approx 113^{\circ}C)$ , composites prepared by using particles of the parent complex  $[Fe(NH_2trz)_3]Cl_2$  (NH<sub>2</sub>trz = 4-amino-1,2,4-triazole) [Fe(NH<sub>2</sub>trz)<sub>3</sub>]Cl<sub>2</sub>/NaPSS, exhibit a wide thermal hysteresis loop around room temperature (see figure 1),

thus allowing the investigation of the viscoelastic properties for both spin states (HS and LS) at room temperature. The investigation of the rheological properties of the composite gel (see figure 2a) reveals that the HS composite exhibits a critical gel behavior, indicated by the presence of a power law dependence of the relaxation modulus G(t) with time, while the LS composite relaxation follows a stretched exponential, as expected for viscoelastic fluids. Further, both G' and G" are increased as compared to the LS state at the same temperature (see figure 2b). This is an important indication for the structuring effect of the spin crossover phenomenon in this composite system.

On the other hand, remarkable coupling between the magnetic state of the nanoparticles and the viscoelastic and the fluorescent properties is observed that becomes possible through the aromaticity of the NaPSS component (figure 3). We observe a strong increase in fluorescence intensity for the HS state as compared to the LS state. While the origin for this is not yet fully understood, we anticipate that this effect could arise from the partial photobleaching of the emission band caused by absorption of the LS state, and/or from local conformational changes of the PSS chains in the vicinity of the nanoparticles, due to the increased lattice volume of the particles in the HS state.

<sup>&</sup>lt;sup>1</sup> Univ. Brest, CEMCA, UMR 6521, UBO, 6 Av. V. Le Gorgeu, CS 93837-29 238 BREST Cedex 3, and University of Cologne, Department for Chemistry and Biochemistry, Cologne, Germany, matthieu.kermarrec@univ-brest.fr <sup>2</sup> Univ. Brest, IRDL,UMR 6027, UBO, 6 Av. V. Le Gorgeu, CS 93837-29 238 BREST Cedex 3.

<sup>&</sup>lt;sup>3</sup> Institut des Sciences Chimiques de Rennes, UMR CNRS-INSA 6226, 20 Av. des Buttes des Coësmes, CS 70839, 35708 RENNES Cedex 7

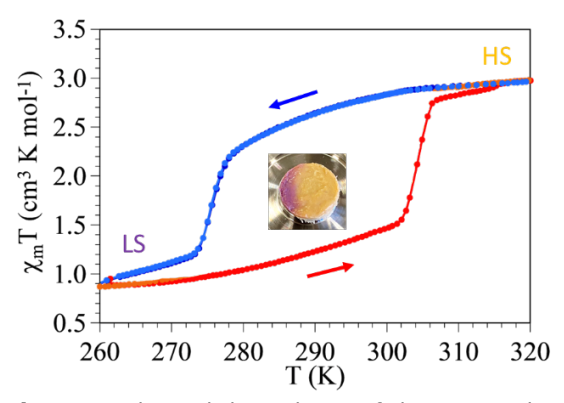


**Figure 1.** Thermal dependence of the  $\chi_m T$  product of the composite [Fe(NH<sub>2</sub>trz)<sub>3</sub>]Cl<sub>2</sub>/NaPSS, recorded at 2.0 K.min<sup>-1</sup>. The red and blue arrows represent heating and cooling respectively, while HS and LS domains are indicated in yellow and purple respectively. (Insert: picture of the composite during a LS-to-HS transition).

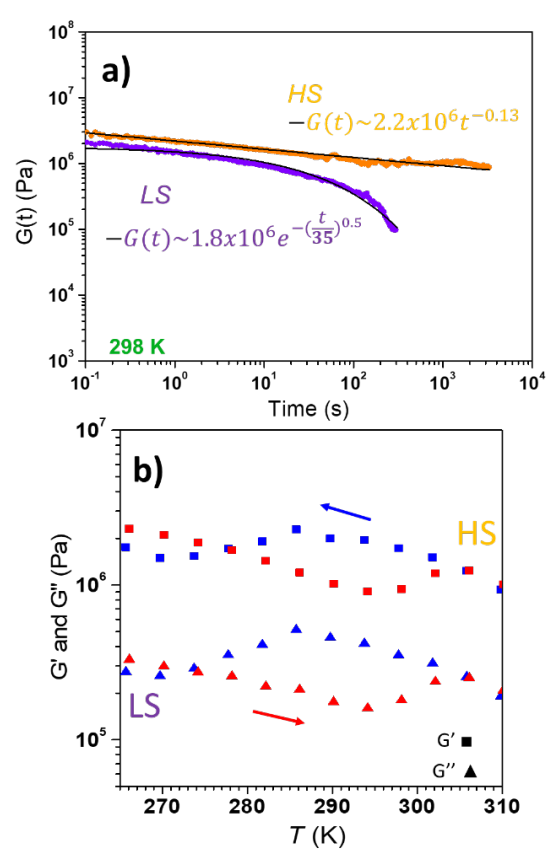


**Figure 2. a)** Stress relaxation modulus G(t) of  $[Fe(NH_2trz)_3]Cl_2/PSS-HS$  (orange), fitted with a power law (black line), and of  $[Fe(NH_2trz)_3]Cl_2/PSS-LS$  (purple) fitted with a stretched exponential (black line), performed at 298 K; **b)** storage  $G'(\blacksquare)$  and loss  $G''(\blacktriangle)$  moduli of the composite versus temperature (K), performed at 2 K.min<sup>-1</sup>. Both experiments are performed in the linear-viscoelastic regime.

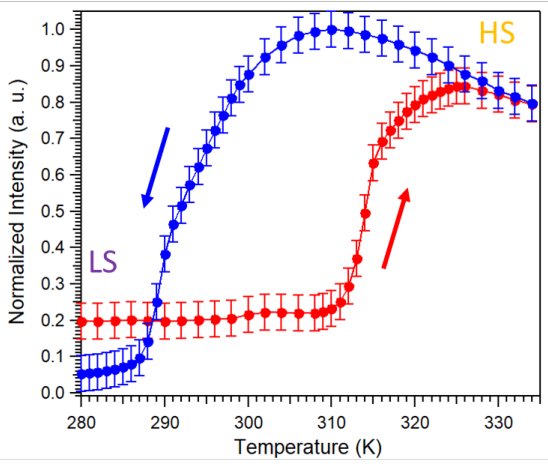


**Figure 3.** Normalized emission intensity ( $E_{max}$ ) as a function of temperature (K) for [Fe(NH<sub>2</sub>trz)<sub>3</sub>]Cl<sub>2</sub>/NaPSS (stabilized with ethylene glycol), recorded at 2.0 K.min<sup>-1</sup> under an excitation wavelength of  $\lambda = 312$  nm. The maximum emission wavelength obtained in the LS and HS states are as followed:  $\lambda_{em}(LS, 273 \text{ K}) = 392$  nm and  $\lambda_{em}(HS, 326 \text{ K}) = 400$  nm.

- [1] A. Enriquez-Cabrera, A. Rapakousiou, M. Piedrahita Bello, G. Molnár, L. Salmon, A. Bousseksou, Coord. Chem. Rev., 2020, V 419, 213396.
- [2] P. Gütlich, H.A. Goodwin, Top Curr. Chem., 2004, 233, 1–47.
- [3] H. Voisin, C. Aimé, A. Vallée, A. Bleuzen, M. Schmutz, G. Mosser, T. Coradin, C. Roux, J. Mater. Chem. C., 2017, 5, 11542.
- [4] M. Kermarrec, C.J. Gómez-García, M. Marchivie, P. Roquefort, T. Aubry, S. Triki, J. Mater. Chem. C, 2025, 13, 5779–5787.
- [5] K.J. Le Goff, D. Jouanneau, C. Garnier, T. Aubry, J. Appl. Polym. Sci., 2014, 131, 40676.
- [6] N.K. Reddy, Z. Zhang, M.P. Lettinga, J.K.G. Dhont, J. Vermant, J. Rheol., 2012, 56, 1153– 1174.
- [7] S. Cocard, J-F. Tassin, T. Nicolai, J. Rheol., 2000, 44, 585–594

# Time-resolved magnetic particle spectroscopy to investigate aneurysm phantoms

B. Kluwe<sup>1</sup>, L. Truttenbach<sup>1,3</sup>, M. Löffler<sup>2</sup>, U. Heinen<sup>3</sup>, S. Dutz<sup>2</sup>, F. Wiekhorst<sup>1</sup>

<sup>1</sup> Physikalisch-Technische Bundesanstalt, Berlin, Germany, <sup>2</sup>University of Applied Science Zwickau, Zwickau, Germany, <sup>3</sup>Faculty of Technology, University of Pforzheim, Pforzheim, Germany

Non-invasive diagnosis and monitoring of intracranial aneurysms (IA) represent an important challenge in modern medicine, as undetected aneurysm could lead to rupture and hemorrhage with high risks of permanent neurological damage or death. The annual global incidence of a subarachnoid hemorrhage (SAH) lies around 6.1 per 100,000 people [1] but with a mortality rate of approx. 35% [2]. Current diagnostic methods are indispensable in initial diagnostics, but reach their technical limits when it comes to quantifying hemodynamic parameters and time-resolved tracking of contrast tracers [3]. Due to their special magnetic properties, magnetic nanoparticles (MNP) enable novel quantitative imaging techniques such as magnetic particle imaging (MPI) and the associated spectroscopic analysis method, magnetic particle spectroscopy (MPS). MPS enables the investigation of the flow behavior of an MNP bolus quantitatively and time-resolved with high sensitivity in model vascular systems. First studies already showed the feasibility of investigating the hemodynamics in aneurysm phantoms with MPI [4,5].

The focus of this work is the development and characterization of a measurement setup for time-resolved quantification of MNP boluses in additively manufactured aneurysm phantoms using MPS. For this purpose, a setup was assembled and validated that enables controlled injections of boluses into a flow system consisting of a simplified aneurysm phantom and a MPS flow cell, see Figure 1a. Aneurysm phantoms were designed based on anatomical reference data from the circle of Willis and aneurysm sizes are selected according to clinical classification of IA with diameters between 4 - 26 mm (Fig. 1b). The phantoms are manufactured using stereolithography with a resin 3D printer.

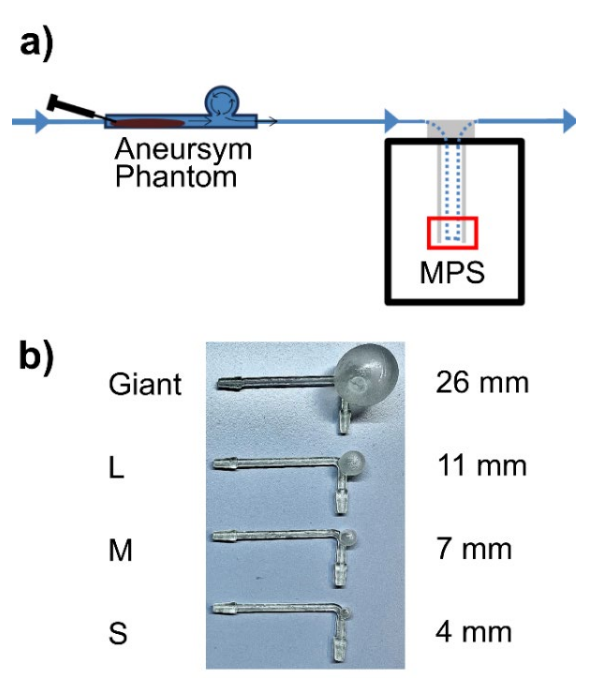


**Figure 1: (a)** flow-based measurement setup consisting of an aneurysm phantom, in which a MNP bolus is injected and time-resolved measured with MPS, **(b)** 3D-printed IA phantoms with different aneurysm sizes (inner diameters).

During the experiment, distilled water is pumped as carrier medium into the flow setup using a peristaltic pump. Then a bolus of MNP (Berlin Heart 10 nm, Berlin Heart GmbH, Germany) is injected into the phantom using a syringe. Propelled by continuous flow in the system, the bolus then passes the aneurysm and finally enters the MPS flow cell (MPS-3, Bruker Biospin, Germany), which records the magnetic response of the particles and enables time-resolved quantification. MPS and an optical detection unit (sepmag A 200 mL, sepmag systems SL, Spain) as reference measurement were employed to characterize the dynamics of the MNP bolus in the aneurysm. The third harmonic amplitude  $(A_3)$  of the MPS spectra measured over time revealed that the descent phase of the A<sub>3</sub> signals broadens with increasing aneurysm size (Fig. 2a).

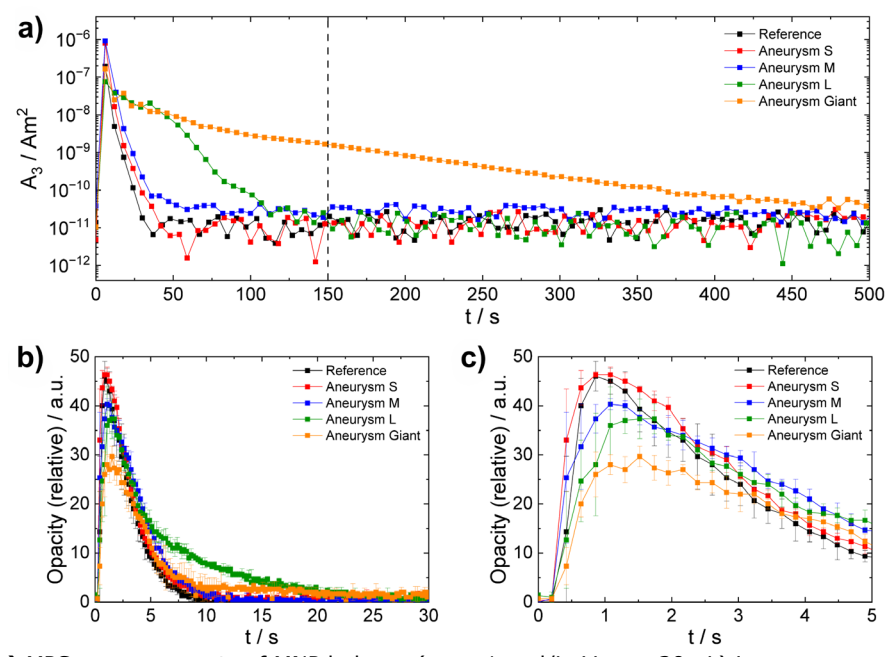


**Figure 2**: (a) MPS measurements of MNP boluses ( $C_{Fe} = 1 \text{ mol/L}$ ,  $V_{Bolus} = 20 \mu L$ ) in aneurysm-phantoms with different sizes, results from time-dependent third harmonic amplitude values (A<sub>3</sub>), (b) Time-resolved optical measurements of MNP boluses,

(c) Enlarged period of 5 s to illustrate the initial course of the signal showing the effect of aneurysm size.

The longer descent phase of the A<sub>3</sub> curve is attributed to a larger MNP retention for increasing aneurysm size. Thus, it can be postulated that the flow velocities and the vortex flow in the aneurysm decrease with larger aneurysm volumes. The optical data (Fig. 2b / 2c) complement the MPS measurements by showing a decrease in opacity resulting from diminished MNP concentration. The method captures the short rise phase of the bolus with high temporal resolution, whereas MPS quantitatively measures the washout phase over several minutes at low MNP concentrations with outstanding high sensitivity.

By combining both methods, the complete profile of an MNP bolus can be measured in an anatomically relevant vascular model with aneurysms of different sizes. Evaluation of the data showed also that it is possible to mathematically estimate the aneurysm size with an exponential fit, which will be further investigated in future work. In addition, the temporal resolution of the MPS should be improved to decrease uncertainties in size calculations. A future setup will also combine MPS and the optical method in one setup for better comparability of the data. With these improvements, the method thus possesses great potential to investigate the influence of different aneurysm morphologies

on hemodynamics and could further be employed as a diagnostic tool in future clinical applications to classify and monitor aneurysm progression.

#### **Acknowledgments**

This work was funded by the DFG project "harmoMPI" (project no 540326102).

- [1] R. G. Tawk, T. F. Hasan, C. E. D'Souza, J. B. Peel, and W. D. Freeman, Mayo Clin. Proc. 96, 1970 (2021).
- [2] S. N. Neifert, E. K. Chapman, M. L. Martini, W. H. Shuman, A. J. Schupper, E. K. Oermann, J. Mocco, and R. L. Macdonald, Transl. Stroke Res. 12, 428 (2021).
- [3] N. K. Yoon, S. McNally, P. Taussky, and M. S. Park, Neurovascular Imaging **2**, 6 (2016).
- [4] J. Sedlacik, A. Frölich, J. Spallek, N. D. Forkert, T. D. Faizy, F. Werner, T. Knopp, D. Krause, J. Fiehler, and J.-H. Buhk, PLOS ONE **11**, e0160097 (2016).
- [5] O. Kosch, A. F. Sanches, Y. Özpeynirci, T. Liebig, and F. Wiekhorst, Trans. Addit. Manuf. Meets Med. 808 Pages (2023).

# Two time scales drive the formation of transient networks in a ferrogranular experiment, and how to control them

A. Lakkis<sup>1</sup>, M. Biersack<sup>1</sup>, O. Bilous<sup>2</sup>, S.S. Kantorovich<sup>2</sup>, R. Richter<sup>1</sup>

<sup>1</sup>Experimentalphysik V, Universtät Bayreuth, 95440 Bayreuth (Germany) <sup>2</sup>University of Vienna, Sensengasse 8, 1090 Vienna (Austria)

#### Introduction

Magnetised steel spheres self-assemble due to anisotropic magnetic interactions. If one shakes a mixture of glass and steel beads with a supercritical vibration amplitude (3.3g), inter-particle collisions hinder the aggregation and keep the mixture in a "gas phase" [1]. Below a critical vibration amplitude, magnetic forces lead, first, to the formation of individual chains and rings that merge into a network [2] as the system relaxes as shown in Fig. 1. If given enough time, the network eventually compacts into crystalline-like islands of magnetic beads.

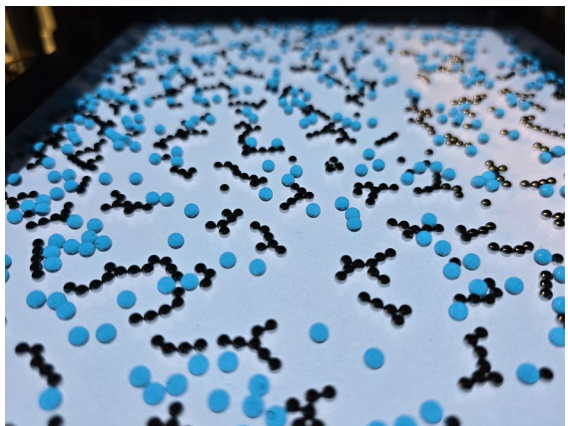


**Figure 1** Snapshot of ferrogranular networks emerging after a quench of the vibration amplitude.

This scenario resembles the viscoelastic phase separation (VPS) introduced by Tanaka [3] for molecular mixtures. There phase separation arises from the different time scales of both components, labelled as dynamic asymmetry by Tanaka. In previous experiments and computer simulations we found some evidence that the ferrogranular coarsening can be describes as a VPS in the macroscale [3]. A homogeneous magnetic field oriented in vertical direction was shown (in experiment

and in silico) to hinder the coarsening dynamics [5,6]. This is, because the magnetized steel spheres eventually repel each other.

Likewise, the value of the subcritical acceleration amplitude  $\Gamma$  plays a crucial role for the type of emerging pattern [1]. In the following we examine the coarsening dynamics for different values of  $\Gamma$ .

#### **Experiment**

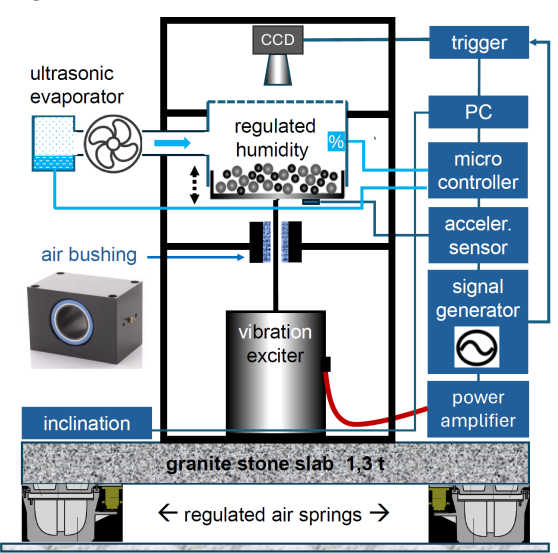


Figure 2. Scheme of the experimental setup.

A computer-controlled signal generator feeds a sinusoidal voltage signal into an amplifier which drives a vibration exciter from TIRA vib Co. The vibrations are coupled via a long rod (guided by a precision air bearing) to the experimental vessel to avoid the magnetic stray field of the exciter. The vessel is filled with glass and steel beads with a diameter of 4 (3) mm, respectively. Pictures are recorded by means of a camera triggered in phase with the driving. To avoid electrostatic charges a micro controller stabilizes the humidity in the range 80%-85%RH. The setup is mounted on a stone plate

(m=1.6t) which is floating on 4 air springs and can be levelled to 10 µm.

#### **Experimental Results**

We are investigating the transient networks by the number of edges of each node, i.e. its degree  $k = \{0,1,...,6\}$ , and the corresponding fraction of nodes Fk = Nk / NS, where NS denotes the total number of steel spheres, and Nk those with k neighbors. Because the networks are largely made up of chains, F2 is a suitable order parameter to monitor their generation and decay, as displayed in Fig. 3.

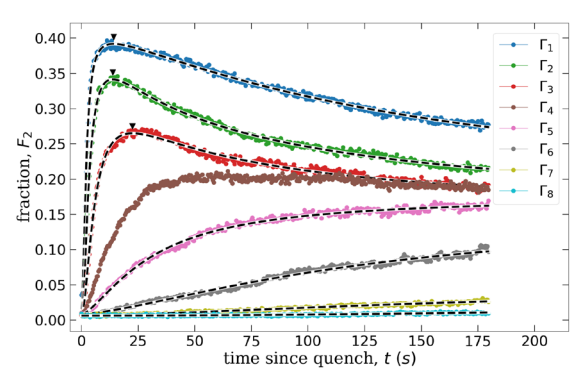


**Figure 3.** Temporal evolution of  $F_2$  for increasing shaking amplitudes  $\Gamma_i$ , as listed in table1.

For a deep quench \( \tau^1 \) we see a fast buildup of chains and networks, which are then diminished on a much longer time scale. A quantitative description can be given by a bi-sigmoidal growth function [6,7]

$$A(t) = A_{\text{ini}} + \sum_{i=1}^{N=2} A_{\text{gro},i} \left( 1 - \frac{1}{1 + \left( \frac{t}{t_{1/2,i}} \right)^{p_i}} \right)$$

of a time-dependent quantity A(t). Here Aini denotes an offset, present at t<0s, and Agro,i. the maximal growth (or decay). The half-value period t1/2,i is the time when A=Aini+1/2 Agro,i, and p is a scaling exponent.

$\Gamma_n$	(g)	$F_{2,ini}$	$F_{2,gro,1}$	$t_{1/2,1}(s)$	$p_1$	$F_{2,gro,2}$	$t_{1/2,2}(s)$	$p_2$
$\Gamma_1$	1.49	0.015	0.40	2.06	2.00	-0.25	144.21	1.21
$\Gamma_2$	1.57	0.010	0.50	3.36	1.75	-0.38	33.93	0.74
$\Gamma_3$	1.65	0.008	0.50	6.29	1.51	-0.36	23.13	0.93
$\Gamma_4$	1.73	-	-	-	-	-	-	-
$\Gamma_5$	1.80	0.008	0.17	31.64	1.43	-	-	-
$\Gamma_6$	1.88	0.009	0.14	128.47	1.45	-	-	-
$\Gamma_7$	1.96	0.007	0.04	200.35	1.55	-	-	-
$\Gamma_8$	2.02	0.006	0.08	715.22	2.00	-	-	-

Table 1 Acceleration amplitudes and fitting parameters to the data displayed in Fig. 3.

Table 1 presents in the 2nd line two half-value-times which differ by 142s. This difference is diminishing with  $\Gamma$ , until for  $\Gamma$ >

 $\Gamma_5$  only one time scale is left, capturing the monotonous growth of  $F_2$ .

To conclude, the two time scales – an initial rapid assembly and a slower coarsening may be specific for a ferrogranulate composed of susceptible dipolar hard spheres (SDHS) [2]. The initial regime is driven by dipolar interaction, while the latter is governed by susceptibility. Thus, internal magnetic complexity leads to VPS. Injecting kinetic energy facilitates the direct arrangement of clusters, bypassing the networks.

#### Acknowledgments

The authors acknowledge financial support of the German-Austrian project "Coarsening dynamics of ferromagnetic granular networks – experiment and simulation" via Ri 1054/7-1 and I5160 FWF.

- [1] D.L. Blair and A. Kudrolli, Phys. Rev. E 67 (2003) 021302.
- [2] A. Kögel, P. Sanchez, R. Maretzki, T. Dumont, E. S. Pyanzina, S. S. Kantorovich, and R. Richter. Soft Matter, 14 (2018) 1001.
- [3] H. Tanaka, J. Phys: Condens. Matter 12 (2000) R207
- [4] M. Biersack, A. Lakkis, R. Richter, O. Bilous, P.A. Sanchez, S.S. Kantorovich Phys. Rev. E. 108 (2023) 054905.
- [5] A. Lakkis, M. Biersack, O. Bilous, S. Kantorovich, R. Richter, J. Magn. Magn. Mater. 589 (2024) 171620.
- [6] A. Tsoularis, J. Wallace, Mathematical bioscience 179 (2002) 21.
- [7] A. Lakkis, M. Biersack, O. Bilous, S.S. Kantorovich, R. Richter, Soft Matter (2025) submitted. For movies of the experiment cf. https://doi.org/10.17605/OSF.IO/6S4FM

# Ultralow-frequency AC-susceptometry for the analysis of complex fluids

### J. Landers<sup>1</sup>, S. Salamon<sup>1</sup>, H. Nádasi<sup>2</sup>, A. Eremin<sup>2</sup>, H. Wende<sup>1</sup>

<sup>1</sup> Faculty of Physics and Center for Nanointegration Duisburg-Essen (CENIDE), University of Duisburg-Essen <sup>2</sup> Institute of Physics, Otto-von-Guericke University Magdeburg

AC-susceptometry is a well-established technique for the study of Brownian and Néel relaxation mechanisms in ferrofluids and soft magnetic composite materials. Here, we report on the usage of a SQUID-magnetometer with integrated AC-option for magnetic AC-susceptometry at ultralow frequencies and variable temperature. The setup allows the application of maximum AC magnetic fields of  $H_{AC,max} = 0.42$  mT ( $H_{DC,max} = 5$  T) at frequencies from  $3.5 \cdot 10^{-4}$  to 1500 Hz and temperatures of 5 to 400 K.

To be sensitive to slow particle magnetization dynamics is especially important, e.g., in high-viscosity fluids and complex media, where spatial constrictions can modify particle mobility. In the following, several such materials are presented exemplarily. One main advantage of this approach with a wide attainable parameter space is the ability to probe Néel- as well as Brownian system parameters. This is demonstrated in fig. 1, showing an AC-susceptometry ( $\chi''$ ) mapping for elongated Fe<sub>3</sub>O<sub>4</sub>/CoFe<sub>2</sub>O<sub>4</sub> core-shell particles in an organic carrier medium.

Other exemplary sample systems are used to demonstrate the determination of hydrodynamic particle diameters in highly viscous fluid media,[2] the comparability

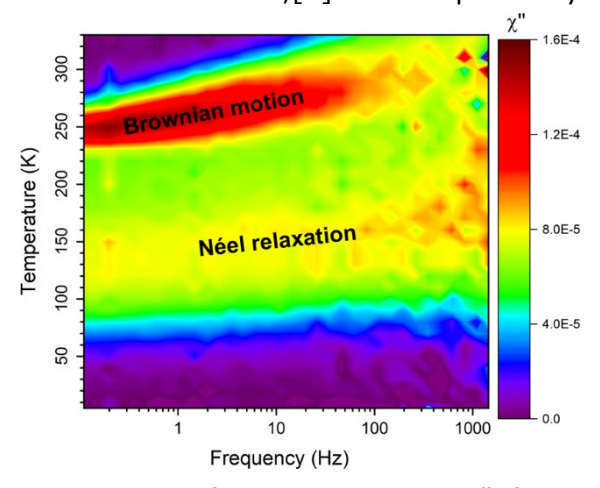


Fig. 1: Mapping of imaginary component  $\chi''$  of magnetic susceptibility of Fe<sub>3</sub>O<sub>4</sub>/CoFe<sub>2</sub>O<sub>4</sub> core-shell particles recorded at 0.1–1500 Hz and 5–330 K.[1]

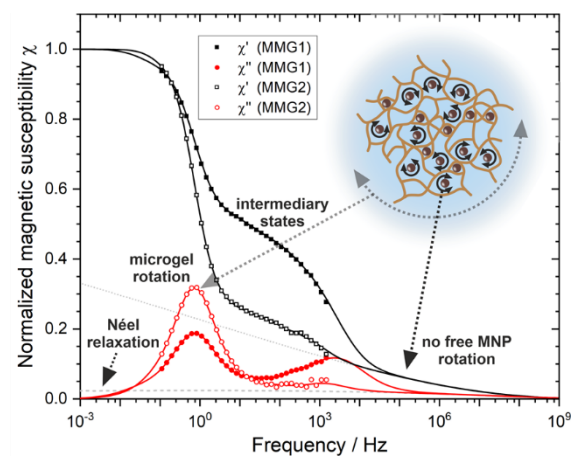


Fig. 2: Magnetic susceptibility  $\chi$  of CoFe<sub>2</sub>O<sub>4</sub> nanoparticles embedded in 2 types of PNIPAM microgel recorded at 293 K.[4]

of slow Brownian dynamics determined from AC-susceptometry data to translational particle motion in Mössbauer spectroscopy [3] and the effect of spatial constraint on the mobility of  $CoFe_2O_4$  particles in temperature-responsive PNIPAM microgel networks, as shown in fig. 2.[4] Special emphasis is given to the rotational dynamics of Sc-doped  $BaFe_{12}O_{19}$  nanoplatelets dispersed in liquid crystal and butanol, respectively, displaying ferronematic properties.

#### **Acknowledgments**

Financial support by CRC/TRR 270 (subproject B05, project number 405553726) is gratefully acknowledged.

- [1] M. Hähsler et al. Magnetic Properties and Mössbauer Spectroscopy of Fe<sub>3</sub>O<sub>4</sub>/CoFe<sub>2</sub>O<sub>4</sub> Nanorods, Inorg. Chem. 59, 3677-3685 (2020)
- [2] R. Müller et al. *Mobility Investigations of Magnetic Nanoparticles in Biocomposites* Mater. Chem. Phys. **193**, 364-370 (2017)
- [3] J. Landers et al. Simultaneous Study of Brownian and Néel Relaxation Phenomena in Ferrofluids by Mössbauer spectroscopy, Nano Lett. **16**, 1150-1155 (2016)
- [4] M. Witt et al. Magnetic response of CoFe<sub>2</sub>O<sub>4</sub> nanoparticles confined in a PNIPAM microgel network, Soft Matter 18, 1089-1099 (2022)

## Chirality and Instabilities in Ferrogel Torsional Actuators under Uniaxial Magnetic Fields

A. Leon-Cecilla,<sup>1,2</sup> F. J. Vazquez-Perez,<sup>2</sup> L. Álvarez de Cienfuegos,<sup>3</sup> J. E. Martin<sup>4</sup>, M. T. Lopez-Lopez<sup>2</sup>

#### Introduction

Ferrogel actuators are made of soft and magneto-responsive polymeric materials that can bend, elongate, contract, or twist under magnetic fields. The magnetic field stands out among other stimuli because it can be instantly applied, produce a quick response, and naturally penetrate most materials. Particularly, by introducing hard magnetic particles (MPs) into the polymeric matrix, complex deformations can be achieved because of their magnetic remanence. However, these particles are highly toxic, which hinders their use in biological environments, the main application space of these systems.

In this work, we present the fabrication and actuation of ferrogel cylinders including iron-based soft MPs, which under adequate experimental conditions, showed a chiral response and two types of instabilities. The polymeric matrix is composed of either alginate or acrylamide and cellulose as a semi-interpenetrating polymeric network (SIPN) [1]. During gelation, a uniform magnetic field is applied normally to the cylindrical axis to organize the soft MPs into chains that are permanently fixed by the gelation process. This fabrication process serves as a straight-forward alternative for the creation of an anisotropic magnetic susceptibility in composites. This simple method for the preparation of ferrogel actuators relies solely on moderate strength magnetic fields in contrast to recently reported methods that require complex magnetic fields or deformable molds [2]. The response of these actuators is based on the anisotropy of the magnetic susceptibility of the ferrogel because of the MP arrangement. When an external field is applied to the cylinder,

the ferrogel deforms because of the partial alignment of MP chains with the magnetic field lines to reduce magnetostatic energy. Experimentally, when one end of the composite is fixed, a chiral twist can be induced in the actuator under moderate magnetic fields, and two types of instabilities are observed. A simple theoretical model is developed that predicts the torsional response of the actuator, and the observed instabilities [3].

#### Theory

Consider a cylindrical ferrogel of a high aspect ratio whose MPs have been structured by a uniaxial field applied perpendicular to the cylinder axis during gelation. If after gelation, a uniaxial field is applied to the composite perpendicularly to its axis, it will rotate so that the MP chains align with the field. If, however, one end of the composite is fixed, the field can induce a significant torsional deformation whose extent depends on the angle  $\theta_0$  between the MPs chains at the fixed end, and the perpendicular direction to the applied field. By studying the magneto-elastic balance of this system, it is possible to obtain an expression for the torsional deformation of the ferrogel cylinder

$$\frac{d\theta(z)}{dz} = \frac{2}{R^2 G} \mu_0 H_0^2 (A_{\parallel} - A_{\perp}) \int_z^L \sin(2\theta(z')) dz'$$

where R is the radius, L the length, G the shear modulus,  $A_{\parallel}$  and  $A_{\perp}$  the effective susceptibility parallel and perpendicular to the MP chains respectively,  $\mu_0$  the vacuum magnetic permeability, and  $H_0$  the applied magnetic field strength. This integro-differential equation is nontrivial to solve, but it can be done numerically [3].

<sup>&</sup>lt;sup>1</sup> University of Cologne, Department for Chemistry and Biochemistry, Greinstr. 4 – 6, 50939 Köln, Germany <sup>2</sup> Universidad de Granada, Departamento de Física Aplicada and Research Unit "Modeling Nature" (MNat), C.U. Fuentenueva, Granada, E-18071, Spain

<sup>&</sup>lt;sup>3</sup> Universidad de Granada, Departamento de Química Orgánica, Unidad de Excelencia Química Aplicada a Biomedicina y Medioambiente, C.U. Fuentenueva, Granada, E-18071, Spain

<sup>&</sup>lt;sup>4</sup> Sandia National Laboratories, Albuquerque, New Mexico 87059, USA

#### Methodology

To characterize the actuation, three different experiments are carried out:

Magnetically induced torsional deformation. The base of the actuator is fixed at a given angle  $\theta_0$ , whilst the other end is free to rotate. The strength of the uniaxial magnetic field is then increased progressively.

Mechanically induced instability. Under a constant magnetic field, the base of the actuator is rotated, starting parallel to the field ( $\theta_0 = +90^\circ$ ). As  $\theta_0$  changes, a metastable point is reached where  $\theta_0 < 0$ , whilst the angle at the free end remains positive ( $\theta > 0$ ). Further rotation induces an instability where the free end abruptly rotates to negative angles ( $\theta < 0$ ).

Field-induced instability. In this experiment, to create a metastable state, the base of the actuator is rotated so that the base angle changes sign, whilst the free end remains in the same direction. The magnetic field is then decreased until the instability is reached wherein the free end abruptly rotates to the opposite direction.

#### **Results**

The cylindrical ferrogel actuators show a torsional deformation (Figure 1A) that translates into a chiral twisted state. Moreover, the actuators showed two types of instabilities induced by the mechanical rotation of the base of the composite (Figure 1B) or reducing the magnetic field in a twisted state (Figure 1C). The theory of their response to magnetic fields predicts their detailed deformation, as well as the existence of nonequilibrium, metastable states, and the existence of instabilities as we see experimentally. The experimental results of the actuation are in good agreement with the theoretical model in most cases, including the angles at which the instabilities occur. However, SIPNs show some discrepancies that are explained by the overestimation of the susceptibility anisotropy in these composites. Field-induced instabilities are experimentally observed, but the discrepancy between the model and the experiment is tangible because of the technical difficulties in performing these types of experiments.

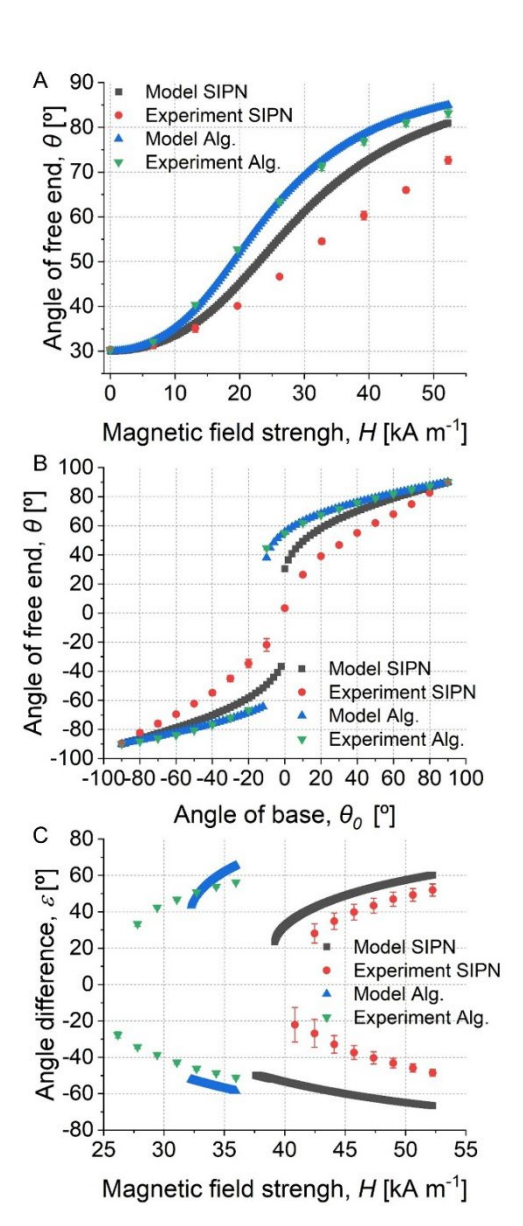


Figure 1. A) Torsional deformation (base at 30°). B) Mechanically induced instability. C) Field-induced instability ( $\varepsilon = \theta \pm \theta_0$ ). Figure adapted from [3], under CC BY-NC 4.0 license.

#### **Acknowledgments**

This study was supported by the grant PID2023-151913NB-I00 funded by MICIU/AEI/10.13039/501100011033, Spain, and by ERDF, EU.

- [1] Leon-Cecilla, A. et al. Int. J. Biol. Macromol. **260**:129368 (2024)
- [2] Vazquez-Perez, F. J. et al. ACS Appl. Mater. Interfaces, **15**(45):53017–53030 (2023)
- [3] Vazquez-Perez, F. J., Leon-Cecilla, A. et al. Adv. Funct. Mater. e15721 (2025). DOI: 10.1002/adfm.202515721

# harmoMPI: Phantoms for Harmonizing Magnetic Particle Imaging Across Global Scanner Systems

Marcus Löffler<sup>1</sup>, Bruno Kluwe<sup>2</sup>, Christian Fiedler<sup>1</sup>, Frank Wiekhorst<sup>2</sup>, Silvio Dutz<sup>1,3</sup>

Magnetic particle imaging (MPI) is a promising tracer-based tool in medical diagnostics [1]. In the past, different hardware, such as a single-sided MPI scanner or head-sized devices, was built. Different reconstruction methods, like the common system matrix approach or the x-space theory of projection, exist. Use cases in the fields of angiography, cell tracking, or cancer treatment have been explored [2, 31. To test and quantify these techniques, different scanner specific phantoms were used [4, 5]. To enable a consistent comparison and to harmonize between these different MPI developments, scanner independent specific phantoms and operation recommendations are mandatory.

Therefore, we designed a workflow based on literature, tests, and the experience of the research community. The workflow includes the development of static-flow-and physiological phantoms as well as a planning tool to determine the optimal scanner configuration for a given problem.

The planning tool should further enhance the efficiency of experiment planning, support quality assurance, and minimize unnecessary animal testing by reducing trial-and-error approaches.

The workflow incorporates the continuous feedback of the interested MPI research community. For the first iteration, we developed a straightforward static test obiect and segmented a vessel structure to print a physiological phantom shown in figure one. We use the 3D printed test object to compare the Revopoint MINI 3D Scanner, a photometric method, and a tactile measurement method for quantifying geometry, and enable quality assurance in terms of printed geometry sizes. The obtained information is used to assess the accuracy of MPI measurements using the developed phantoms, enabling consistent comparisons between different MPI techniques and approaches.

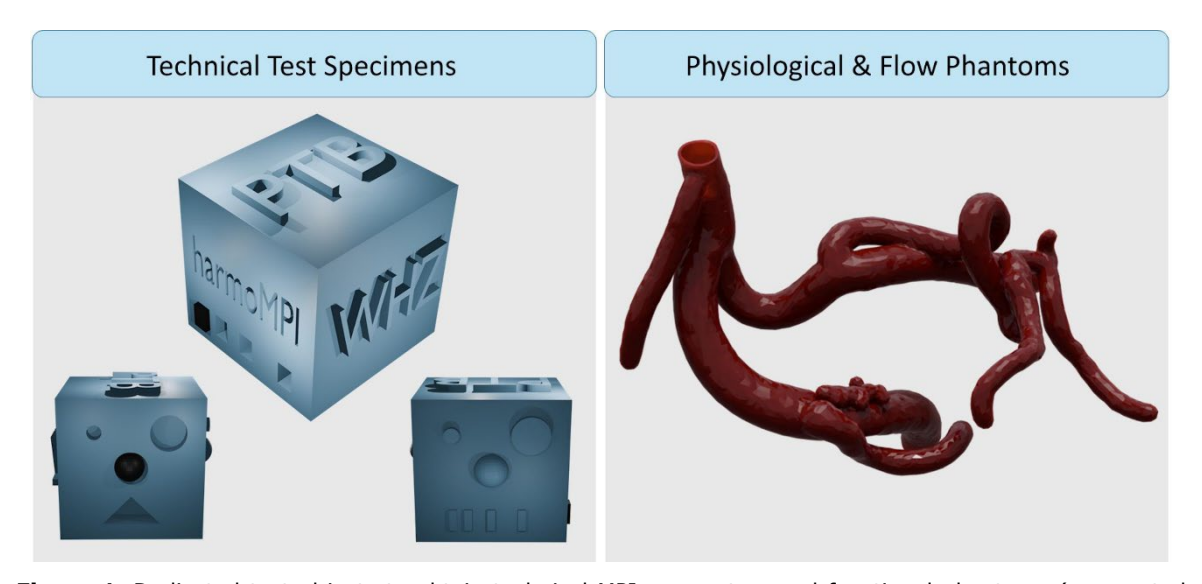


**Figure 1.** Dedicated test objects to obtain technical MPI parameters and functional phantoms (segmented vessel phantom) to provide controlled physiological conditions.

<sup>&</sup>lt;sup>1</sup> University of Applied Science Zwickau, Zwickau, Germany, Faculty of Physical Engineering/Computer Sciences

<sup>&</sup>lt;sup>2</sup> Physikalisch-Technische Bundesanstalt, Berlin, Germany

<sup>&</sup>lt;sup>3</sup> Technische Universität Ilmenau, Institute of Biomedical Engineering and Informatics, Ilmenau, Germany

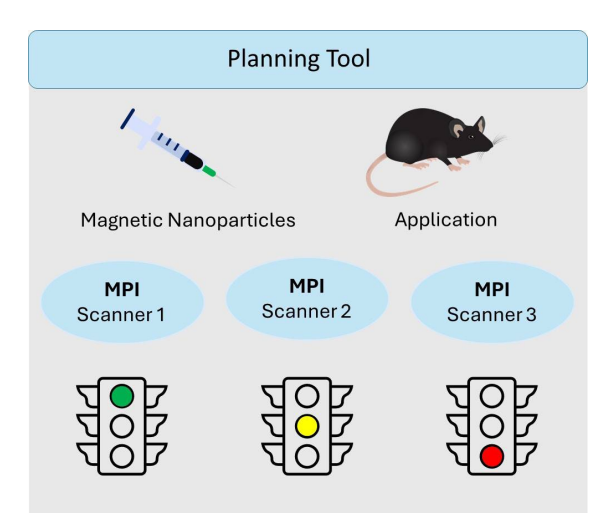


**Figure 2.** Schematic of the planning tool to be developed to enable assessing of the success of envisaged MPI investigations.

#### **Acknowledgments**

This work was funded by the DFG project "harmoMPI: Harmonization of quantitative Magnetic Particle Imaging by scanner-specific, functional phantoms" (project no 540326102).

- [1] N. Löwa, J.-M. Fabert, D. Gutkelch, H. Paysen, O. Kosch, und F. Wiekhorst, "3D-printing of novel magnetic composites based on magnetic nanoparticles and photopolymers", *Journal of Magnetism and Magnetic Materials*, Bd. 469, S. 456–460, Jan. 2019, doi: 10.1016/j.jmmm.2018.08.073.
- [2] A. Remmo, O. Kosch, L. Kampen, A. Ludwig, F. Wiekhorst, und N. Löwa, "Counting cells in motion by quantitative real-time magnetic particle imaging", *Sci Rep*, Bd. 14, Nr. 1, S. 4253, Feb. 2024, doi: 10.1038/s41598-024-54784-5.
- [3] E. U. Saritas u. a., "Magnetic Particle Imaging (MPI) for NMR and MRI researchers", Journal of Magnetic Resonance, Bd. 229, S. 116–126, Apr. 2013, doi: 10.1016/j.jmr.2012.11.029.
- [4] H. Bagheri u. a., "A mechanically driven magnetic particle imaging scanner", Applied Physics Letters, Bd. 113, Nr. 18, S. 183703, Okt. 2018, doi: 10.1063/1.5052646.
- [5] N. Löwa, J.-M. Fabert, D. Gutkelch, H. Paysen, O. Kosch, und F. Wiekhorst, "3D-printing of novel magnetic composites based on magnetic nanoparticles and photopolymers", *Journal of Magnetism and Magnetic Materials*, Bd. 469, S. 456–460, Jan. 2019, doi: 10.1016/j.jmmm.2018.08.073.

# Influence of microstructure on magnetic properties of anisotropic magnetic elastomers

N. Magin, D. Borin, S. Odenbach

Chair of Magnetofluiddynamics, Measuring and Automation Technology, TU Dresden, 01069 Dresden, Germany

#### **Introduction and Objectives**

Composites based on magnetic particles and an elastic polymer matrix are called magnetic elastomers. Depending on the size and concentration of magnetic particles and the elasticity of the matrix, such materials can have a significant magnetorheological (MR) effect and are traditionally referred to as MR elastomers [1]. Regardless of the above parameters and the magnitude of the MR effect, the presence of a magnetic component makes such composites magnetically sensitive. The application of an external homogeneous magnetic field during the polymerisation process makes it possible to obtain anisotropic material due to the structuring of particles in the initially liquid polymer matrix. It is obvious that the induced anisotropy significantly changes the magneto-mechanical response of composites to an external magnetic field. Recently, the influence of the mutual orientation of particle aggregates and the external magnetic field applied during magneto-mechanical tests on the macroscopic mechanical properties of MR elastomers was systematically investigated, see e.g. [2,3]. At the same time, the known results of measuring magnetisation curves and determining the corresponding magnetic properties of magnetic elastomers depending on the mutual orientation of particle structures and the external field in the experiment are extremely limited. The known publications consider parallel and perpendicular orientations only [4,5]. On the other hand, varying the concentration of magnetic filler and the magnitude of the magnetic field applied during material crosslinking makes it possible to obtain a composite with different morphology of particle aggregates, see e.g. [6]. However, the relationship between the morphology of particle aggregates and

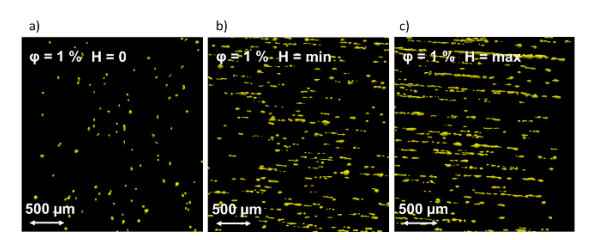
the macroscopic properties of the material has not been sufficiently investigated to date. The question of the influence of the spatial orientation of different particle structures relative to the direction of the magnetic field applied in the experiment remains open. Accordingly, this study examines the influence of the angle between the direction of particle aggregates of different morphologies and the direction of the field applied during magnetic measurements on the macroscopic material response. Measurements of the magnetic characteristics of various composite samples are accompanied by microstructural studies.

#### **Material and Methodology**

The study examines elastomeric composite samples based on two-component polydimethylsiloxane matrix (silicone and crosslinker NEUKASIEL RTV 230 and A149). Sigma-Aldrich iron powder with a particle average diameter of 44 µm are used as magnetic filler. The specimens are fabricated by mechanical mixing of all components, vacuum degassing and crosslinking at room temperature. The structuring magnetic field is provided by the electromagnet of a vibrating sample magnetometer (Lake Shore VSM 7407s), which is further used for magnetic measurements. The spatial orientation of particle structures relative to the direction of the external field in magnetic measurements was changed by rotating the VSM rod with the sample holder around the vertical axis. Microstructural investigations are conducted using the own laboratory X-Ray microtomography setup and reconstruction process is performed calculating a three-dimensional model from the individual radiographs with a software package developed in house [7].

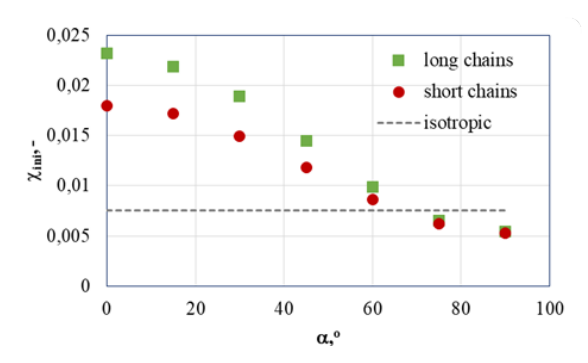
#### **Results and Discussion**

Figure 1 shows visualization of the different internal microstructure of a magnetic elastomer with the same microparticle content. A composite with short chains formed by structuring in a low (<100 mT) magnetic field (b) and a composite with long chains formed by structuring in a high magnetic field (>1T) (c) are shown next to the isotropic sample (a).



**Figure 1:** Microstructure of specimens with  $\sim 0.13$  vol.% particles in VSM specimen holder: a) isotropic composite, b) short chain composite, c) long chain composite

Figure 2 shows the dependence of the initial magnetic susceptibility  $X_{\text{ini}}$  on the tilt angle of the particles  $\alpha$  relative to the direction of the magnetic field applied during the magnetic measurements. The values of  $X_{\text{ini}}$  are obtained from the magnetization curves of these samples. The smaller the tilt angle of chain aggregates relative to the applied field, the higher the initial magnetic susceptibility.



**Figure 2:** Initial magnetic susceptibility of samples with  $\sim 0.13$  vol.% particles as a function of the angle of spatial orientation of particle chains relative to the external magnetic field.

The composite with long chains has the highest susceptibility. At higher tilt angle  $(a>60^{\circ})$ , the susceptibility of anisotropic

composites is comparable to that of isotropic material. The obtained results are obviously related to the demagnetizing factor of chain aggregates and its variation with the change of the tilt angle of the chains. It should also be noted that a similar trend is observed for filled composites (~10 vol.%) with thick clusters and/or network-like aggregates of particles, i.e. composites with a morphology fundamentally different from individual chains.

#### **Summary and outlook**

The morphology of the structures of magnetic microparticles and their orientation relative to the external field has a significant influence on the magnetic properties of anisotropic magnetic elastomers.

#### **Acknowledgment**

We thank the Deutsche Forschungsgemeinschaft (German Research Foundation, DFG) for support through the Research Unit FOR 5599 on structured magnetic elastomers, project no. 511114185, via DFG grant reference no. OD 18/35-1.

- [1] Wereley N. (ed.), Magnetorheology, RSC Publishing, Cambridge, 2014.
- [2] Yao J. et al. Magnetorheological elastomers with particle chain orientation: modelling and experiments. Smart Mater. Struct. 2019; 28, 095008.
- [3] Wang L. et al. Magneto-mechanical properties of anisotropic magnetorheological elastomers with tilt angle of magnetic chain under compression mode. J. Magn. Magn. Mater. 2023; 570, 170441.
- [4] Stepanov G.V. et al. Motion of ferroparticles inside the polymeric matrix in magnetoactive elastomers. J. Phys. Condens. Matter, 2008; 20, 204121.
- [5] Borin D., Odenbach S. Initial magnetic susceptibility of the diluted magnetopolymer elastic composites. J. Magn. Magn. Mater. 2017; 431, 115-119.
- [6] Borin D. Targeted patterning of magnetic microparticles in a polymer composite. Phil. Trans. R. Soc. A 2020; 378: 20190256.
- [7] Borin D., Odenbach S. in Magnetic Soft Matter, ed. J. de Vicente, The Royal Society of Chemistry, 2023, ch. 8, pp. 213-228.

# Application of the Scharr edge detection algorithm for microstructure assessment of magnetic composites

N. Magin, S. Odenbach

Chair of Magnetofluiddynamics, Measuring and Automation Technology, TU Dresden, 01069 Dresden, Germany

#### **Introduction and Objectives**

The microstructure of magnetic composites exerts a significant influence on properties including the MR effect and initial magnetization. Conducting a precise analysis of the microstructure is therefore of paramount importance. Following the imaging of the structure of a magnetic composite, for instance by means of X-ray computed tomography, the resulting data is typically displayed as a binary image. One methodology for achieving this objective would be to implement the thresholding technique subsequent to the denoising process. However, it should be noted that if the threshold value is set too high, there is a risk of losing information about the extent of the features [1]. In order to achieve this objective, it is advantageous to employ the Scharr operator for the purpose of edge detection, thereby facilitating the acquisition of a more precise representation of the microstructure. The Scharr operator is a gradient-based method for edge detection. In comparison to alternative boundary detection operators, this method demonstrates superior performance in the presence of noise and exhibits rotational invariance [2].

#### **Material and Methodology**

The focus of the study is the microstructure of elastomeric composite samples based on a two-component polydimethylsiloxane matrix (silicone and crosslinker NEUKASIEL RTV 230 and A149). Sigma-Aldrich iron powder, with a particle average diameter of 44 µm and spherical particles of BASF SP-I with a diameter of 5-8 µm is used as a magnetic filler. The specimens are fabricated by mechanical mixing all components, followed by vacuum degassing and crosslinking at room temperature. A vibrating sample magnetometer (Lake Shore VSM 7407s) is used to provide a magnetic field for the struc-

turing of some of the samples. The investigation of microstructural properties is conducted through the utilisation of the in-house laboratory X-ray microtomography apparatus. Subsequent to this, a three-dimensional model is reconstructed and X-ray artefacts are corrected from the individual radiographs using a software package developed in-house [3]. The microstructure is then examined using a self-developed algorithm that uses the Scharr filter to determine the edges between the sample holder and the matrix, as well as between the matrix and the particles. The image is then subjected to a denoising process that involves the application of a filter. This results in the conversion of the image into a binary format, achieved by the implementation of a threshold. Subsequently, a three-dimensional examination of the particles is possible for properties such as size and orientation.

#### **Results and Discussion**

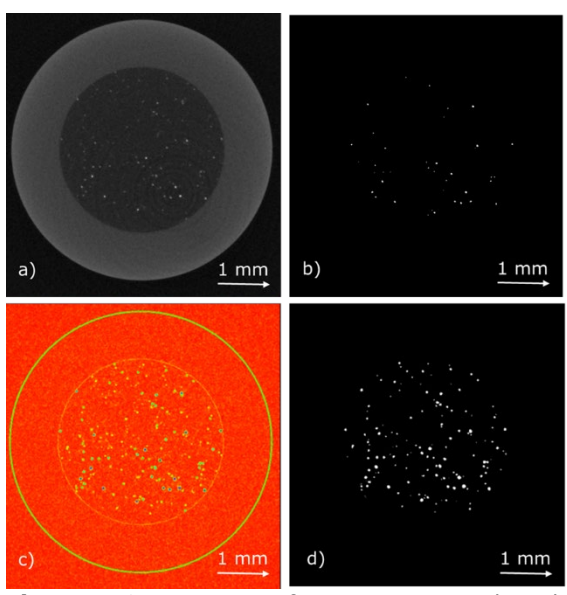


**Figure 1:** Cross-section of an isotropic sample with  $\sim 0.13$  vol.% in a sample holder a) reconstructed and artifact-cleaned, b) after application of a threshold, c) after application of Scharr edge detection algorithm, d) isolated particles as the end result.

As illustrated in Figure 1a, a cross-section through the centre of a reconstructed and artifact-cleaned isotropic sample is presented. The application of a threshold with the lowest possible threshold value produces Figure 1b. Conversely, the application of the edge detection sharpening operator, as demonstrated in Figure 1c, has been shown to result in a more accurate reproduction of the structure of individual particles. This is particularly evident when directly comparing Figure 1d, which was binarized from Figure 1c, with Figure 1b, the binary image without edge detection. However, due to the high spatial resolution of the particles achieved in this way, the artefacts caused by X-ray computed tomography, such as ring artefacts, are also strongly accentuated and must be corrected beforehand. However, the potential disadvantages are mitigated by the improvements observed.

#### **Summary and outlook**

As evidenced by the research, the implementation of an edge detection algorithm results in a significant enhancement of the process of particle detection for isotropic samples. Evidence regarding the use of structured samples will be presented subsequently.

#### **Acknowledgment**

We thank the Deutsche Forschungsgemeinschaft (German Research Foundation, DFG) for support through the Research Unit FOR 5599 on structured magnetic elastomers, project no. 511114185, via DFG grant reference no. OD 18/35-1.

- [1] Siebert, J. M. U., Odenbach, S. Transport in Porous Media 151.7 (2024):1607-1626.
- [2] Weickert, J., Scharr, H. Journal of Visual Communication and Image Representation 13.1-2 (2002): 103-118.
- [3] Borin D., Odenbach S. in Magnetic Soft Matter, ed. J. de Vicente, The Royal Society of Chemistry, 2023, ch. 8, pp. 213-228.

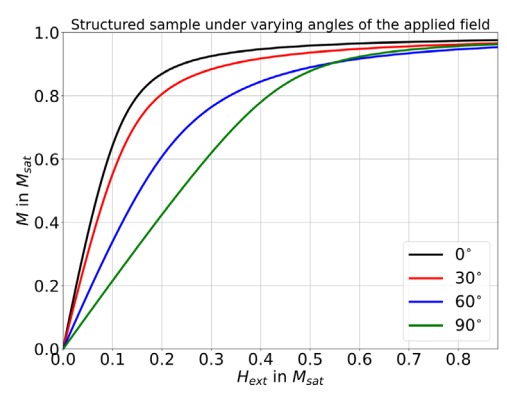
# Structured magneto-active elastomers under inclined fields and an approximation for the nearfield effect in particle clusters

### P. Patel, M. Saphiannikova, D. Romeis

Leibniz-Institut für Polymerforschung Dresden e.V., Hohe Straße 6, 01069 Dresden

In our research we address magnetoactive elastomers (MAEs) as composites of magnetically soft particles embedded inside an elastic matrix. In the course of manufacturing, basically two different types of such MAEs can be distinguished: unstructured samples prepared without any magnetic field during the matrix curing, leading usually to an isotropic, or random, distribution of particles in the matrix. And structured samples that are cured under a magnetic field, which leads to a columnar- or chain-like particle structure that is aligned along the curing magnetic field. To describe the difference in the magnetization behavior between structured and unstructured samples, we developed an effective magnetization approach. It turns out that in the limit of infinite magnetic susceptibility the effective magnetization approach resembles the theory by J.J. Abbott et al. [2] for non-spherically shaped samples of soft-magnetic bulk material in external magnetic field. In comparison with corresponding measurements of the magnetization behavior of structured MAE samples at different angles of the applied magnetic field we can prove now that our approach represents a generalization of the theory [2]. Our approach allows to describe the effect of sample shape and inscribed particle microstructure simultaneously for arbitrary magnetization functions or material parameters, i.e., for finite magnetic susceptibility. The agreement with the experiment is very convincing, although the effective magnetization approach, so far, relies on the dipole approximation for the magnetic interactions among the particles. In highly filled samples, as well as in structured MAEs, the particles are often very close to each other. In such situation the dipole approximation underestimates the interactions among magnetizable objects. Yet, for only 2 spherical particles

the analytic solution is quite complex, resulting in a slowly converging series expansion. When considering many particle systems only computationally elaborate methods like a Finite Element Approach can provide numerical solutions. Based on a more compact generic function for the 2-body problem presented in [3], we suggest a mean-field approximation for many-body systems including the near-field effect in a similar fashion as



we developed our cascading mean-field approach for pure dipole interactions previously [4]. Using further simplifications, a correction factor to our dipole formulation for effective particle concentrations is obtained. Considering these corrections due to the near-field effect, we further investigate the role of cluster formation and dispersion of particles in initially isotropic MAE samples as the applied magnetic field is either increasing or decreasing. The thereby described hysteresis effect in elastically ultrasoft samples is analyzed in more detail.

#### **Acknowledgments**

Financial support by German Research Foundation (DFG) via research projects 380321452/GRK2430 and RO6756/3-1 is gratefully acknowledged.

#### References

- [1] D. Romeis, M. Saphiannikova. Effective magnetic susceptibility in magnetoactive composites.
  - J. Magn. Magn. Mat. **565**: 170197 (2023).
- J.J. Abbott et.al.. Modeling magnetic torque and force for controlled manipulation of softmagnetic bodies.
   IEEE Trans. Robot. 23: 1247 (2007).
- [3] A.M. Biller, O.V. Stolbov, Y.L. Raikher. Modeling of particle interactions in magnetorheological elastomers.
  - J. Appl. Phys. **116**: 114904 (2014).
- [4] D. Romeis, M. Saphiannikova. A cascading mean-field approach to the calculation of magnetization fields in magnetoactive elastomers.

Polymers 13: 1372 (2021)

# Micromagnetic Simulations of Magneto-Plasmonic Nano-Objects with Tunable Domain Architectures

### M. Raphael, A. M. Schmidt

Institute for Light and Matter, Department for Chemistry and Biochemistry, University of Cologne, Cologne, Germany

#### **Background and Motivation**

Magnetic nanoparticles (MNPs), particularly those based on ferrites, are of growing interest for a wide range of applications including actuation, hyperthermia, and smart materials. [1,2] Recent advances have focused on combining magnetic and plasmonic domains into single nanostructures to enable multifunctional behavior at the nanoscale, accelerated by promising property combinations. [3,4]

We have developed a modular synthetic approach to anisotropic  $Pt-[CoFe_2O_4]_z$  (= CF-z) nanostructures with well-defined geometry and tunable domain number.

The systematic variation of precursor composition, surfactant concentration, and seed-to-precursor ratio enabled precise control over the number, size, and geometry of CoFe<sub>2</sub>O<sub>4</sub> domains on Pt nanocubes (Figure 1). This structural modulation translated directly into tunable magnetic properties, including shifts in saturation magnetization, remanence, and interdomain coupling. By establishing a robust heteroepitaxial interface with minimal lattice mismatch, we ensured consistent and anisotropic growth. The resulting hybrid nanostructures demonstrate a clear structure-function relationship, wherein nanoscale architectural design governs collective magnetic behavior.

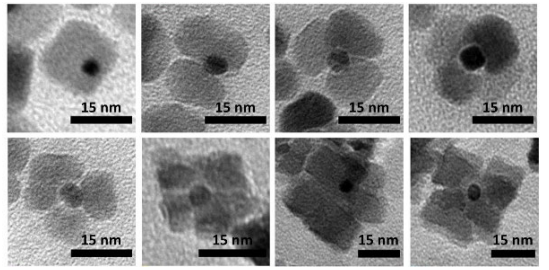


**Figure 1.** TEM images of CF-z nanoparticles with z = 1 to z = 8 CFO moieties.

Due to their lattice-matched interfaces and spacing, these complex nano-objects present an ideal system to study domain interaction and programmable magnetic response based on geometric design in low dimensions.

This framework paves the way for engineered magnetic-plasmonic systems for future applications in nanoscale motion control, field-guided self-assembly, and magnetic sensing platforms.

#### **Object symmetry**

Nano-objects with a central cuboidal Pt core and a predetermined number of corner-attached CoFe<sub>2</sub>O<sub>4</sub> cuboids display interesting symmetry properties. In particular, CF-1 objects are characterized by a C<sub>3</sub> axis formed by the Pt-CoFe<sub>2</sub>O<sub>4</sub> connection. However, the preferred magnetization direction (easy axis) of the CoFe<sub>2</sub>O<sub>4</sub> cuboid is unlikely to match this symmetry axis: Considerations of the CoFe<sub>2</sub>O<sub>4</sub> anisotropy lead to magnetically easy axes in (1,0,0) direction, thus perpendicular to the cuboids faces and thus three equivalent and perpendicular axes for each individual cuboid. For CF-1 objects, this leads to a symmetry break and an expected angle between geometric axis and magnetic axis of 54.74° (magic angle). In other geometries of interest, in particular, CF-3 (trigonal-pyramidal, C<sub>3</sub> point group) and CF-8 (supercube cuboid group), the prediction of the magnetization axes and their orientation with respect to the object symmetry is even more complex. E. g., for the CF-3 system, 38 different configurations of the magnetization axes within the three cuboids can be identified.

#### Methodology

To gain a deeper understanding of the micromagnetic interactions within the cobalt ferrite cubes in such magnetic nanoobjects, micromagnetic simulations using MuMax3 are conducted. Therefore, we

employed the fundamental magnetic properties such as anisotropy constants (exchange constant  $A_{\rm ex}=1.2\cdot 10^{-11}~{\rm J\cdot m^{-1}}$ , saturation magnetization  $M_{\rm s}=5.0\cdot 10^5~{\rm A\cdot m^{-1}}$ , cubic anisotropy constants  $K_1=3.0\cdot 10^5~{\rm J\cdot m^{-3}}$  and  $K_2=-7.0\cdot 10^5~{\rm J\cdot m^{-3}}$  [5–7]) in a simulation box comprising a single object, and obtained the minimized micromagnetic state by using the deepest descent method.

Starting point for the CF-3 simulations are the  $6^3 = 216$  different configurations of the cuboids' magnetic moments in the arrangement. We realize that a total of 16 distinct energy levels between 1.17 10<sup>-18</sup> J and 1.38 10<sup>-18</sup> J can be identified (Figure 2). At ambient temperature, Boltzmann statistics reveal over 98 % of the total population is expected to be in the ground state, represented by two of the 38 unique starting configurations. In this state, the magnetization of two cubes is oriented oppositely, while the third cube adopts an orthogonal orientation, enabling a minimization of the total external magnetization (Figure 3) approximately equivalent to that of a single cube. Again, the angle between geometric axis and net magnetization direction is 54,74 ° under these conditions.

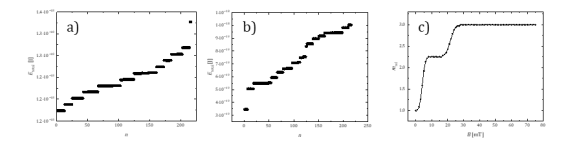


**Figure 2.** Variation of total energy  $(E_{\rm total})$  across all 216 states, a) without magnetic field, b) in a magnetic field of 75 mT, magnetic moment of the CF-3 nano-objects in dependence of the magnetic field.

To investigate the influence of an external magnetic field, simulations are performed under varied magnetic field strength up to 75 mT, oriented along the net magnetic moment of the particle system. The energetically most favorable state is field dependent, and already at a few mT, the Zeeman energy results in an increased relative total magnetic moment of the objects (Figure 2c). In an external field of about 30 mT or higher, the cuboids' magnetization is likely to be parallelly ori-

ented. Again, the angle between the geometric axis and the magnetization orientation is the magic angle of 54.74°. The relative net magnetization now corresponds to the parallel arrangement of all three domains, and the energy distance to the next state is much larger than in the field-free state (**Figure 2b**). At intermediate field strengths, a third configuration is observed to be dominant (**Figure 3**), with a relative net magnetic moment equivalent to that of 2.25 CoFe<sub>2</sub>O<sub>4</sub> cubes.

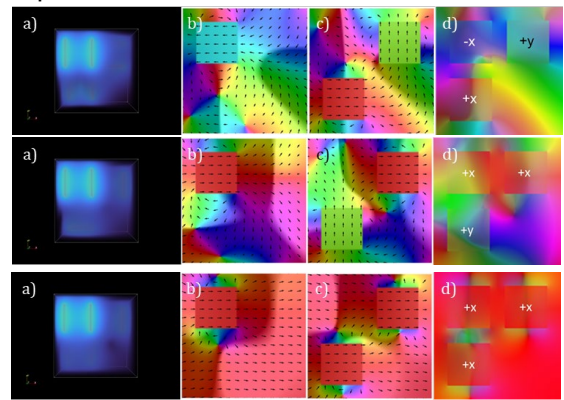


**Figure 3.** MuMax3 simulation results of the a) demagnetization and b)-d) magnetization fields passing through b) the front cube, c) the back cubes, and d) the full voilume of a single CF-3 particle of the lowest energy states in (upper) absence of, (middle) the presence of an external magnetic field of 10 mT and (lower) 75 mT.

- [1] B. Costa, E. Pereira, V. C. Ferreira-filho, A. S. Pires, L. C. J. Pereira, P. I. P. Soares, M. F. Botelho, F. Mendes, M. P. F. Graça, S. S. Teixeira, *Pharmaceutics* 2025, *17*, 1.
- [2] M. Vassallo, D. Martella, G. Barrera, F. Celegato, M. Coïsson, R. Ferrero, E. S. Olivetti, A. Troia, H. Sözeri, C. Parmeggiani, D. S. Wiersma, P. Tiberto, A. Manzin, ACS Omega 2023, 8, 2143.
- [3] B. Muzzi, M. Albino, A. Gabbani, A. Omelyanchik, E. Kozenkova, M. Petrecca, C. Innocenti, E. Balica, A. Lavacchi, F. Scavone, C. Anceschi, G. Petrucci, A. Ibarra, A. Laurenzana, F. Pineider, V. Rodionova, C. Sangregorio, ACS Applied Materials and Interfaces 2022, 14, 29087.
- [4] L. León Félix, J. A. H. Coaquira, M. A. R. Martínez, G. F. Goya, J. Mantilla, M. H. Sousa, L. D. L. S. Valladares, C. H. W. Barnes, P. C. Morais, Scientific Reports 2017, 7, 1.
- [5] A. Franco, F. C. E Silva, *Applied Physics Letters* 2010, *96*, DOI 10.1063/1.3422478.
- [6] G. Sheet, A. R. Cunliffe, E. J. Offerman, C. M. Folkman, C. B. Eom, V. Chandrasekhar, Journal of Applied Physics 2010, 107, DOI 10.1063/1.3393745.
- [7] R. Perthel, G. Elbinger, W. Keilig, *Physica Status Solidi (B)* 1966, *17*, 151.

## Tailoring Magnet Setups for Field Homogeneity: An Interactive GUI for Design and Exploration

I. Rehberg<sup>1</sup>, P. Blümler<sup>2</sup>

#### Introduction

Special arrangements of permanent magnets along a ring yield an almost homogeneous field useful for applications [1]. A dipole orientation  $\alpha=2\varphi$ , as originally introduced for extended magnetic rods [2], yields a reasonable amount of homogeneity even for such finite-size magnets as shown in Fig. 1. A slight modification of this arrangement in the plane, namely

$$\tan\alpha = \frac{3\sin(2\varphi)}{6\cos^2\varphi - 2},\tag{1}$$

optimizes the field strength [3] and increases its homogeneity [4]. Adapting this approach to the third dimension leads to so-called focussed configurations [4].



Figure 1. Sixteen neodymium 1 cm<sup>3</sup> cubes form a prototype used for the focussed configuration measurements in [4].

#### **Methods**

An open-source Python script supports interactive exploration of the findings of Ref. [4]. It provides a graphical user interface (GUI) available for download to aid the design of novel experimental arrangements [5]. This presentation indicates some of the capabilities of that GUI.

#### **Results for Rings and Sandwiches**

In the following, screenshots from [5] highlight five key results of [4].

- **Halbach Rings:** If built of *N* infinitely long rods the centre field forms a saddle point of order *N* shown in Fig. 2.

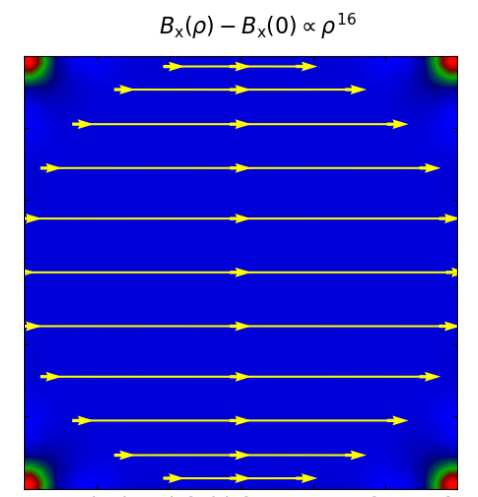


Figure 2. Calculated field for a ring of 16 infinitely long rods. The extreme flatness means that a change is only visible at the largest distance from the centre, the 4 corners.

- **Finite-size magnets:** For cuboids, disks, spheres, and other finite-size shapes, the field changes generically with the second power, e.g. Fig. 3.

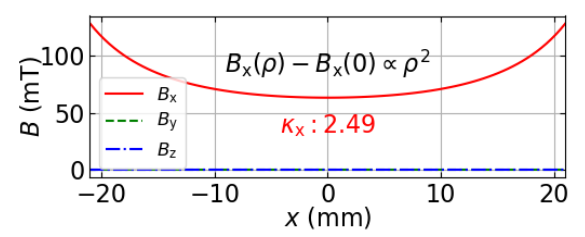


Figure 3. The change of the fields with the distance from the centre.

- **Tilt:** Allowing for a tilt (Fig. 4) of the magnets with respect to their ring planes focusses the field to finite distances from that ring, a feature useful for single-sided NMR and other applications.

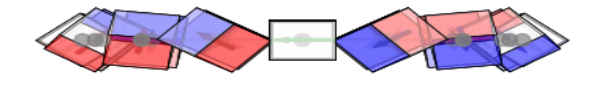


Figure 4. Side view of tilted cuboids located along a ring.

<sup>&</sup>lt;sup>1</sup> Institute of Physics, University of Bayreuth

<sup>&</sup>lt;sup>2</sup> Institute of Physics, Johannes Gutenberg-Universität Mainz

- **Singular arrangements:** At singular heights of a stacked (sandwich, see Fig. 5) ring configuration, the centre field might achieve a quartic (flat) maximum.

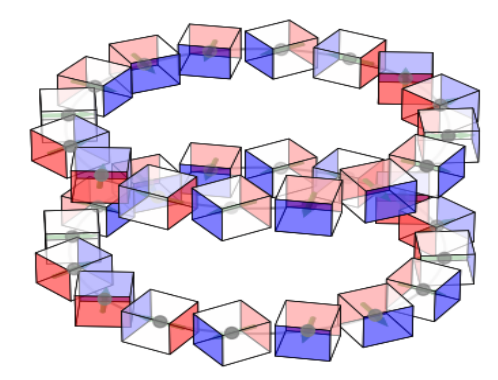


Figure 5. A sandwich construction of two planar rings.

- **Twist:** To achieve the circular homogeneity desirable for imaging applications, a twisted sandwich is helpful (Fig. 6).

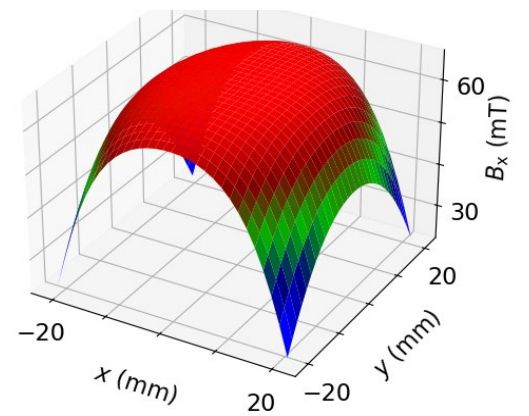


Figure 6. The strength of  $B_{\scriptscriptstyle X}$  forms a quartic maximum here due to a suitable twist in a stack of two rings.

# Annular and Spherical Arrangements: Outlook

Another interactive tool for designing magnet distributions to achieve homogeneous fields experimentally will be available in the updated version of the GUI [5]. Based on the theory for continuous distributions of magnetization for both annular disks and spherical shells it allows estimating the field on a percentage level with a compact analytic formula and an interactive modification of the inner and outer diameter of the annular disk. Figure 7 illustrates, e.g., that one cannot afford an inner radius R<sub>in</sub> which is larger than the height of the magnets h, to obtain field strengths of 50 % of the remanence Br of the magnets.

In contrast to this restriction, spherical distributions produce fields that diverge logarithmically with the outer radius  $R_{\rm out}$  of the spherical shell. A practical approach to optimized spherical distributions of magnetization is to arrange magnets at the vertices of Platonic solids.

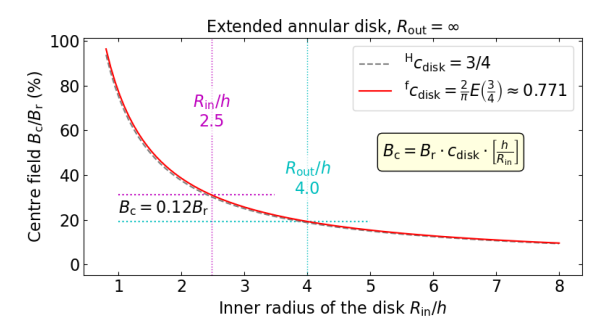


Figure 7.The field stemming from a continuous distribution of magnetization on an infinite annular disk following either the Halbach (grey dashed) or the focussed orientation (red solid line). Screenshot from an update of [5].

Focussing onto the origin yields the configuration with the largest field [4]. Version 2.1.1 of the *Dipole Cluster Inspector* visualizes the orientations and fields for all Platonic and Archimedean solids [6].

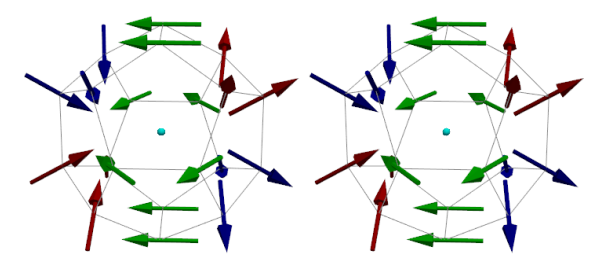


Figure 8. A stereoscopic image of the magnetic dipoles arranged at the vertices of a dodecahedron and set in the focussing orientation. Screenshot from an update of [6].

- [1] Blümler, P. (2021). Magnetic Guiding with Permanent Magnets: Concept, Realization and Applications to Nanoparticles and Cells. Cells 10, 2708. https://doi.org/10.3390/cells10102708
- [2] Halbach, K. (1980). Design of permanent multipole magnets with oriented rare earth cobalt material. <u>Nucl. Instrum. Methods</u> 169, 1–10.
- [3] Zijlstra, H. (1985). Permanent Magnet Systems for NMR Tomography. <u>Philips J. Res.</u> 40, 259–288.
- [4] Rehberg, I. and Blümler, P. (2025). Analytic approach to creating homogeneous fields with finite-size magnets. <a href="https://pex.eps.123">Phys. Rev. Appl. 23</a>, 064029.
- [5] Rehberg, I. and Blümler, P. (2025). Hal-bach\_two\_point\_oh: Optimize Uniform Fields with Permanent Magnets (V2.0.0). Zenodo. https://doi.org/10.5281/zenodo.16322091.
- [6] Rehberg, I. (2025). Dipole Cluster Inspector A Duty-Free Python GUI for Exploring 569 Dipole Clusters (V2.1.0). Zenodo. https://doi.org/10.5281/zenodo.10084573.

## Ferrofluidic gears and seals for space applications

# Y. Remane, S. Hestermann, A. Wagner, M. Ehresmann, G. Herdrich

Institute of Space Systems, University of Stuttgart

Ferrofluid and magnetic-based technology may be a unique opportunity for solving challenges in space systems, especially in mechanisms exposed to dusty and vacuum environments. Their self-healing and magnetically controllable characteristics set them up to be uniquely suitable as a replacement for conventional tribological components in gears and seals. Compared to traditional solutions, ferrofluidic systems offer lower wear and improved reliability, especially for long-duration missions where maintenance is impractical [4].

#### Ferrofluidic seals

At the Institute of Space Systems, University of Stuttgart, ongoing research currently focuses on ferrofluid-based sealing and torque transmission concepts for space-relevant applications. Coming from already existing earth applications, e.g. vacuum chambers, a preliminary modular ferrofluidic pressure seal has been developed and tested for use in astronautical systems, such as wrist disconnects in extravehicular activity (EVA) suits. This design employs ferrofluid to form atomically tight, dust-repelling seals capable of quasi-frictionless rotation and sustaining pressure differentials exceeding 30 kPa per barrier [2].

Dust contamination poses a critical threat to spacesuit integrity, particularly in lunar environments where abrasive regolith (e.g. lunar dust) rapidly degrades conventional rubber seals or metal gaskets. The proposed ferrofluidic sealing concept leverages the self-healing capability of ferrofluids and their selective particle rejection due to internal magnetic pressure [5]. Experimental campaigns using NdFeB magnets and two ferrofluid types, EFH-1 and J12, demonstrated that EFH-1, with higher magnetic susceptibility, achieved a maximum pressure differential of 30.11 kPa, while J12, with higher viscosity,

reached 15.70 kPa. This appears to be strongly correlated to the maximum magnetic saturation of the utilized ferrofluid. Pressure retention tests confirmed that higher viscosity provides more controlled leakage in failure scenarios, reducing contamination risk.

Due to limited magnet resources, configuration trials identified a staggered axial arrangement as optimal for forming multiple radial seal barriers. In regolith resilience tests using a lunar mare simulant, including high-magnetic-content fractions, no particle ingress was detected after prolonged mechanical agitation. The seals maintained integrity even under heavy particulate loading, while trapped particles at the interface reinforced the sealing effect.

A modular wrist disconnect was developed to integrate ferrofluid reservoirs and bayonet fasteners, meeting ergonomic, sealing, and operational requirements. This configuration enables easy attachment and removal, allows for the inspection and replenishment of ferrofluid, and ensures long-term operational performance. These results support the feasibility of ferrofluidic seals for future lunar missions, offering enhanced durability, pressure retention, and resistance to particulate contamination [2].

#### Ferrofluidic gears

Alongside sealing technologies, research is being conducted on ferrofluidic gear systems for space actuation applications. These designs utilize magnetic coupling and ferrofluid-wetted bearings to transmit torque without direct mechanical contact, or with ferrofluid serving as a magnetic bridge to enhance coupling efficiency due to increased magnetic permeability. In the case of spur gears, radially outward-facing Halbach arrays are particularly advantageous for such couplings, as they increase the effective magnetic field range

and improve torque transfer across the gap. While at the same time, the unused "inner" side of the gear sees minimal magnetic fields. This approach can be applied to all other examined gear types. For gear bearings mostly ring magnets are used. The ferrofluid layer naturally selfdistributes within the available magnetic potential field, forming near-perfect circularity in toroidal or ring magnet arrangements. This behavior not only contributes to uniform load distribution but also improves the vibration profile of rotating components, which can be useful to optimize dynamic performance. By eliminating solid contact, these concepts inherently enable wear-free torque transmission, which is valuable for sustainable, low-maintenance drive systems.

Potential applications in space include torque transmission in robotic manipulators, precision pointing mechanisms for scientific instruments, and encapsulated drive systems for environments prone to dust, such as the lunar surface.

To evaluate the performance of various gear configurations, including axial, planetary, spur, and bevel types, a dedicated test stand is currently under construction. It features a motor and a torque sensor, enabling systematic testing under controlled conditions, including an integrated brake system with adjustable torque output, allowing fine-tuning from maximum to lower levels.

The ferrofluidic gearing and sealing research builds on the results of previous microgravity experiments, including PAPELL, FerrAC, FARGO, FerrAS, and FINIX, and is part of a broader effort to replace traditional mechanical interfaces

with ferrofluid-based subsystems [3]. The most recent project, FOX (Ferrofluid Optics Experiment), will expand the scope by evaluating ferrofluid-supported adaptive optics for in-space use, further demonstrating the multifunctional potential of magnetic nanoliquids in future spacecraft systems [1].

Within the research history of the Institute of Space Systems University of Stuttgart, ferrofluids and magnetorheological liquids have been used as bearings, seals, as well as heat and electric conductors, as manipulation subjects for droplet generation, splitting, merging and movement in microgravity, as a vital component to achieve wear less pumps systems, reaction wheels and switches.

#### **Acknowledgments**

This work, titled "Wear-resistant magnetic gears with ferrofluid technology" (Verschleißarme magnetische Getriebe mit Ferrofluidtechnologie), is funded under grant number BW8\_1382 through the bwInvest program.

- [1] FOX project page, https://ksatstuttgart.de/projekte/fox/, accessed 11.08.2025
- [2] A. Wagner, et al.: Dust-Resistant Pressure Seals Utilizing Ferrofluids, 54th ICES; 2025
- [3] S. Zajonz et al.: Development of a Ferrofluid Based Attitude Control Actuator for Verification on the ISS, Aerotecnica Missili & Spazio 103(3), 2024
- [4] S. Sütterlin et al.: Fargo: validation of spacerelevant ferrofluid applications on the ISS, CEAS Space Journal, 2024
- [5] Odenbach, S.: Ferrofluids. Magnetically Controllable Fluids and Their Applications. Springer-Verlag GmbH, Berlin (2002)

## A data-driven decoupled multiscale scheme for the modeling of structured magnetorheological elastomers

H. T. Roth<sup>1</sup>, P. Gebhart<sup>2</sup>, K. A. Kalina<sup>1</sup>, T. Wallmersperger<sup>2</sup>, M. Kästner<sup>1</sup>

Structured magnetorheological elastomers (MREs) are composite materials consisting of a soft elastomer matrix with embedded magnetizable particles arranged in chain-like patterns. For the simulation of real-world samples, explicitly resolving the microstructure is infeasible, necessitating a multiscale modeling approach.

We present a framework based on physics-augmented neural networks (PANNs) [1,2] for the macroscale modeling of structured MREs, incorporating their transversely isotropic behavior. The developed PANN macroscopic model respects key physical constraints, including objectivity, material symmetry, thermodynamic consistency, and the vanishing free energy, stress, and magnetization in the absence of external mechanical and magnetic loads [1].

Assuming the absence of electric fields and current densities, as well as quasistationary conditions, both the microscale and macroscale problems are formulated based on a variational principle for magneto-hyperelastic materials [3] and are solved using the finite element (FE) method

In the first step, training data is generated via numerical homogenization: sampled magneto-mechanical loads are applied to a representative volume element (RVE) in FE simulations, and the resulting microscale responses are homogenized to form a database for training and testing the PANN. In the second step, the PANN

is trained using a Sobolev training approach, enabling the model to automatically detect the direction of particle chain alignment [2].

The trained model accurately predicts magnetization, mechanical stress, and total stress within the range of the training data and is capable of reasonable extrapolations of the magnetization curve. Finally, the PANN is used to simulate the magnetostrictive response of a spherical MRE sample, demonstrating contraction along the magnetic field direction when it aligns with the particle chains.

#### **Acknowledgments**

We thank the Deutsche Forschungsgemeinschaft (German Research Foundation, DFG) for support through the Research Unit FOR 5599 on structured magnetic elastomers, project no. 511114185, via DFG grant reference no. KA 3309/22-1.

- [1] K. A. Kalina, P. Gebhart, J. Brummund, L. Linden, W. Sun, M. Kästner: Neural network-based multiscale modeling of finite strain magneto-elasticity with relaxed convexity criteria. Computer Methods in Applied Mechanics and Engineering 421, (2024).
- [2] K. A. Kalina, J. Brummund, W. Sun, M. Kästner: Neural networks meet anisotropic hyperelasticity: A framework based on generalized structure tensors and isotropic tensor functions. Preprint, arXiv:2410.03378, (2024).
- [3] P. Gebhart: Skalenübergreifende Modellierung magneto-aktiver Polymere auf Grundlage energie-basierter Variationsprinzipien. PhD thesis. TU Dresden (2024).

<sup>&</sup>lt;sup>1</sup> Chair of Computational and Experimental Solid Mechanics, TU Dresden, 01062 Dresden, Germany.

<sup>&</sup>lt;sup>2</sup> Chair of Mechanics of Multifunctional Structures, TU Dresden, 01062 Dresden, Germany.

# Exploring the Mechanisms of Particle-Matrix Coupling in Magnetic Gels by Means of Simulations and Experiments

R. Stephan<sup>1</sup>, S. Ranoo<sup>2</sup>, P. Kreissl<sup>1</sup>, C. Pabshettiwar<sup>1</sup>, J. Kubis<sup>3</sup>, C. Holm<sup>1</sup>, R. von Klitzing<sup>4</sup>, A. Schmidt<sup>3</sup>, R. Weeber<sup>1</sup>

Magnetic gels are soft hydrogels into which magnetic nanoparticles (MNP) are embedded. Thus, they exhibit the viscoelastic properties known from hydrogels, while features such as shape and stiffness can be tuned by external magnetic fields.

The exact nature of the coupling between magnetic nanoparticles and polymers is crucial for the materials' stimuli-responsive properties, and is determined by several competing interaction mechanisms including hydrodynamics, van der Waals forces, electrostatics, and the local structure of the polymer network.

Here, we explore the role of these mechanisms by juxtaposing results for a PAAm hydrogel loaded with cobalt ferrite particles and for a simulation model resolving particles, polymers, and hydrodynamic interactions.

In experiments, the polymer mesh size is controlled by varying the degree of cross-linking and the monomer fraction. In simulations, in addition to the mesh size, the nanoparticle-polymer interaction is varied. We probe the coupling mainly using magnetic AC susceptibility spectra, which can be obtained both experimentally and in simulations, allowing for a direct comparison and for elucidating the role of different factors in the coupling.

The most notable feature in experimental spectra is a systematic decline of the low-frequency susceptibility as the mesh size shrinks, despite the MNPs being only physically trapped rather than covalently linked into the polymer network.

Simulations show that purely hydrodynamic or isotropic Lennard-Jones-like interactions cannot reproduce this drop. A reduction of low frequency susceptibility as observed in the experiments appears only when anisotropic surface patches that attract polymer segments to the MNP are introduced.

In simulations, isotropic coupling influences the time scale. Specifically, hydrodynamic interactions shift the Brownian peak to lower frequencies in proportion to the local polymer density, but leave the zero-frequency susceptibility unchanged.

However, our simulations show that an affinity between the MNP and the polymers can mask mesh size effects:

strong polymer–MNP attraction distorts the network around the particle, homogenizing the hydrodynamic environment and partly suppressing the mesh size dependence of the relaxation time.

The experimentally observed reduction of low-frequency susceptibility can be reproduced in simulations when including patchy attractions of a few kT between the MNP surface and the polymers.

In summary, our results highlight both, the local polymer environment and surface heterogeneity of the magnetic particles — chemical or topographical — as important factors in MNP-polymer coupling.

#### **Acknowledgments**

RW, CP and CH acknowledge funding by the Cluster of Excellence SimTech (EXC 2075)

<sup>&</sup>lt;sup>1</sup> Institute for Computational Physics (ICP), Universität Stuttgart

<sup>&</sup>lt;sup>2</sup> Institute Chemistery Biologz Innovation (CBI), Ecole Supérieure de Physique et de Chimie Industrielles (ES-PCI) Paris

<sup>&</sup>lt;sup>3</sup> Institute of Physical Chemistry (PC), Universität zu Köln

<sup>&</sup>lt;sup>4</sup> Insitute for Condesnsed Matter Physics (IPKM), Technische Universität Darmstadt

# Light induced coating of iron oxide nanoparticles with Cu and assessment of their catalytic activity for electrochemical reduction of NO<sub>3</sub>- to NH<sub>4</sub>+

A. Weidner<sup>1</sup>, M. Kurniawan<sup>1</sup>, B. Hankiewicz<sup>2</sup>, S. Dutz<sup>3,4</sup>, A. Bund<sup>1</sup>

#### Introduction

Iron oxide nanoparticles (IONP) are interesting materials due to easy availability and low cost. Their magnetic properties enable a wide range of applications like magnetic manipulation, heating or imaging. Also, they show photothermal and photoelectrical properties with high absorption rates in the visible light spectrum making them interesting candidates for photohyperthermia or catalysis [1,2]. To add catalytic properties, the deposition of Cu is favorable for reducing costs for catalysts, making them reusable and developing multifunctional materials, as Cu NP have high potential in catalysis (e.g., CO<sub>2</sub>or NO<sub>3</sub>--reduction) and biomedical engineering (e.g., tumor therapy, diagnostic testing, antibacterial activity) [3,4].

Therefore, the aim of this research is to develop a synthesis route to deposit Cu by intrinsic heating with a visible light source and to assess the catalytic behavior of the resulting Cu-coated IONP.

#### Preparation and characterization

Preparation of IONP: Ferrimagnetic large single domain particles (LSDP) were prepared following [5]. In short, a 0.1 M FeCl<sub>2</sub> solution was added to a stirred solution with 0.021 M NaOH and 0.185 M NaNO<sub>3</sub> under N<sub>2</sub> atmosphere and held at 35 °C for 1 d. The resulting LSDP were magnetically washed with distilled water, analyzed by transmission electron microscopy (TEM, JEOL JEM 1011, JEOL GmbH, Germany) and vibration sample magnetometry (VSM, MicroSense EZ, Quantum Design, Taiwan).

To load the IONP with Cu, an electroless copper process (see [6]) was performed

using an alkaline Cu bath (pH = 12,8, adjusted with NaOH, 0.2M CuSO<sub>4</sub>) with 0.1 M trisodium citrate as complexing agent and formaldehyde as reducing agent. The electrolyte was mixed with the IONP suspension, and three samples  $(V = 3 \text{ ml}; \beta \sim 1 \text{ g/l})$  were filled in separate borosilicate glasses. One sample was irradiated for 1 h (1hL) at a distance of 3.5 cm with a high intensity white light LED (60 W Shenzhen Aixinde Technology Co., Ltd.; China) focused by a glass lens. The second one was kept for 1 h at 75 °C in an oil bath (1h 75 °C) and a third was kept without treatment (noL). Afterwards, the IONP were magnetically washed to remove excess electrolyte. The Cu content was determined by atom absorption spectroscopy (AAS, contrAA 800F, Analytik Jena GmbH+Co. KG) and the morphology was investigated by TEM.

Investigation of catalytic behavior: To test the catalytic behavior of the Cu coated IONP an electrochemical setup with a Nafion<sup>™</sup> separated H-cell was used (see Fig. 1 a) to investigate the conversion reaction of  $NO_3^-$  to  $NH_4^+$  [7]. At the cathode side a glassy carbon sample holder with a permanent magnet on the back serving as working electrode (WE) was placed with an Ag/AgCl (sat.) reference electrode (RE) either in a  $0.5 \text{ M} \text{ K}_2\text{SO}_4 + 0.01 \text{ M}$ KNO<sub>3</sub> or 0.5 M K<sub>2</sub>SO<sub>4</sub> solution for comparison, purged for 10 min with Ar. The glassy carbon was taped and isolated except for a circle in the middle ( $\emptyset \sim 4$  mm; see Fig. 1 b), where IONP samples were placed (pristine IONP, 1hL, and 1h75°C Cu coated IONP;  $\sim 40 \mu g$ ). The permanent magnet at the back held the IONP in contact with the glassy carbon. At the anode side, filled with 0.5 M K<sub>2</sub>SO<sub>4</sub> solution, an inert Pt electrode served as counter

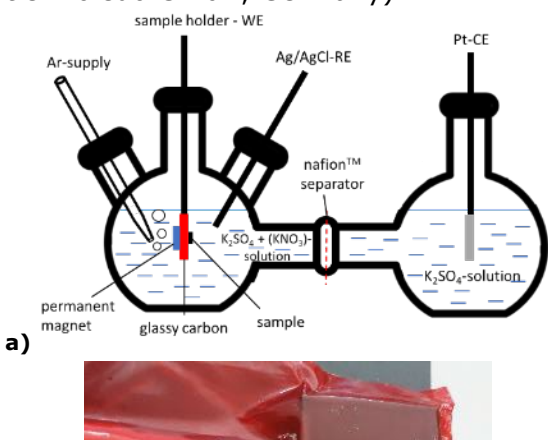
<sup>&</sup>lt;sup>1</sup> Fachgebiet Elektrochemie und Galvanotechnik, Technische Universität Ilmenau, Germany

<sup>&</sup>lt;sup>2</sup> Institut für Physikalische Chemie, Universität Hamburg-Harburg, Hamburg, Germany

<sup>&</sup>lt;sup>3</sup> Leupold Institute for Applied Natural Sciences (LIAN), Westsächsische Hochschule Zwickau, Germany

<sup>&</sup>lt;sup>4</sup> Institut für Biomedizinische Technik und Informatik (BMTI), Technische Universität Ilmenau, Germany

electrode (CE). Cyclic voltammetry (CV; dE/dt = 20 mV/s,  $E_0$  = open circuit potential; 10 cycles; -0.5 - -1.2 V vs. Ag/AgCl (sat.)) and chronoamperometry (CA, t = 30 min;  $E_A$  = -1.2 V vs. Ag/AgCl (sat.)) were performed with a potentiostat BioLogic VSP (BioLogic GmbH, Germany). pH-values were measured before and after CA (pH-meter Seven2Go, Mettler Toledo GmbH, Germany).



b)

**Fig. 1) a)** Electrochemical setup and **b)** loaded sample holder for IONP

To investigate the catalytic behavior for reduction of  $NO^{3-}$  to  $NH_4^+$ , IONP samples were administered on a glassy carbon sample holder (untaped circle Ø  $\sim$  4 mm) serving as working electrode (WE) in an electrochemical setup. The IONP were held in contact with a permanent magnet on the back.

#### **Results and discussion**

Preparation of IONP: LSDP with similar ferrimagnetic properties and morphology as in [5] were prepared. Using a white light LED the IONP could be loaded with  $\beta_{Cu-AAS}$  (1hL)  $\sim 17-19$  wt-%, which was slightly higher than for the 1h75°C-sample ( $\beta_{Cu-AAS} \sim 11-17$  wt-%). No Cu was detected for the noL-sample. The results can be explained with the reduction of Cu by intrinsic heat generation and possible photoelectrical processes on the IONP-surface absorbing visible light in the transparency window of the electrolyte ( $\lambda \sim 400-600$  nm). TEM revealed no significant change in morphology.

Investigation of catalytic behavior: Using CV and CA for all IONP tested in  $K_2SO_4$  solution, currents in the  $\mu A$  range could be observed. After adding KNO<sub>3</sub> solution, the currents for pristine IONP were in the  $\mu A$ 

range, whereas for 1hL and 1h75°C samples, currents in the mA range could be determined. For these samples, the pH changed from pH 6.5 – 6.7 to 10.3 – 10.7 after 30 min of CA at the cathode side. This is in accordance with the consumption of H<sup>+</sup> for the reduction reaction [7] and proves catalytic activity. After CA in KNO<sub>3</sub> containing solution, Cu deposition could be observed on the glassy carbon. An explanation could be the oxidation and dissolution of Cu in the presence of NO<sub>3</sub>- and redeposition on the glassy carbon [8].

#### **Summary and outlook**

A synthesis route to obtain Cu coated magnetic IONP with  $\beta_{Cu\text{-}AAS} \sim 17-19$  wt-% by using intensive visible light was successfully established. The catalytic activity of these IONP for NO<sub>3</sub>- reduction was shown in an electrochemical setup using the magnetic properties of the IONP to connect them to a glassy carbon WE.

Follow-up investigations will focus on optimizing the synthesis route to reach higher Cu contents by, e.g., adapting the light source and composition of the electrolytes or using different core structures (multi-core, single-core IONP). Also, further characterization is planned, e.g., by X-ray Photoelectron Spectroscopy (XPS) to determine the chemical state of the Cu. Another aim is to adapt the synthesis route to deposit noble metals like Ag or Au for different functionalization. Furthermore, an optimization of the electrochemical setup to enable easier handling, e.g., by making the permanent magnet removable, and to quantify the products is planned. Also, the setup can be used to investigate other magnetic NP or other catalytic reactions, like the oxidation of glucose or the reduction of azo dyes.

- [1] Ali et al., 2021;
  - DOI: 10.3389/fchem.2021.629054 Ximin Cui et al., 2023;
- DOI: 10.1021/acs.chemrev.3c00159
- [3] Pathak et al., 2024; DOI: 10.1007/s10853-024-09546-z
- [4] Wei et al., 2024; DOI: 10.1016/j.cej.2024.149040
- [5] Zahn et al., 2022; DOI: 10.3390/nano12030343Zahn
- [6] Kurniawan et al., 2021; DOI: 10.1007/s10853-021-06058-y
- [7] Karamad et al., 2023;
- DOI: 10.1039/D2FD00145D [8] Yoon et al., 2025;
- DOI: 10.1038/s41563-024-02084-8

# Hyperthermal-active and reprocessable composites based on magnetic nanoparticles in responsive polymer networks

M. Weißpflog<sup>1</sup>, G. Signorato<sup>1</sup>, <u>P. Schütz<sup>1</sup></u>, B. Hankiewicz<sup>1</sup>, V. Abetz<sup>1,2</sup>.

The field of stimuli-responsive soft materials is rapidly evolving, particularly with recent advances in the design and fabrication of magnetic soft materials. By incorporating superparamagnetic nanoparticles (MNPs) into an elastic polymer matrix, materials with rapid and fully reversible mechanical responses to magnetic fields can be created, making them highly suitable for the development of flexible, remote-controlled soft robots.[1] However, conventional crosslinked elastomer materials often lack reprocessability and recvclability, limiting the material's lifetime, especially when it is subjected to repeated mechanical stress. These limitations can be overcome by using vitrimers as the elastic matrix. Vitrimers are dynamically crosslinked polymers that can be reshaped at high temperatures and offer valuable features such as self-healing and recyclability. The dynamic mechanical properties of the material can be tailored depending on the applications by adjusting parameters like the building blocks, the crosslink density, the amount and size of MNPs, or the way the particles are integrated into the matrix.

In this work, we present a magnetic elastomer with a MNP content of 5 wt% based on  $Co_x Fe_{3-x}O_4$ -MNPs (x = 0.42 - 0.49), the biologically derived building block psorbitol, and the commercially available trifunctional amine Jeffamine T403 (Figure 1a).[2] The dynamic nature of the materials is given by the vinylogous urethane bonds, which allow a reshuffling of the network without a catalyst at elevated temperatures.[3] The MNPs are synthesized in a hydrothermal approach in the presence of the functionalized sorbitol monomer, allowing for a precise size control between 3 and 20 nm in diameter, depending on the concentration of the capping agent.[2,4] Acetoacetylated sorbitol, which is also a building block of the matrix, was chosen as a coating to ensure that the particles blend in with the vitrimer matrix and segregation under high temperature and pressure during the material's processing is suppressed. To obtain the magnetic elastomer, MNPs are mixed with functionalized sorbitol and the Jeffamine T403 crosslinker (Figure 1a). The resulting material could be molded into the desired shape and directly used.

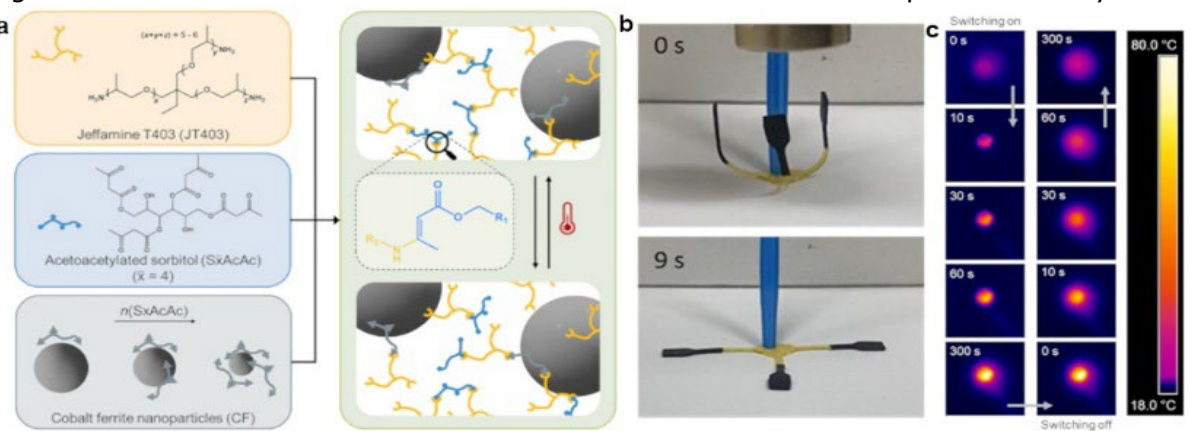


**Figure 1:** a) Schematic of the single components of the system and the magnetic vitrimer nanocomposite. b) Elastic deformation and return to the original shape. c) Heating of the nanocomposite using an alternating magnetic field ( $H_0 = 12-36$  mT and f = 142.70 kHz).

<sup>&</sup>lt;sup>1</sup> Institute of Physical Chemistry, University of Hamburg, Grindelallee 117, 20146 Hamburg, Germany. <sup>2</sup> Institute of Membrane Research, Helmholtz-Zentrum Hereon, Max-Planck-Straße 1, 21502 Geesthacht, Germany.

Still, more complex structures are easily created by welding the pure matrix material and the nanocomposite to fabricate defect-free structures with more complex deformation behavior (Figure 1b).[3] Moreover, the magnetic properties and thermo-reversibility can be combined using alternating magnetic fields ( $H_0 = 12$ -36 mT and f = 142.70 kHz) to induce localized heating (Figure 1c) and trigger the self-healing behavior or a reshaping of the material (Figure 2a). For example, a composite containing 7 nm MNPs with a mass of around 45 mg, which is exposed to a frequency of 142.70 kHz and a field amplitude of 36 mT, reaches a temperature rise of up to 78 °C. To optimize the coupling of magnetic heating and the material's response, the relaxation mechanisms of MNPs with different sizes were investigated using temperature and fielddependent X-ray photon correlation spectroscopy (XPCS), revealing the ability of the particles to freely rotate in the elastic matrix. The findings affirm the significance of the particles' anchoring within the matrix, since covalent binding of the particles inhibits the rotation, while a loose particle coating allows for Brownian relaxation to occur.

Finally, the recyclability of the material was investigated to show the full mechanical reprocessability (Figure 2b) without a macroscopic segregation of the magnetic particles using heat compression. Additionally, the chemical recycling of the composites using 0.5 M acetic acid was investigated, showing that the MNPs and the matrix can be easily separated using

a permanent magnet (Figure 2c). A reformation of the prune matrix by removing the acetic acid and water, as well as the recovery of MNPs without changing their morphological and magnetic properties, was realized (Figure 2d).

In conclusion, we demonstrated that smart magnetic elastomers can be easily fabricated using dynamic polymer networks, known as vitrimers, which exhibit rapid mechanical responses to magnetic and temperature-dependent shape memory and self-healing properties that can be remotely triggered *via* magnetic heating using alternating magnetic fields.

#### **Acknowledgments**

This work was funded by the Deutsche Forschungsgemeinschaft (DFG) within the RTG2536 and SFB986 "M3" subproject A2.

- [1] G. Dong, Q. He, S. Cai, *Soft matter* **2022**, *18*, 7604.
- [2] M. Weißpflog, G. Signorato, V. S. Schulze, J. L. Hansen, N. F. Torres, B. Hankiewicz, V. Abetz, in preparation.
- [3] G. Signorato, L. R. Klauke, P. Haida, T. Vossmeyer, V. Abetz, *Polymer* 2025, 318, 127968.
- [4] M. Weißpflog, N. Nguyen, N. Sobania, B. Hankiewicz, J. Phys. Chem. C 2024, 128, 15598.

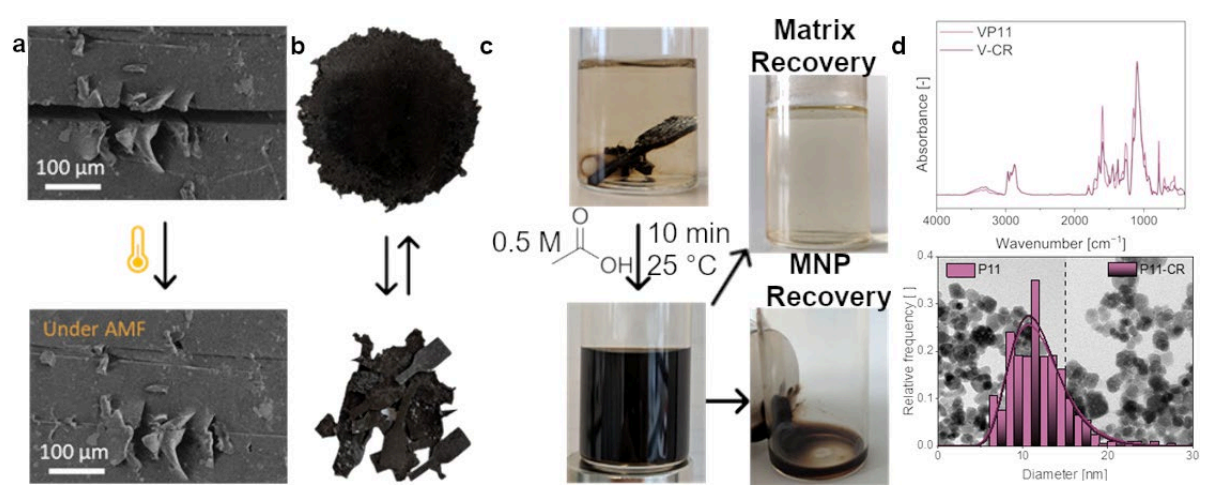


**Figure 2:** a) Self-healing of a surface cut due to the heating *via* alternating magnetic fields. b) Mechanical recycling of the nanocomposite. c) Chemical recycling of the nanocomposite and separation of the components. d) FTIR-spectra of the matrix and the recovered matrix, and TEM histograms from the used MNPs and the recovered particles.

## Advection of superparamagnetic nanoparticles in branched arterial networks

L. C. P. Wille<sup>1</sup>, S. Lyer<sup>2</sup>, G. Fischer<sup>1</sup>, J. Kirchner<sup>1,3</sup>

#### Introduction

The application of SPIONs (super paramagnetic iron oxide nanoparticles) for various in-body medical treatments is proposed frequently in the literature [1][3]. One central property of SPIONs is their steerability by utilizing magnetic forces applied by external magnets [2]. This technique is often discussed in the approach of magnetic drug targeting (MDT), where the SPIONs are used as transporters and are coupled with medication [1]. By guiding the particles through the human circulatory system towards the diseased region, the effectivity of treatments could be significantly increased, without any invasive work except the injection of particle solution.

The magnetic force  $F_m$  acting on the particles is relatively weak as it grows with the particle volume  $F_m \sim V$ , which increases strongly with the iron cluster diameter as  $V \sim D^3$ . Multiple iron cores form one cluster with a typical size of D=10~nm [1]. The iron cluster within one particle is encapsuled by a coating resulting in a larger hydrodynamic diameter. Due to the small size, the particle propagation is also heavily affected by the blood flow conditions through the drag force. The prediction of reasonable steering strategies is therefore heavily reliant on the knowledge of fluidic conditions.

# Particle propagation in branched arterial networks

The propagation of particles in a network of vessels is depicted in Fig. 1. Particles are injected usually in mid-sized arteries experiencing laminar flow conditions [1]. Due to the small hydrodynamic size, the particle response time to changes in the drag force is relatively small in the order of sub-nanosecond. Any velocity changes in the flow can be assumed to instantaneously affect the particle.

In the past, models have been proposed to predict propagation of particles within a single channel as in [5]. Additionally, testbeds have been developed to measure the timely arrival of a particle bolus at a fixed sensor position downstream [4].

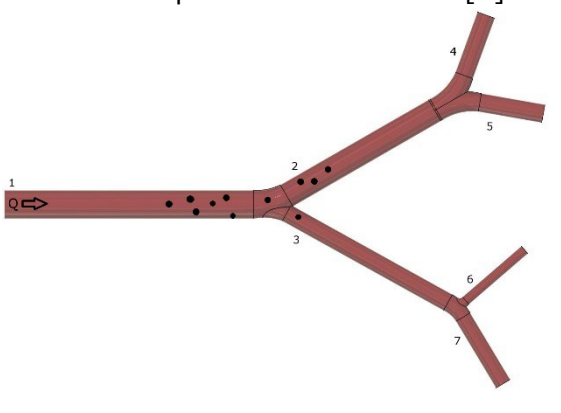


Figure 1: Arterial network consisting of 7 vessels. As the arteries branch, the vessels shrink in diameter. Particles within this network are indicated by black circles.

In this work we want to simulate the particle propagation in a network of 7 vessels with 3 branches, thus introducing a more complicated scenario than the usual single vessel setup. The network is shown in Fig. 1 with the single vessel indices. The inlet diameter corresponds to a typical mid-sized artery and the other diameters have been set accordingly smaller:  $\{1.6\ mm, 0.7\ mm, 0.51\ mm, 0.52\ mm, 0.52\ mm, 0.27\ mm, 0.46\ mm\}$ . The lengths of these vessels are set to:  $\{15\ mm, 12\ mm, 12\ mm, 5\ mm, 5\ mm, 5\ mm, 5\ mm, 5\ mm\}$ .

We set our focus on predicting the particle arrival in a network of vessels without any external forces. Insights into the undisturbed movement of particles can then later be used for optimizing the magnet position for MDT purposes.

#### Simulation Methodology

<sup>&</sup>lt;sup>1</sup> Institute for Smart Electronics and Systems (LITES), Friedrich-Alexander-Universität, Erlangen-Nürnberg, Germany

<sup>&</sup>lt;sup>2</sup> Section of Experimental Oncology and Nanomedicine (SEON), Universitätsklinikum Erlangen, Germany

<sup>&</sup>lt;sup>3</sup> Fachhochschule Dortmund, University of Applied Sciences and Arts, Germany

In the beginning we briefly introduced that the blood flow induces a drag force on the particles. For analyzing particle movement, a CFD simulation of the flow condition is necessary. We utilize the simpleFoam solver from the OpenFOAM simulation environment to numerically solve the velocity and pressure within this vessel network in 3D based on the Navier-Stokes equations. The inflow boundary condition of the inlet vessel is set to  $Q_{in} =$  $10 \frac{ml}{min}$  similar to [4], while the outlet pressures of vessels No. 4-7 are set to zero. The viscosity of blood (non-Newtonian fluid) is shear rate dependent and is calculated based on a Casson model.

Afterwards in a second simulation step, particles are introduced at an initial injection location inside the first vessel and are then advected by the fluid movement. This is solved with the <code>icoUncoupledKinematicParcelFoam</code> solver. The particle count is set to  $5\cdot 10^4$  and particles are uniformly distributed over the cross section of the vessel at the injection region.

#### **Simulation Results**

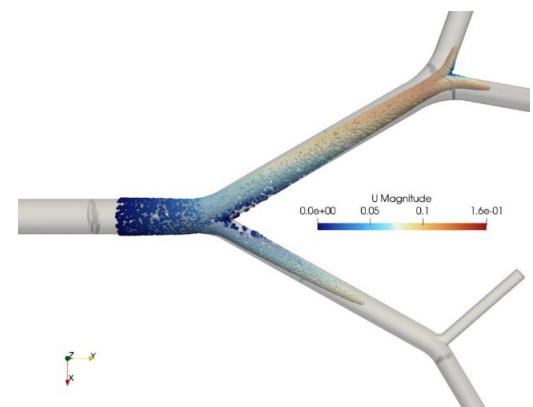


Figure 2: The particle cloud travelling through the vessel network at 0.12 s. The velocity of the particles is indicated by the colour. The upper branches are reached earlier than the lower branches.

A snapshot of the particles shortly after the injection is shown in Fig. 2. The larger vessels seem to acquire a higher particle share, since they are better perfused. This effect becomes even more visible by evaluating the particle count at the four outlets over time in Fig. 3. The smallest vessel No. 6 only receives about 1.3% of the total particles.

#### **Outlook**

We showed that the particle arrival can differ a lot between similar sized vessels.

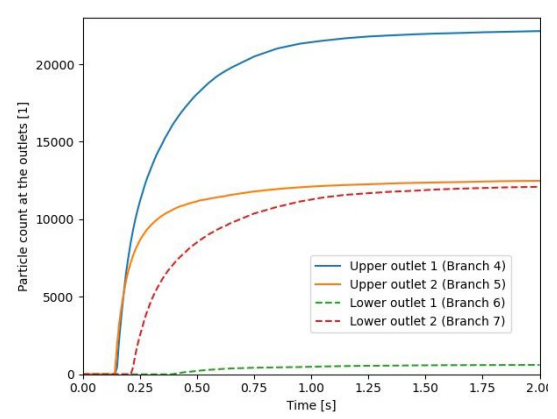


Figure 3: SPION count at the four outlets over time.

In the future we would like to incorporate the magnetic forces acting on the SPIONs into the particle simulation. This would allow us to optimize particle steering methods, by iteratively adjusting simulation parameters and evaluating the particle arrival results. Furthermore, since simulating larger networks with hundreds of vessels in 3D becomes numerically challenging, we want to create simpler mathematical models to predict the spread of nanoparticles in connected vessels of different size and orientation. These simpler models will speed up any computational prediction.

**Acknowledgments** This work was funded by the Deutsche Forschungsgemeinschaft (German Research Foundation) – GRK 2950, project-ID 509922606.

- [1] A. S. Thalmayer, L. Fink, and G. Fischer (2025). Experimental and simulative characterization of a hybrid magnetic array for steering super-paramagnetic nanoparticles in drug targeting. *IEEE Transactions on Biomedical En*gineering.
- [2] R. Van Durme, G. Crevecoeur, L. Dupr'e, and A. Coene (2023). Improved magnetic drug targeting with maximized magnetic forces and limited particle spreading. *Medical Physics*.
- [3] M. Mahmoudi, S. Sant, B. Wang, S. Laurent and T. Sen (2011). Superparamagnetic iron oxide nanoparticles: Development, surfacemodification and applications in chemotherapy. Advanced Drug Delivery Reviews.
- [4] M. Bartunik, G Fischer, and J. Kirchner (2023). The Development of a Biocompatible Testbed for Molecular Communication With Magnetic Nanoparticles. *IEEE Transactions on Molecular, Biological and Multi-Scale Communications*.
- [5] L. Y. Debus, M. J. Wilhelm, H. Wolff, L. C. P. Wille, T. Rese, M. Lommel, J. Kirchner, F. Dressler (2025). Blood Makes a Difference: Experimental Evaluation of Molecular Communication in Different Fluids. IEEE Transactions on Molecular, Biological and Multi-Scale Communications.

# Magnetic particle spectroscopy based biosensing for antigens and nucleic acids

F. Wolgast, R. Sack, Y. Wang, R. Amin, A. Lak, M. Schilling, T. Viereck

Institut für Elektrische Messtechnik und Grundlagen der Elektrotechnik (EMG) and Laboratory for Emerging Nanometrology (LENA), TU Braunschweig, Braunschweig, Germany

#### Introduction

Food safety, environmental safety, quality assurance and medical diagnostics have one thing in common: they depend on fast and reliable tests for the detection of proteins, peptides, lipids, nucleic acids, toxins and pathogens. In this field of pointof-care (POC) diagnostics, lateral flow assays (LFA) are widely used due to their ease of use and the availability of results within less than half an hour. However, it is not possible to detect the smallest amount of an analyte with the LFA. In addition, they only provide qualitative results. Therefore, especially in medical diagnostics, the polymerase chain reaction (PCR) is used as the leading technology for nucleic acid detection, but it requires well-equipped laboratories and sophisticated equipment as well as time-consuming enzymatic reactions, which makes this method unsuitable for POC diagnostics in everyday clinical practice. Magnetic biosensing platforms promise advances in the field of POC testing in terms of their sensitivity with regard to antigen detection as well as the speed at which they can detect deoxyribonucleic acid (DNA).

#### Antigen detection

A homogeneous magnetic assay (MA) is realized by the addition of the analyte to functionalized magnetic nanoparticles (MNP), in this case BNF particles with a size of 80 nm (BNF80) from micromod GmbH, resulting in a hydrodynamic change in size of the MNP. This influences the sensitive relaxation dynamics of the MNP, which can be detected by measuring the magnetization response using Magnetic Particle Spectroscopy (MPS). Consequently, the presence of the analyte can be inferred. When evaluating the MPS signals, the harmonic ratio of the fifth to the

third harmonic is considered because it is a concentration-independent metric. Furthermore, the harmonics are independent of any para- or diamagnetic background and can therefore be directly associated to the particles.

Our assays for detecting antigens are based on the formation of clusters by adding the analyte, as shown in Fig. 1. The added antigen (AG) is captured up by the antibodies (AB) on the MNP surface. Since there are typically several AB on an MNP as well as the AG has several binding sites. large magnetic clusters are formed form the single particles leading to a decrease of the harmonic amplitudes [1, 2]. As a result, the MA achieve a greater relative size change for the same amount of analyte, which leads to an increase in sensitivity. The influence of the functionalization of the MNP on the hydrodynamic size is shown in Fig. 2. In both cases, BNF80 particles were functionalized with AB or Fv against SARS-CoV-2. While the pure MNPs have a hydrodynamic diameter of around 83 nm, those with AB on the surface are already 97 nm in size. This contrasts with the Fv functionalized MNP at 86 nm in diameter. Therefore, this type of functionalization represents a good starting point for more sensitive antigen detection. The next step is to perform an MA with the MNPs with Fv on the surface to determine the detection limit for this type of assay.

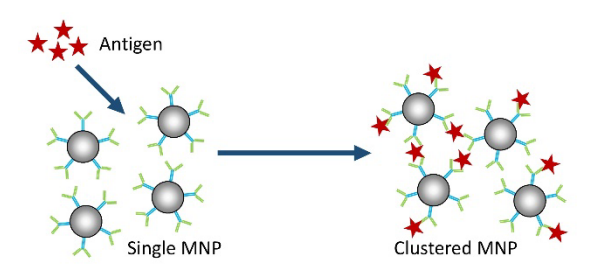


Figure 1: Schematic of clustering-based antigen detection.

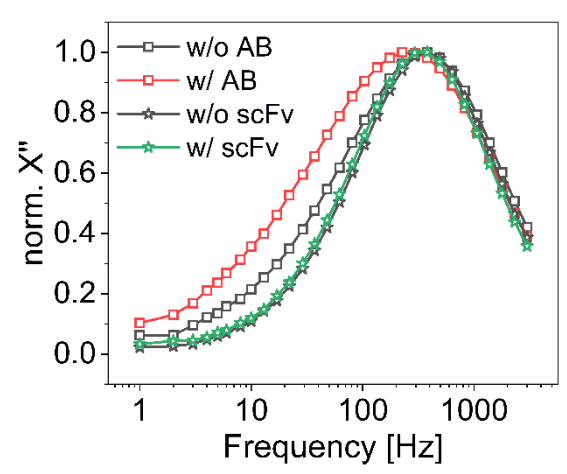


Figure 2: Normalized imaginary part of the AC susceptibility for BNF80 without (w/o) and with (w/) AB or Fv functionalization.

#### **DNA** detection

The platform we have developed for DNA detection uses MA, which are wash-free and enable enzyme-free signal amplification. The magnetic signal amplification circuit (MAC) illustrated in Fig. 3 is used for the sensitive detection of DNA strands.

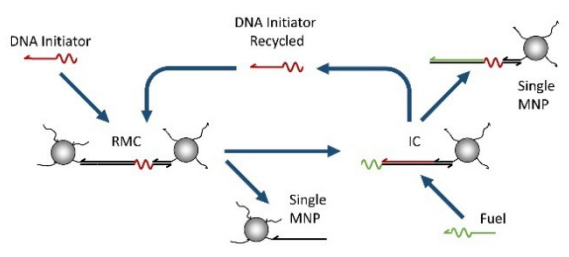


Figure 3: Schematic design of the MAC.

A declustering-based approach is used, as this offers a higher specificity compared to clustering due to unspecific binding. Brownian dominated MNP form responsive magnetic clusters (RMC) are disassembled by toehold-mediated strand displacement (TMSD) reactions that are highly specific for the corresponding target nucleic acid sequence. The cycle begins with the DNA initiator step binding to the RMC and releases a single MNP from the intermediate complex (IC). Afterwards a fuel DNA binds to the IC and releases the DNA initiator so that it can be reused. The RMC decay in a cyclic process, which changes the magnetic signal caused by the low target concentration.

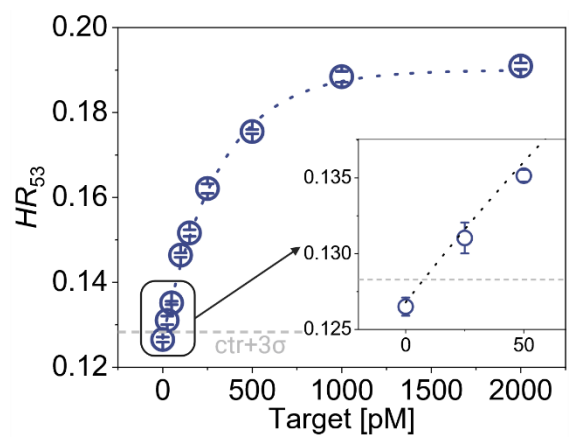


Figure 4: Detection limit for the improved MAC approach measured with MPS [4].

Consequently, the amplitude of the harmonics in the MPS increases. [3, 4]. Using the MAC approach, a detection limit of 27 pM DNA strands after 24 h incubation time was previously demonstrated [3]. In Fig. 4 one can see the results with the finally improved MAC concept described above using BNF80 particles. Both, the assay time and the detection limit could be improved, so that 7.6 pM can be detected after only 2 h incubation time [4].

#### **Acknowledgments**

This work was supported by the Deutsche Forschungsgemeinschaft (DFG, German Research Foundation) under the DFG Research Training Group 1952 Metrology for Complex Nanosystems as well as the DFG project VI 892/4-1. We also gratefully acknowledge the support by the Braunschweig International Graduate School of Metrology B-IGSM.

- [1] F. T. Wolgast et al., Low-Cost Magnetic Particle Spectroscopy Hardware for Low-Viral-Load Immunoassays, IEEE Trans. Instrum. Meas. vol. 73, pp. 6008509, August 2024.
- [2] T. Kahmann et al., Improvements of magnetic nanoparticle assays for SARS-CoV-2 detection using a mimic virus approach, J. Appl. Phys., vol. 127, pp. 233901, May 2020.
- [3] E. L. Rösch et al., Amplification- and Enzyme-Free Magnetic Diagnostics Circuit for Whole-Genome Detection of SARS-CoV-2 RNA, Chem-BioChem, vol. 25, p. e202400251, June 2024.
- [4] R. Sack et al., Mismatch-Assisted Toehold Exchange Cascades for Magnetic Nanoparticle-Based Nucleic Acid Diagnostics, bioRxiv, 2025.03.14.643268, March 2025 (preprint).

# Molecular Dynamics Simulation of Zipped Chainlike agglomeration of the SPIONs

K. Xiao<sup>1</sup>, S. Lyer<sup>2,3</sup>, J. Kirchner<sup>1,4</sup>, G. Fischer<sup>1</sup>

<sup>1</sup> Institute for Smart Electronics and Systems (LITES), Friedrich-Alexander-Universität Erlangen-Nürnberg (FAU), Erlangen, Germany

#### Introduction

The widespread application of superparamagnetic iron-oxide nanoparticles (SPION) is attributable to their exceptional magnetic response properties. When the size of a magnetic nanoparticle is below a critical threshold, they can be regarded as single magnetic domains. This implies that each nanoparticle possesses a unique magnetic moment, leading to non-negligible magnetic dipole-dipole interactions between them. These dipolar interactions are the primary driving force for the formation of agglomerates.

Furthermore, an external magnetic field can induce these agglomerates to form long, straight chains. The existence of these field-induced chain-like agglomerations has been verified by various imaging techniques [1,2] and simulations [3,4]. However, in contrast to the single chains often depicted in simulations, experimental images frequently reveal hexagonally arranged, zipped chain-like agglomerations. In other words, the chains are not isolated but interact to form bundles.

Nevertheless, many studies suggest that the van der Waals (vdW) forces between particles are the essential factor responsible for the formation of these zipped chain-like agglomerations [2,6]. Therefore, it is necessary to validate this assertion through simulations.

Molecular dynamics simulation, which can account for particle forces at the nanoscale, is well-suited for investigating the influence of van der Waals interactions on the formation of such zipped structures.

#### **Model and Method**

Van der Waals forces, electrostatic interactions, and steric hindrance exist between SPIONs. Among these, the van der Waals force is attractive, while the other two are repulsive. The colloidal stability of SPIONs is maintained by the balance between these attractive and repulsive forces.

The Lennard-Jones (LJ) potential is a simple mathematical model used to represent the sum of these interactions, as shown in (1):

$$V(r) = 4\epsilon \left[ \left( \frac{\sigma}{r} \right)^{12} - \left( \frac{\sigma}{r} \right)^{6} \right]$$
 (1)

where  $\epsilon$  is the depth of the potential well,  $\sigma$  is the particle size and r is the distance between the SPIONs.

To exclude the van der Waals attraction, the Weeks–Chandler–Andersen (WCA) potential can be employed, as shown in (2). The potential is set to zero when the separation distance r exceeds the cutoff distance  $r_{\rm cut}$ . To ensure the function is continuous at  $r_{\rm cut}$ , a constant shift,  $c_{\rm shift}$ , is introduced. In this manner, the LJ potential from (1) is modified into a purely repulsive version.

$$V(r) = \begin{cases} 4\epsilon \left[ \left( \frac{\sigma}{r} \right)^{12} - \left( \frac{\sigma}{r} \right)^{6} \right] + c_{\text{shift}} & 0 < r \le r_{\text{cut}} \\ 0 & r > r_{\text{cut}} \end{cases}$$
 (2)

The simulation code was adapted from the relevant tutorials on the official ESPResSo website [7], incorporating van der Waals interactions and a homogenous magnetic field. The magnetic field was applied in the horizontal direction. The simulation results are presented in Figure 1.

<sup>&</sup>lt;sup>2</sup> Department of Otorhinolaryngology, Head and Neck Surgery, Section of Experimental Oncology and Nanomedicine (SEON), Else Kröner-Fresenius-Stiftung Professorship, Universitätsklinikum Erlangen, Erlangen, Germany <sup>3</sup> Department of Otorhinolaryngology, Head and Neck Surgery, Section of Experimental Oncology and Nanomedicine (SEON), Professorship for AI-Controlled Nanomaterials, Universitätsklinikum Erlangen, Erlangen, Germany <sup>4</sup> Fachhochschule Dortmund, University of Applied Sciences and Arts, Dortmund, Germany

#### **Results and Discussion**

As can be seen in Figure 1, SPIONs form agglomerates regardless of the presence of a magnetic field or van der Waals forces. This phenomenon occurs due to the dipole-dipole interactions, as previously mentioned. Upon the application of an external magnetic field, Figures 1(c) and 1(d) clearly show chain-like agglomerates aligned with the field direction. Under these conditions, the magnetic moments of the SPIONs, influenced by the external field, orient themselves in the same direction.

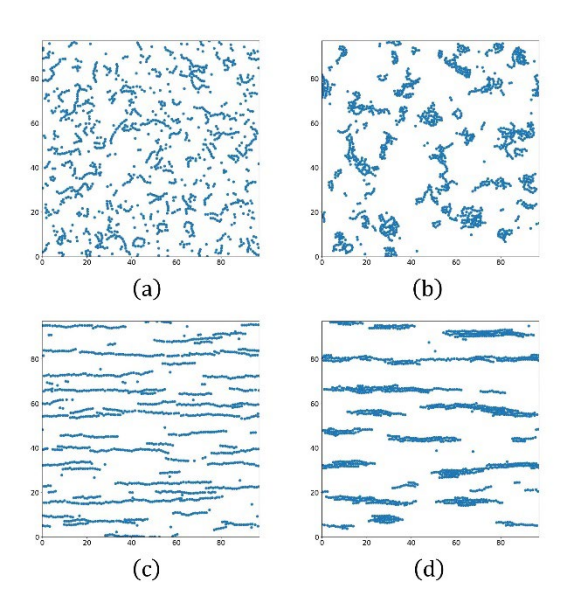


Figure 1. Snapshots from molecular dynamics (MD) simulations illustrating the agglomeration of SPIONs under four conditions: (a) without magnetic field and vdW forces; (b) without magnetic field, but with vdW forces; (c) with an applied magnetic field, but without vdW forces; and (d) with an applied magnetic field and vdW forces.

Notably, a comparison between Figures 1(b)(d) and 1(a)(c) reveals that the van

der Waals forces induce stacking among the chain-like agglomerates, resulting in thicker structures. This observation confirms that van der Waals interactions are responsible for the formation of the hexagonally arranged, zipped chain-like agglomerations.

#### **Acknowledgments**

This work was funded by the Deutsche Forschungsgemeinschaft (DFG, German Research Foundation) – GRK 2950 – project-ID 509922606.

- [1] Butter, K., Bomans, P., Frederik, P. et al. Direct observation of dipolar chains in iron ferrofluids by cryogenic electron microscopy. Nature Mater 2, 88–91 (2003). https://doi.org/10.1038/nmat811
- [2] N. S. Susan Mousavi, Sachin D. Khapli, Sunil Kumar; Direct observations of field-induced assemblies in magnetite ferrofluids. J. Appl. Phys. 14 March 2015; 117 (10): 103907. https://doi.org/10.1063/1.4914484
- [3] Ku, J., Chen, H., He, K., & Yan, Q. (2015). Simulation and observation of magnetic mineral particles aggregating into chains in a uniform magnetic field. *Minerals Engineering*, 79, 10-16.
- [4] Climent, E., Maxey, M. R., & Karniadakis, G. E. (2004). Dynamics of self-assembled chaining in magnetorheological fluids. *Langmuir*, 20(2), 507-513.
- [5] Blümler, P. Magnetic Guiding with Permanent Magnets: Concept, Realization and Applications to Nanoparticles and Cells. Cells 2021, 10, 2708. https://doi.org/10.3390/cells10102708
- [6] Heinrich, D., et al. "Dynamics of the Field-Induced Formation of Hexagonal Zipped-Chain Superstructures<? format?> in Magnetic Colloids." *Physical Review Letters* 106.20 (2011): 208301.
- [7] Weik, F., Weeber, R., Szuttor, K. et al. ES-PResSo 4.0 an extensible software package for simulating soft matter systems. Eur. Phys. J. Spec. Top. 227, 1789–1816 (2019). https://doi.org/10.1140/epjst/e2019-800186-

#### **List of Participants**

#### Günter K. Auernhammer

Polymer Interfaces Leibniz-Institut für Polymerforschung Dresden Hohe Straße 6 1069 Dresden Germany

Tel.: +49 (0) 351 4658 486 E-mail: auernhammer@ipfdd.de

#### Tatiana Becker

Fachgebiet Mechanik Nachgiebiger Technische Universität Ilmenau Max-Planck-Ring 12 98693 Ilmenau Germany

Tel.: 03677 / 69-1845 E-mail: becker.tatiana@gmx.de

#### Silke Behrens

Institut für Katalyseforschung und technologie Karlsruher Institut für Technologie Hermann-von-Helmholtz-Platz 1 76344 Eggenstein-Leopoldshafen Deutschland

Tel.: 0721 608 26512 E-mail: silke.behrens@kit.edu

#### Oksana Bilous

Computational and Soft Matter Physics Faculty of Physics University of Vienna Kolingasse 14-16 1090 Vienna Austria

Tel.: 380503905997

E-mail: oksana.bilous@univie.ac.at

#### **Dmitry Borin**

Chair of Magnetofluiddynamics, Measuring and Automation Technology TU Dresden George-Baehr-Str. 3 1062 Dresden

Tel.: 4935146332307

E-mail: dmitry.borin@tu-dresden.de

#### Maria Daniela Contreras Mateus

Chair of Magnetofluiddynamics, Measuring and Automation Technology Technische Universität Dresden - TU Dresden George-Bähr 3 1069 Dresden

Germany

Tel.: +49 351 463-35584

E-mail: maria.contreras@tu-dresden.de

#### **Dietmar Eberbeck**

Aug.23 PTB Abbestraße 02.Dez 10587 Berlin

Tel.: 3034817208

E-mail: dietmar.eberbeck@ptb.de

#### Clemens Friedrich

MFD TU Dresden Zwötzener Weg 7a 7551 Gera Deutschland

Tel.: 4915204408116

E-mail: clemens.friedrich@mailbox.tu-

dresden.de

#### Yashas Tejaskumar Gandhi

Institute of Computational Physics/ University of Stuttgart Allmandring 3 70569 Stuttgart Germany

Tel.: 49711685567719

E-mail: ygandhi@icp.uni-stuttgart.de

#### Philipp Gebhart

Institut für Festkörpermechanik/ Professur für Mechanik multifunktionaler Strukturen TU Dresden George-Bähr-Straße 3c 1069 Dresden Deutschland

Tel.: 49312292

E-mail: philipp.gebhart@tu-dresden.de

#### Konstantin Gerstenberger

P/P3 IPF Hohe Straße 6 1069 Dresden Deutschland Tel.: 15237974285

E-mail: gerstenberger@ipfdd.de

#### Yaser Hadadian

Biosignals, Metrology for magnetic nanoparticles Physikalisch-Technische Bundesanstalt Institute Berlin/PTB Abbestraße 02.Dez 10587 Berlin Germany Tel.: 3034817572

E-mail: yaser.hadadian@ptb.de

#### Birgit Hankiewicz

Physical Chemistry University of Hamburg Grindelallee 117 20146 Hamburg Germany

Tel.: +49 40 42838-8347 E-mail: birgit.hankiewicz@uni-

hamburg.de

#### Karl Kalina

Institute of Solid Mechanics TU Dresden George-Bähr-Straße 3c 1069 Dresden Germany

Tel.: 0351 463-33284

E-mail: karl.kalina@tu-dresden.de

#### Matthieu Kermarrec

Department of Chemistry Universität zu Köln Illien serpil 580 29470 Plougastel Daoulas France

Tel.: 33630305685

E-mail: matthieu.kermarrec@univ-

brest.fr

#### Jens Kirchner

Lehrstuhl für Intelligente Technische Elektronik und Systeme FAU Erlangen-Nürnberg Theodor-von-Zahn-Str. 24.Jan 91052 Erlangen Germany

Tel.: 0049 160 95082599 E-mail: jens.kirchner@fau.de

#### **Bruno Kluwe**

Metrology for Magnetic Nanoparticles Physikalisch-Technische Bundesanstalt Abbestraße 02.Dez 10587 Berlin Germany

Tel.: +49 3034817588 E-mail: bruno.kluwe@ptb.de

#### Ali Lakkis

Experimental physics 5 Universität Bayreuth Brandeburger Strasse 34a 95448 Bayreuth Germany Tel.: 1731728566

E-mail: Ali.Lakkis@uni-bayreuth.de

#### Joachim Landers

Faculty of Physics University of Duisburg-Essen Lotharstr. 1 47057 Duisburg Germany

Tel.: +49 203 379 2384

E-mail: joachim.landers@uni-due.de

#### Alberto Leon-Cecilla

Department of Chemistry University of Cologne Greinstraße 6 50939 Cologne Germany

Tel.: 34673321607 E-mail: lece\_al@hotmail.es

#### Marcus Löffler

Physikalische Technik/Informatik Westsächsische Hochschule Zwickau Kornmarkt 1 8056 Zwickau Germany Tel.: 0375 536 2134

E-mail: Marcus.loeffler@fh-zwickau.de

#### Stefan Lyer

ENT Clinic, Section of Experimental Oncology and Nanomedicine Universitätsklinikum Erlangen Glückstraße 10a 91054 Erlangen Germany

Tel.: 0160 91 94 77 06

E-mail: stefan.lyer@uk-erlangen.de

#### Nils Magin

Professur für Magnetofluiddynamik, Mess- und Automatisierungstechnik TU Dresden George-Bähr-Straße 3 1069 Dresden Germany

Tel.: 4935146335159

E-mail: nils.magin@tu-dresden.de

#### **Andreas Menzel**

Faculty of Natural Sciences / Institute of Physics / Theory of Soft Matter & **Biophysics** 

Otto von Guericke University Magdeburg Universitatsplatz 2 39106 Magdeburg

Tel.: +49 391 6757490 E-mail: a.menzel@ovgu.de

#### Jakob Mihatsch

Institut für Physik Otto-von-Guericke-Universität Magdeburg Universitätsplatz 2 39106 Magdeburg Germany

Tel.: 4917654324377

E-mail: jakob.mihatsch@ovgu.de

#### Stefan Odenbach

Magnetofluiddynamik, Mess- und Automatisierungstechnik TU Dresden George-Bähr-Str. 3 1069 Dresden Germany

Tel.: 35146332062

E-mail: stefan.odenbach@tu-dresden.de

#### **Anton Ostler**

Private Private In Gerold 2 82493 Klais Deutschland Tel.: 1758765712

E-mail: ostler-t@web.de

#### **Pawan Nimesh Patel**

Theory of Polymers Leibniz Institut für Polymerforschung Hohe Straße 05.Jan 1069 Dresden Germany Tel.: 3514658793133

E-mail: patel-pawan@ipfdd.de

#### **Harald Pleiner**

MPI Polymer Forschung Am Muehlborn 5 55218 Ingelheim Germany

Tel.: 06132 3086

E-mail: pleiner@mailbox.org

#### Ingo Rehberg

Physics Bayreuth University Grace-Hopper-Str. 3a 23562 Lübeck Germany Tel.: 0451 48900475

E-mail: Ingo.Rehberg@uni-bayreuth.de

#### **Marius Reiche**

Mechanics of Compliant Systems Group Technische Universität Ilmenau Max-Planck-Ring 12 98693 Ilmenau Deutschland

Tel.: 3677691884

E-mail: marius.reiche@tu-ilmenau.de

#### Henning Reinken

Institut für Physik Otto-von-Guericke-Universität Magdeburg Universitätsplatz 2 39106 Magdeburg Germany

Tel.: 4916092356583

E-mail: henning.reinken@ovgu.de

#### Yolantha Remane

Plasma wind tunnels - Electric space Institute of Space Systems/University of Stuttgart Pfaffenwaldring 29 70569 Stuttgart Germany

Tel.: +49 176 72808103

E-mail: remaney@irs.uni-stuttgart.de

#### Reinhard Richter

Experimentalphysik 5 Universität Bayreuth Gotthelfstrasse 2 95447 Bayreuth DE

Tel.: 92150862806

E-mail: reinhard.richter@uni-bayreuth.de

#### **Dirk Romeis**

Theorie der Polymere Leibniz-Institut für Polymerforschung Dresden e.V. Hohe Strasse 6 1069 Dresden Germany Tel.: 491638781339

E-mail: romeis@ipfdd.de

#### Heinrich Roth

Chair of Computational and Experimental Solid Mechanics TU Dresden George-Bähr-Straße 3c 1069 Dresden Germany

Tel.: +49 351 463-33450 E-mail: heinrich.roth@tu-dresden.de

#### Annette Schmidt

Chemistry Department Universität zu Köln Greinstr 04.Jun 50939 Koeln DF

Tel.: 0221 4705410

E-mail: annette.schmidt@uni-koeln.de

#### Patrick Schütz

Institut für Physikalische Chemie Universität Hamburg Grindelallee 117 20146 Hamburg Germany Tel.: +49 40 42838-9952

E-mail: patrick.schuetz@uni-

hamburg.de

#### Thilo Viereck

Inst. f. Elektrische Messtechnik (EMG) TU Braunschweig Hans-Sommer-Straße 06.Mrz 38106 Braunschweig Deutschland Tel.: +49 531 391-3860

E-mail: t.viereck@tu-braunschweig.de

#### **Rudolf Weeber**

Physics Institute for Computational Physics, University of Stuttgart Allmandring 3 70553 Stuttgart Deutschland Tel.: 491727136893

E-mail: weeber@icp.uni-stuttgart.de

#### **Andreas Weidner**

FG Elektrochemie und Galvanotechnik TU Ilmenau Gustav-Kirchhoff-Straße 6 98693 Ilmenau Deutschland

Tel.: 15739065010

E-mail: andreas.weidner@tu-ilmenau.de

#### Luiz Wille

EEI - Elektrotechnik Elektronik Informationstechnik LITES - F.A.U. Friedrich Alexander Universität Erlangen/Nürnberg Cauerstraße 08.Jan 91058 Erlangen Deutschland Tel.: +49 9131 85-27651

E-mail: luiz.wille@fau.de

#### Florian Wolgast

Institut für elektrische Messtechnik TU Braunschweig Hans-Sommer-Str. 66 38106 Braunschweig Germany Tel.: 5313913876 E-mail: f.wolgast@tu-bs.de

#### Keyu Xiao

Elektrotechnik-Elektronik-Informationstechnik LITES/Friedrich-Alexander-Universität Erlangen-Nürnberg Cauerstrasse 9 91058 Erlangen

Germany Tel.: +49 9131 85-27651 E-mail: keyu.xiao@fau.de

#### Konstantin Leonidas Zisiadis

Theory of Soft Matter / Biophysics Otto-von-Guericke-Universität Magdeburg Meseberger Weg 34 39128 Magdeburg

Germany Tel.: +49 391 67-51702 E-mail: konstantin.zisiadis@ovgu.de